Spring 2000

Diffusion Problems in Wound Healing and a Scattering Approach to Immune System Interactions

Julia Suzanne Arnold
Old Dominion University

DIFFUSION PROBLEMS IN WOUND HEALING ANDA SCATTERING APPROACH TO IMMUNE SYSTEM INTERACTIONS

by

Julia Suzanne Arnold
B.A. 1963 University of South Florida,
M.A. 1967 University of Georgia,
M.S. 1997 Old Dominion University

A Dissertation Submitted to the Faculty of
Old Dominion University in Partial Fulfillment of the
Requirements for the Degree of

DOCTOR OF PHILOSOPHY

COMPUTATIONAL AND APPLIED MATHEMATICS

OLD DOMINION UNIVERSITY
May 2000

Approved by:

John A. Adam (Director)

John Mark Dorrepaal (Member)

John Heinbockel (Member)

Constance Schober (Member)

Toby Banco (Member)

ABSTRACT

DIFFUSION PROBLEMS IN WOUND HEALING ANDA SCATTERING APPROACH TO IMMUNE SYSTEM INTERACTIONS

Julia Suzanne Arnold
Old Dominion University, 2000
Director: Dr. John A. Adam

A theoretical model for the existence of a Critical Size Defect (CSD) in certain animals is the focus of the majority of this dissertation. Adam [1] recently developed a one-dimensional model of this phenomenon, and chapters I - V address the existence of the CSD in a two-dimensional model and a three-dimensional model. The two-dimensional (or 1-d circular) model is the more appropriate for a study of CSD's. In that model we assume a circular wound of uniform depth and develop a time-independent form of the diffusion equation relevant to the study of the CSD phenomenon. It transpires that the range of CSD sizes for a reasonable estimate of parameter values is 1mm-1cm. More realistic estimates await the appropriate experimental data.

The remainder of this dissertation is devoted to two phenomenological models describing the spread of cancer and the effects of the immune system on that spread. In chapter VI, Tumor Immunity, a PDE similar to Fisher's equation is analyzed in terms of the equilibrium points and their linear stability and similarities are noted with the Spruce-Budworm problem of Ludwig et al (and summarized by Strogatz). This chapter concludes with a standard phase plane analysis of a traveling wave solution.

Chapter VII, Tunneling, introduces a novel and hopefully useful way of looking at cancer growth and the immune system. In the governing differential equation, the cancer cell number represents the independent variable, while the dependent variable is related to the probability of achieving that size cell number. (The square of the dependent variable is the probability). By analogy with quantum mechanics, the idea is introduced that the immune system (represented by a rectangular barrier of height V) may not in all cases prevent the cancer from "penetrating" the barrier i.e. tunneling through. The governing differential equation and boundary conditions represent a classical eigenvalue problem which may be thought of here as a "semi-classical" version of the time-independent Schrödinger equation. Examples are provided which show considerable variation in the effectiveness of the "immune barrier" towards limiting the numerical growth of cancer cells.

I would like to dedicate this thesis to Gayle Tarkelsen and Janet Brock, because of their unending encouragement. They were always sure of my ability to do this and their uplifting words helped me through the tough times. Thank You!

ACKNOWLEDGMENTS

I would like to thank my Lord and Savior, Jesus Christ, for He is responsible for my pursuit of this dream. He closed all other opportunities for me, allowing me to enter the graduate program. When I questioned my ability, He reminded me of the scripture verse " I can do all things through Christ which strengtheneth me."[Phil 4:13 (KJV)]. I would also like to thank my mentor and advisor Dr. John A. Adam, for his input, his patience, and his encouragement. Next, I would like to thank Dr. Toby Barco, a dental surgeon at Portsmouth Naval Hospital, who proposed the question on the critical size defect in wound healing, which became the focus of this dissertation. Finally, I would like to thank the members of my committee, Dr. John Mark Dorrepaal for his diligence in reading and correcting this dissertation, and to Dr. John Heinbockel for his helpfulness in arranging my equations so that they would be clearer to the reader, and to Dr. Constance Schober for her suggestion to supply more details of the solutions which I have summarized in Appendix C. To all my of you I express my sincere appreciation for your help in the culmination of a life-long dream. Last but not least, I would like to thank my husband, David W. Arnold, for his understanding and patience. I know he is glad it is finally finished.

TABLE OF CONTENTS

Page

LIST OF TABLES

LIST OF GRAPHS

CHAPTER I

INTRODUCTION

Lecomte DuNoüy [6] in his book *Biological Time* , written in 1936, wrote these words,

> "The difference between the biological method of approach and the mathematical method borrowed from the physical sciences is ...the multiplicity of the factors and ... the complexity of the problem. The solution had not yet been found, because those who had studied it were *too familiar* with the details of the phenomenon. Knowing a great many physiological factors but ignoring their relative influence, they did not dare eliminate them, and did not know how to take them into account. They were paralysed by their knowledge.
>
> Like the botanist who could not see the forest because of the trees, they could only consider the facts as a function of microscopic biological elements with which they were familiar. My ignorance of these elements freed me from the chains which fettered them. Not knowing how to distinguish the different species, I examined the forest from a distance, as a whole and quantitatively as I had been taught to do for a physical phenomenon."

DuNoüy is saying that sometimes it is necessary to strip the physical situation and consider a mathematically manageable set of parameters and begin the investigation from a distance. The following information gleaned from books and papers represents the basic information from which the following mathematical model was formulated.

THE CRITICAL SIZE DEFECT

Part of the care a neurosurgeon or dental surgeon might give a patient is the treatment of bone wounds. For example, a neurosurgeon removes a portion of the skull

---

The model journal used is *Mathematical And Computer Modelling*.

to expose the brain. When his operation on the brain is finished, he must decide to cover the cavity with a plate or reposition the excised bone, suture it in the hope that it grows back together. An oral surgeon removes a portion of bone while excising a cancerous tumor in the mandible or jaw bone. Is the cavity too large for the bone to regenerate itself? Will he need to provide an alternative treatment to ensure that the bone will heal properly? When teeth are removed from the jaw bone, will the socket fill in with new bone? These are questions that surgeons must ask themselves routinely. Bone wounds, such as breaks, or gouges may at times heal naturally and at other times may not heal without medical treatment. In Winet [30], a critical size defect is defined as the wound size for which the diameter is too large for ossification (the formation of rigid bone), (although the wound is not necessarily circular). This means that the calcification of new bone ceases before reaching the opposite side of the wound, thus leaving spongy bone called cancellous bone in the center of the wound. The objective of this paper is to provide a mathematical basis for the existence of this critical size defect or CSD in bone. In Adam [1], a one dimensional model was used to show this existence. This paper extends his work into both a two-dimensional and three-dimensional setting.

The time development of the wound is not addressed here; only the conditions under which tissue regeneration occurs. The primary objective is to find in each case a critical radius beyond which no healing occurs–the definition of a CSD.

In the two-dimensional and three-dimensional setting, Model I corresponds to a circular cylinder, and a sphere respectively in which bone has been removed and no bone remains in the vacated area. In the two-dimensional problem, Model II examines the case where

a central core of bone remains in the excavated area. (This cannot occur in the three-dimensional setting.)

In each model we assume a thin ring of width δ which influences the mitotic activity up to the wound edge. In the models, C(r,t) represents the concentration of a generic growth stimulator, R being the radius of the wound and t being time, both in appropriate units. For Model I, $R \leq r < \infty$, and for Model II $0 \leq r < \infty$.

THE NORMAL GROWTH PROCESS IN BONE

From Bloom & Fawcett [3] we find that bone is composed of many different types of cells. In order for a bone to grow from "infant size" to "adult size" a process of growth and resorption must occur. The exterior of a bone is covered with a connective tissue membrane called the periosteum. The interior of the bone is made up of a cellular membrane called the endosteum. In the deep layer of periosteum cells are cells called osteogenic cells. During growth it is these osteogenic cells which proliferate giving rise to cells called osteoblasts. A key factor in the bone cell development are the growth factors secreted by these osteoblasts. Some of the growth factors secreted are named bone morphogenetic protein or BMP. (There exist also BMP 2, and BMP 7). In addition there is a transforming growth factor beta called TGF-β, a fibroblastic growth factor beta FGF-β, and others. According to Bennett et al [4], growth factors may act on the producer cell, adjacent cells, or distant cells. When activated these growth factors can stimulate a number of processes including wound healing. The osteoblast cells secrete the intercellular substance of bone, thus adding new bone to the surface and thus

increasing the size or width of the bone. In the endosteum the osteogenic cells produce cells called osteoclasts which have the job of bone resorption. This in turn enlarges the inner shaft creating a larger bone marrow cavity. Since this procedure is part of the growth procedure for new born animals until they reach adulthood where this process then ceases, it is easy to understand why wound healing in bone in young animals may be more successful than in full sized adult animals. Most of the experimental research on the critical size defect was performed on the skull or calvaria of animals. We will now examine how bone wounds heal.

THE NORMAL WOUND HEALING PROCESS

When a bone wound occurs a temporary blood clot seals off damaged blood vessels. A fibrous protein (BMP or other growth factors) develops within the bone near the wound edge. This fibrous substance is referred to as collagen. As the collagen ages the osteoblasts start to build a spongy bone (cancellous bone) on the wound edge until it links the gap. Gradually denser, harder bone replaces the cancellous bone; hard bone is called cortical bone. In some cases the gap is too large and remains filled with a fibrous connective tissue which fails to calcify [3].

THE TIME FACTOR FOR HEALING

EBI Medical Systems and the Mayo Clinic Health Letter describe the time interval for bone healing [7,10] as follows. While the healing process begins immediately, the complete healing of bone may take from two months to two years.

(Although according to Hollinger and Kleinschmidt [16] if a bone defect is not regenerated within one year it is unlikely that it will occur.) During the first few days after a wound has occurred, the spongy bone forms on the wound edge. Within seven to ten days, the gap between the new bone is invaded by embryonic tissue which forms a bridge of connective tissue, called fibrocartilage. This begins at the wound edge and moves toward the center. This generally occurs three to four weeks after the initial wound. In the sixth to eighth week, the process of bone resorption occurs, where the vascular system penetrates the fibrocartilage, breaks it down and absorbs it while replacing the area with fiber bone. The last phase is the change from fiber bone to a rigid bone.

The time-development of the healing process is not taken into consideration in the mathematical models that follow because the timescales justify the assumption of diffusive equilibrium in these models (which is discussed in Chapter II).

CHAPTER II

THE MATHEMATICAL MODELS

THE ONE-DIMENSIONAL MODEL

Adam [1] investigated the CSD phenonenon in a one-dimensional setting. The first model corresponded to bone removed from an infinite plane, in which only a thin band of tissue at the wound edges takes part in bone regeneration. The edges are represented by $x = \pm \frac{L}{2}$. The region $[0, \frac{L}{2}]$ represents the right half of the wound where no tissue or bone remains, and $[\frac{L}{2}, \frac{L}{2}+\delta]$ represents the layer generating growth factor (GF). In a second model in [1], it is assumed some bone remains in the center but is not a source of GF, it merely serves as a passive vehicle through which GF freely diffuses. Simple though these models were, they did provide some upper bounds for the size (width) of the CSD.

THE TWO-DIMENSIONAL MODEL

According to the work of Arnold and Adam [2] model 1 assumes a circular wound of uniform depth in which no bone remains in the wound interior. Model II assumes some bone remains in the wound center but is not a source of growth factors, as indicated above, and in [1]; it is essentially bone in which the GF diffuses.

BASIC CONFIGURATIONS: MODEL I

We position the center of the circular wound at the origin; a disk of radius R being removed . As indicated earlier we suppose that a generic "growth factor" (GF) is produced as a result of the trauma to the system, and it is the distribution of this growth factor that determines whether or not wound healing occurs in this model.

The differential equation describing the space and time distribution of the growth factor concentration C(r,t) is

$$\frac{\partial C}{\partial t} - \frac{D}{r}\frac{\partial}{\partial r}\left(r\frac{\partial C}{\partial r}\right) + \lambda C = PS(r) \qquad (1)$$

where D, λ and P are respectively the diffusion coefficient for the GF in the tissue, the decay or depletion rate of the GF, and the production rate of GF by the enhanced mitotically active cells in the vicinity of the wound's edge. These are assumed to be constant in both models. Furthermore, S(r) is the source term describing the distribution of GF production throughout the active tissue. In both models this is assumed to be uniform; thus

$$S(r) = 1 \text{ for } R \leq r \leq R + \delta$$

$$S(r) = 0 \text{ elsewhere}$$

δ being the width of the active layer producing GF.

In equation (1), the first term represents the time rate of change of GF concentration, the second term describes the spatial change due to diffusion of GF, and the third term is the depletion or decay rate of change of GF as it interacts with the

system as a whole, and is changed or removed. One important assumption made is that of *diffusive equilibrium*. Basically, this means that the process of readjustment of the GF concentration as the wound heals is so fast (when compared with the typical wound-healing time) that, to a first approximation, the distribution of GF may be considered independent of time [1] . A typical diffusion time, from dimensional analysis is

$$T \approx \frac{r^2}{D}$$

where r is a typical wound radius. The value D depends on the particular GF (the higher the molecular weight, the smaller is D). Sherratt and Murray [19,20] carried out a best fit analysis from data on epidermal wound healing and estimated that for epidermal GF, $D \approx 3.1 \times 10^{-7} cm^2\ \mathrm{sec}^{-1}$. Diffusion processes alone will not suffice in bone to provide nourishment for the osteocytes, but capillaries are never far away: the osteocytes are arranged around central capillaries in concentric layers, which form spindle-shaped units known as osteons. Thus pure diffusion is facilitated by the efficient capillary transport system, and we might expect that the effective diffusion coefficient is enhanced compared with the standard value used in [1] (at least for growth factors of the same molecular weight). It is difficult to be more precise at this stage, but again, for the purposes of illustration, we suppose that, compared with the values used in [1], D is increased by a factor of ten. Thus we take $D \approx 3.1 \times 10^{-6} \mathrm{cm}^2\ \mathrm{sec}^{-1}$. Using the first value for D and r values of 1μm (10^{-4}cm), 10μm, 1mm, and 1cm we find typical diffusion times of .03 sec, 3.2 sec, 8.9 hrs, and approximately 37 days. Clearly the approximation is less well justified for GF in wound sizes of order one centimeter. Using the second

value for D and r values of 1μm (10^{-4}cm), 10μm, 1mm, and 1cm we find typical diffusion times of .003 sec, .32 sec, .9 hrs, and approximately 3.7 days. Over this timescale, the diffusive approximation is certainly a very good one for GF distributions. Under these circumstances, we write $\frac{\partial C}{\partial t} = 0$ in equation (1).

MODEL I: EQUATIONS AND SOLUTIONS

If $\alpha^2 = \frac{\lambda}{D}$ then equation (1) can be written as:

$$\frac{d^2C(r)}{dr^2} + \frac{1}{r}\frac{dC(r)}{dr} - \alpha^2 C(r) = \frac{-P}{D}S(r) \quad . \qquad (2)$$

The boundary conditions are:

- C(r) and $\frac{dC(r)}{dr}$ are both continuous at $R + \delta$
- $\lim_{r\to\infty} C(r) = 0$
- $\frac{dC(r)}{dr} = 0$ at $r = R$.

The first two conditions are obvious requirements. The third condition implies

that there is no flux (number of molecules crossing unit area in unit time) at the wound edge. The second model will modify this restriction as we will permit tissue in the wound area capable of dispersing GF.

In terms of the dimensionless variable $x = \alpha r$, equation (2) becomes

$$x^2 \frac{d^2C(x)}{dx^2} + x\frac{dC(x)}{dx} - x^2C(x) = \frac{-P}{D}\frac{x^2}{\alpha^2}S\left(\frac{x}{\alpha}\right) \quad . \tag{3}$$

The solutions to the homogeneous version of (3) are modified Bessel functions of order zero. After some algebra, the solution to the nonhomogeneous equation can be written, in terms of the original variables for $R \le r \le R + \delta$ as

$$C(r) = \frac{-PK_1(\alpha(R+\delta))}{\lambda\beta_\delta} I_0(\alpha r) + \frac{-PK_1(\alpha(R+\delta))}{\lambda\beta_\delta}\frac{I_1(\alpha R)}{K_1(\alpha R)}K_0(\alpha r) + \frac{P}{\lambda} \tag{4}$$

and for $r > R + \delta$ as

$$C(r) = \left[\frac{-PK_1(\alpha(R+\delta))}{\lambda\beta_\delta}\frac{I_1(\alpha R)}{K_1(\alpha R)} + \frac{PI_1(\alpha(R+\delta))}{\lambda\beta_\delta}\right]K_0(\alpha r) \tag{5}$$

$$\text{where } \beta_\delta = \left(I_0K_1 + K_0I_1\right)\left(\alpha(R+\delta)\right) \quad .$$

For the generic parameter values P, $\lambda = 1$, $\alpha R = 2$, and $\alpha\delta = .5$ a typical graph of C(r) is shown in Figure 1.

Using equation (4), we apply the criterion that

$$C(R) \geq \theta$$

where θ represents a threshold value for which wound healing will occur for values of r satisfying this condition. The resulting equation is:

$$\frac{P}{\lambda}\left\{1 - \frac{K_1(\alpha(R+\delta))}{\beta_\delta}\left[I_0(\alpha R) + \frac{I_1(\alpha R)K_0(\alpha R)}{K_1(\alpha R)}\right]\right\} \geq \theta \quad . \tag{6}$$

Using standard identities for the Wronskian [19], inequality 6 simplifies to

$$\frac{(\alpha R + \alpha\delta)K_1(\alpha R + \alpha\delta)}{\alpha R K_1(\alpha R)} \leq 1 - \frac{\lambda\theta}{P} \tag{7}$$

If $\alpha R = y$ and $\alpha\delta = \epsilon$, then inequality (7) can be written as

$$Q(\varepsilon, y) = \frac{(y+\varepsilon)K_1(y+\varepsilon)}{yK_1(y)} \leq 1 - \frac{\lambda\theta}{P} = 1 - \frac{1}{n} \tag{8}$$

where $n = \frac{P}{\lambda\theta}$. Holding y fixed, $Q(\epsilon,y)$ can be thought of as a function of $\epsilon = \alpha\delta$, from

which we can then find a lower bound δ_c (δ critical and also ϵ_c for ϵ critical) for the width δ above which healing can occur. It is not possible to obtain an explicit expression for ϵ_c in general, but if ϵ is small compared with y, then we may use first order Taylor polynomials to simplify the Bessel functions. Thus to first order in ϵ

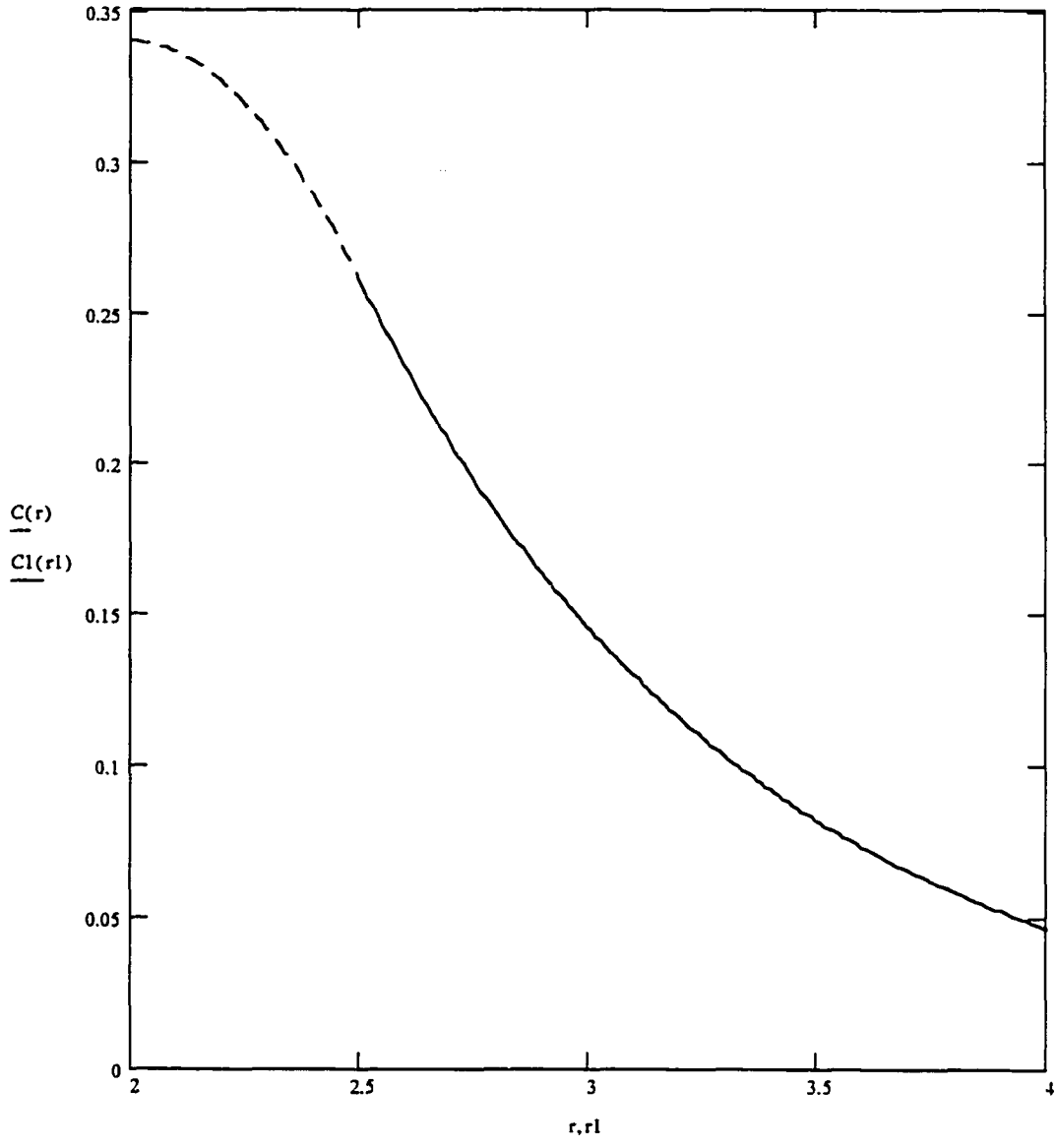

Figure 1: The growth factor concentration C(r) for Model I. For illustrative purposes P and $\lambda = 1$, $\alpha R = 2$ and $\alpha\delta = .5$. C(r) is the dotted graph representing the δ- region, and C1(r1), the solid graph, represents $r > R + \delta$.

$$K_1(y+\varepsilon) \approx K_1(y) + \varepsilon K_1'(y)$$

where $$K_1'(y) = -K_0(y) - \frac{K_1(y)}{y}$$

whence

$$\left[K_1(y) + \varepsilon\left(-K_0(y) - \frac{K_1(y)}{y}\right)\right]\frac{(y+\varepsilon)}{yK_1(y)} \le 1 - \frac{1}{n}$$

which simplifies to:

$$\varepsilon \ge \varepsilon_c = \frac{K_1(y)}{nK_0(y)} \tag{9}$$

i.e.

$$\delta \ge \delta_c = \frac{K_1(y)}{\alpha n K_0(y)}$$

The graph of $\alpha\delta_c$ is given in Figure 2. (See Appendix A for more information.)

With y fixed, Q(ϵ,y) becomes a function of ϵ. Call this function $Q_1(\epsilon)$. If ϵ_c satisfies $Q_1(\varepsilon_c) \le 1 - \frac{1}{n}$, then any $\varepsilon \ge \varepsilon_c$ satisfies $Q_1(\varepsilon) \le 1 - \frac{1}{n}$.

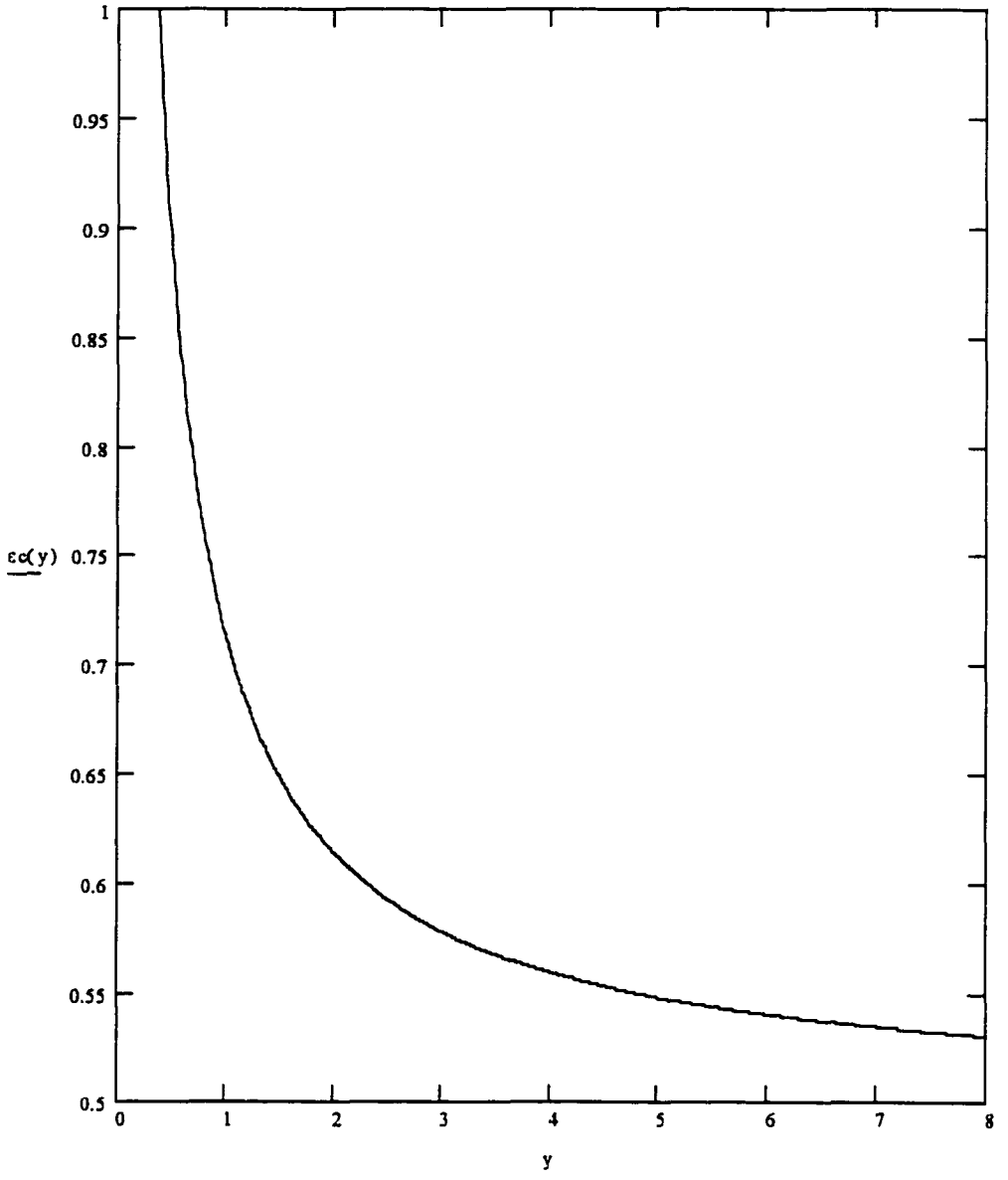

Figure 2: The graph of the width function $\epsilon_c(y) = \alpha\delta_c(y)$, defined by inequality (9). In this graph n = 2.

This follows despite the fact that $K_1(y + \epsilon)$ is monotone decreasing in ϵ, while $(y + \epsilon)$ is monotone increasing in ϵ. The derivative of $(y + \varepsilon)K_1(y + \varepsilon)$ is $-(y + \epsilon)K_0(y + \epsilon)$, hence $(y + \epsilon)K_1(y + \epsilon)$ is monotone decreasing in ϵ. Thus $Q_1(\epsilon_c) \geq Q_1(\epsilon)$ since $\epsilon_c \leq \epsilon$. Hence $Q_1(\epsilon) \leq Q_1(\epsilon_c) \leq 1 - \frac{1}{n}$.

Large values of n denote an active production rate which would certainly be conducive to healing. Alternatively, small values of λ or θ relative to P also imply large values of n. In Figure 3 the graph of $Q_1(\epsilon)$ from equation (8) is illustrated for the parameter values y = 2 and n = 2.

A comparison of the values from the graph of equation (8) referred to as $(\alpha\delta_c)_g$ (with no approximation except rounding) and the values from equation (9) referred to as $\alpha\delta_c$ are given in Table 1.

Using this value of δ_c, a representative for R_c - values can be sought. Using equation (8), we can write

$$Q_2(y) = \frac{(y+\varepsilon)K_1(y+\varepsilon)}{yK_1(y)} \leq 1 - \frac{1}{n} \tag{10}$$

by substituting $\frac{K_1(y)}{nK_0(y)}$ for ϵ in equation (10) and simplifying the result, $Q_2(y)$ becomes

$$Q_2(y) = \left(\frac{nyK_0(y) + K_1(y)}{nyK_0(y)K_1(y)}\right) K_1\left(y + \frac{K_1(y)}{nK_0(y)}\right) \leq 1 - \frac{1}{n} \tag{11}$$

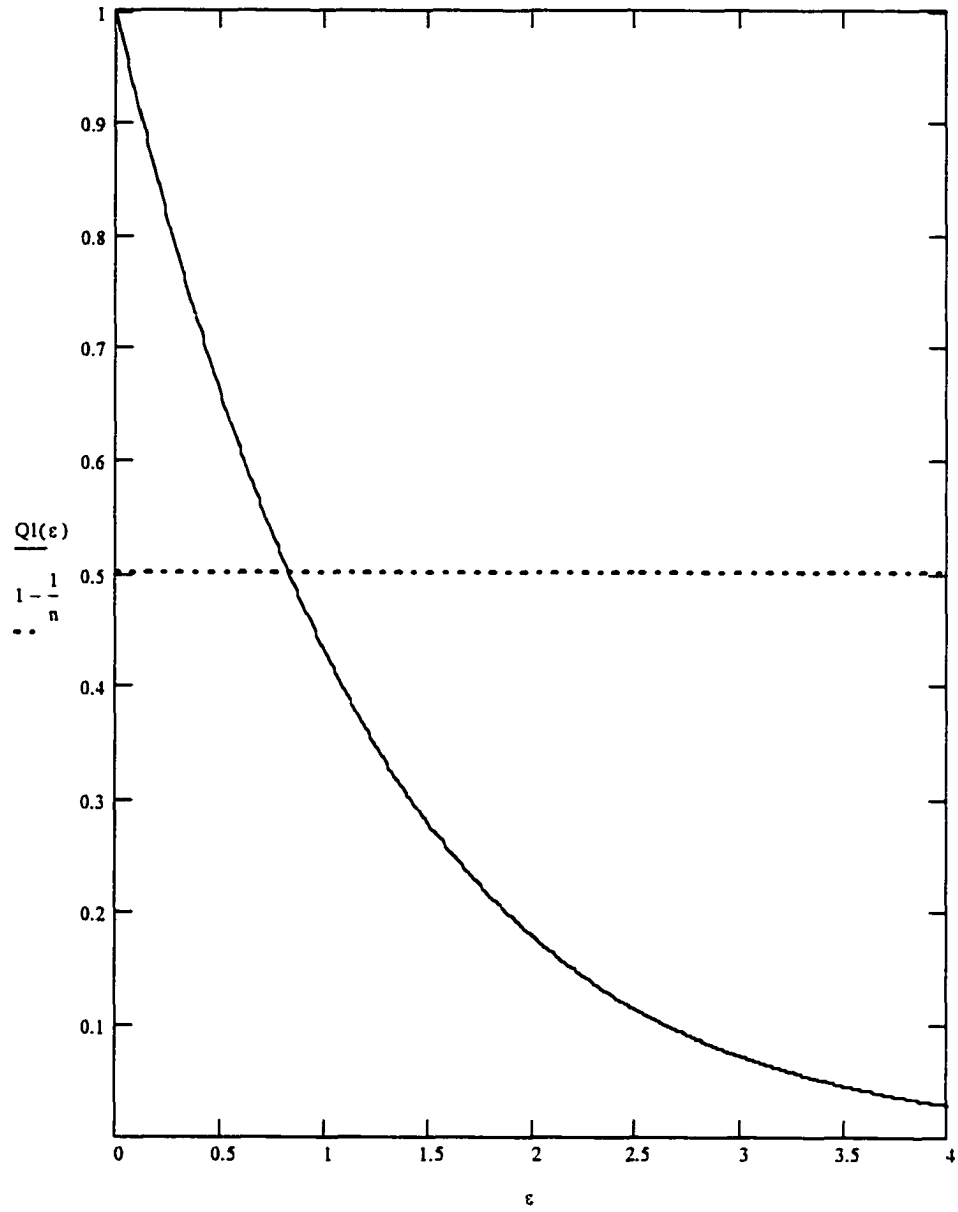

Figure 3: The graph of the function $Q_l(\epsilon)$ defined by equation (8) with y = 2. The parameter value is n = 2. The intersection of the dotted line with the graph of Q_l defines the point which represents the minimum thickness of GF activity, below which no healing can occur for ϵ less than this amount.

the graph of which is given in Figure 4. The parameter value used for Figure 4 is $n = 1.5$.

Solving for y from inequality (11) is not feasible, analytically, at least. However, observe that the graph of $Q_2(y)$ in Figure 4 resembles that of a rational function. Thus by finding a rational function which approximates $Q_2(y)$, it should be possible to approximate R_c by an explicit formula. A rational function which approximates $Q_2(y)$ for various parameter values is

$$F(y) = b - \frac{a}{y}$$

for suitable a, and b, both positive. Solving for y, the formula for $\alpha R_c = y_c$ is

$$y \le y_c = \frac{an}{bn + 1 - n}$$

In Figure 5, for $n = 1.5$ $\quad F(y) = .523 - \frac{.048}{y}$

and $y \approx .253$ while graphical methods give $y \approx .252$. Some additional comparisons are given in Table 2.

An interesting observation is that using the minimum value for $\alpha\delta_c$ will always produce a CSD because of the dependence on n in the equation. (See equation (11)). For n very large, e.g. $n = 200$, the graph of equation (11) is shown in Figure 6.

If we choose an $\alpha\delta > \alpha\delta_c$ such as $\frac{\beta K_1(y)}{nK_0(y)}$ for $\beta \ge 1$, it is possible to create graphs

Table 1. For various values of n and αR, a comparison is made between the approximation for the $\alpha\delta_c$ region and the values found on the graph of $Q_1(\alpha\delta_c)$.

n	1 - 1/n	αR	$\alpha\delta_c$	$(\alpha\delta_c)_g$	$(\alpha\delta_c)_g - \alpha\delta_c$
1.5	.33333	1	.95	1.39	.44
1.5	.33333	3	.77	1.22	.45
1.5	.33333	5	.73	1.15	.42
1.5	.33333	7	.71	1.16	.45
1.5	.33333	10	.70	1.16	.46
1.5	.33333	20	.68	1.13	.45
5.0	.8	1	.29	.307	.017
5.0	.8	3	.23	.253	.023
5.0	.8	5	.22	.244	.024
5.0	.8	7	.21	.235	.025
5.0	.8	10	.21	.235	.025
5.0	.8	20	.20	.226	.026
8.0	.875	1	.18	.190	.01
8.0	.875	3	.14	.154	.014
8.0	.875	5	.14	.145	.001
8.0	.875	7	.13	.145	.015
8.0	.875	10	.13	.140	.01
8.0	.875	20	.13	.137	.007

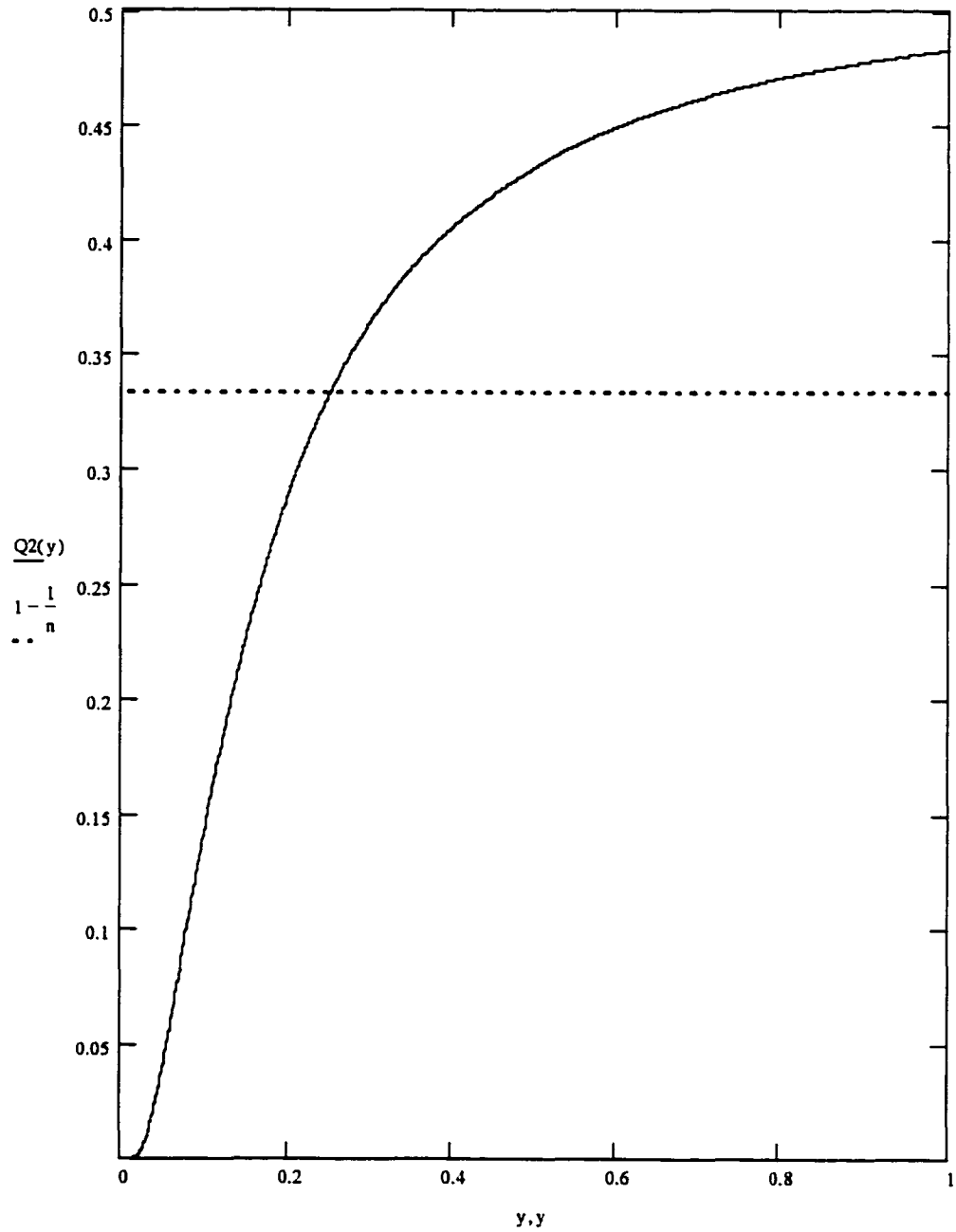

Figure 4: The graph of $Q_2(y)$ where the approximation $\epsilon_e(y)$ replaces ϵ in $Q(\epsilon,y)$. For this graph $n = 1.5$.

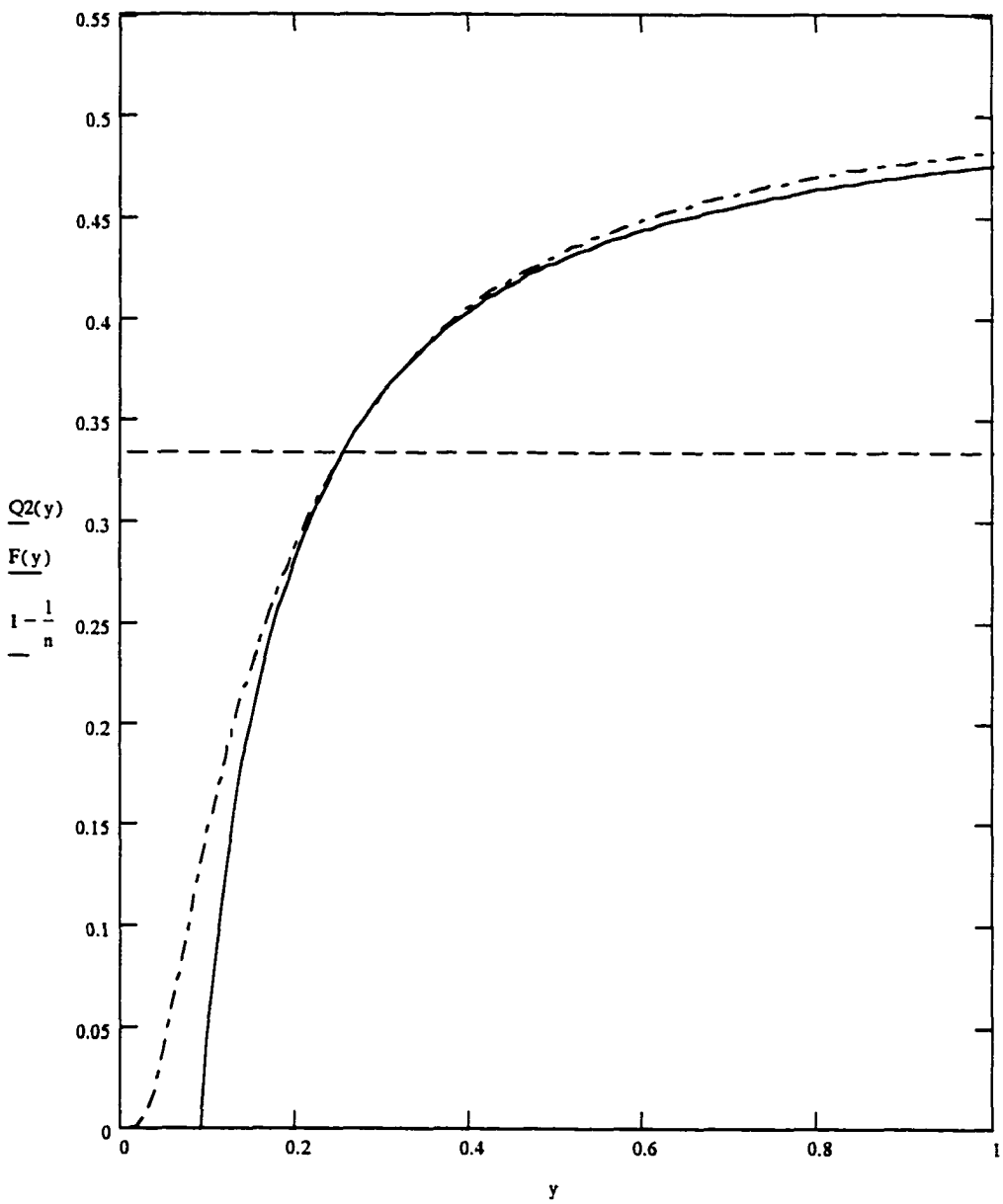

Figure 5: The graph of Figure 4 and its rational approximation F(y). For this graph

n = 1.5, a = .048, and b = .523.

Table 2. For various values of n, αR_c values are found.

n	$1-\frac{1}{n}$	$(\alpha R_c)_g$	αR_c	a	b
1.1	.091	.13	.155	.050	.413
1.5	.333	.252	.253	.048	.523
3.0	.667	.40	.480	.029	.727
5.0	.800	.45	.487	.014	.829
8.0	.875	.54	.572	.010	.892
10	.900	.54	.539	.008	.915
20	.950	.59	.670	.002	.952

which show no CSD is possible. For example; for n = 2 and β_i = 1, 1.2, and 2 for i = 0,1, and 2 respectively, $Q_{2i}(y)$ is defined as follows:

$$Q_{2_i}(y) = \left(\frac{nyK_0(y) + \beta_i K_1(y)}{nyK_0(y)K_1(y)} \right) K_1\left(y + \frac{\beta_i K_1(y)}{nK_0(y)} \right) \leq 1 - \frac{1}{n}, \text{ for } i = 0, 1, 2 \qquad (12)$$

(which is true from an earlier conjecture). The corresponding graphs are given in Figure 7. Thus using an $\alpha\delta$ value larger than the minimum illustrates a situation modeling complete healing. For β = 1, $Q_{20}(y)$ represents ϵ_c substituted for ϵ. For β = 1.2, $Q_{21}(y)$ represents a situation which shows the existence of a CSD. For β = 2, $Q_{22}(y)$ is exhibiting a graph with no CSD which implies complete healing. An examination of the asymptotic expansions of the Bessel functions reveals that when $\beta = 1, \lim_{y \to \infty} Q_2(y) = 1$ for all n. It follows that the graph of $Q_2(y)$ will asymptote to the horizontal line y = 1 and thus exceed $1 - \frac{1}{n}$ for sufficiently large y. Since equality in equation (12) indicates the existence of a CSD, this proves that there is always a CSD when β = 1.

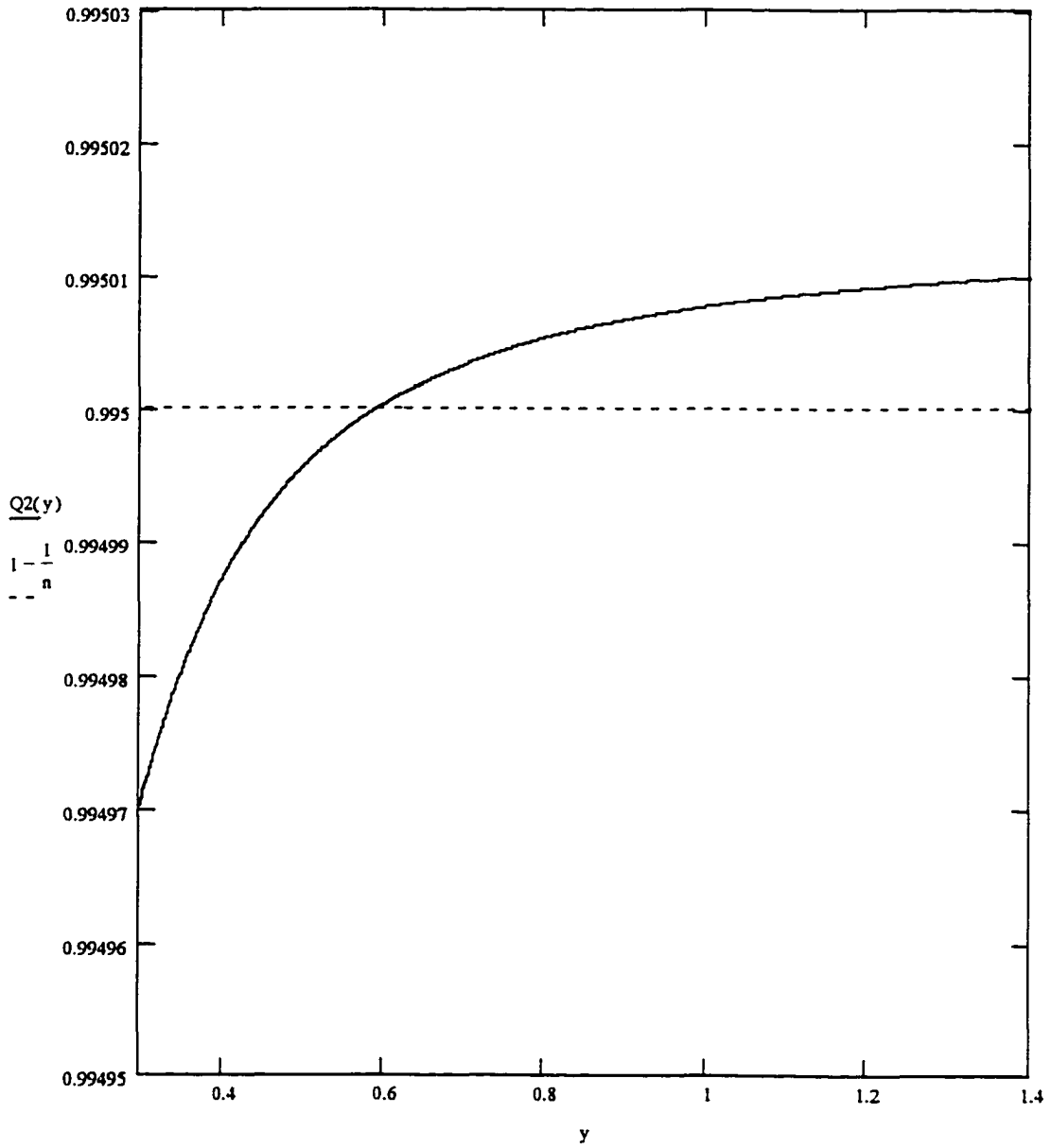

Figure 6: Figure 4 reproduced for n = 200. The purpose of this graph is to illustrate the existence of a CSD when the minimum value $\alpha\delta_c(y)$ is substituted for ϵ.

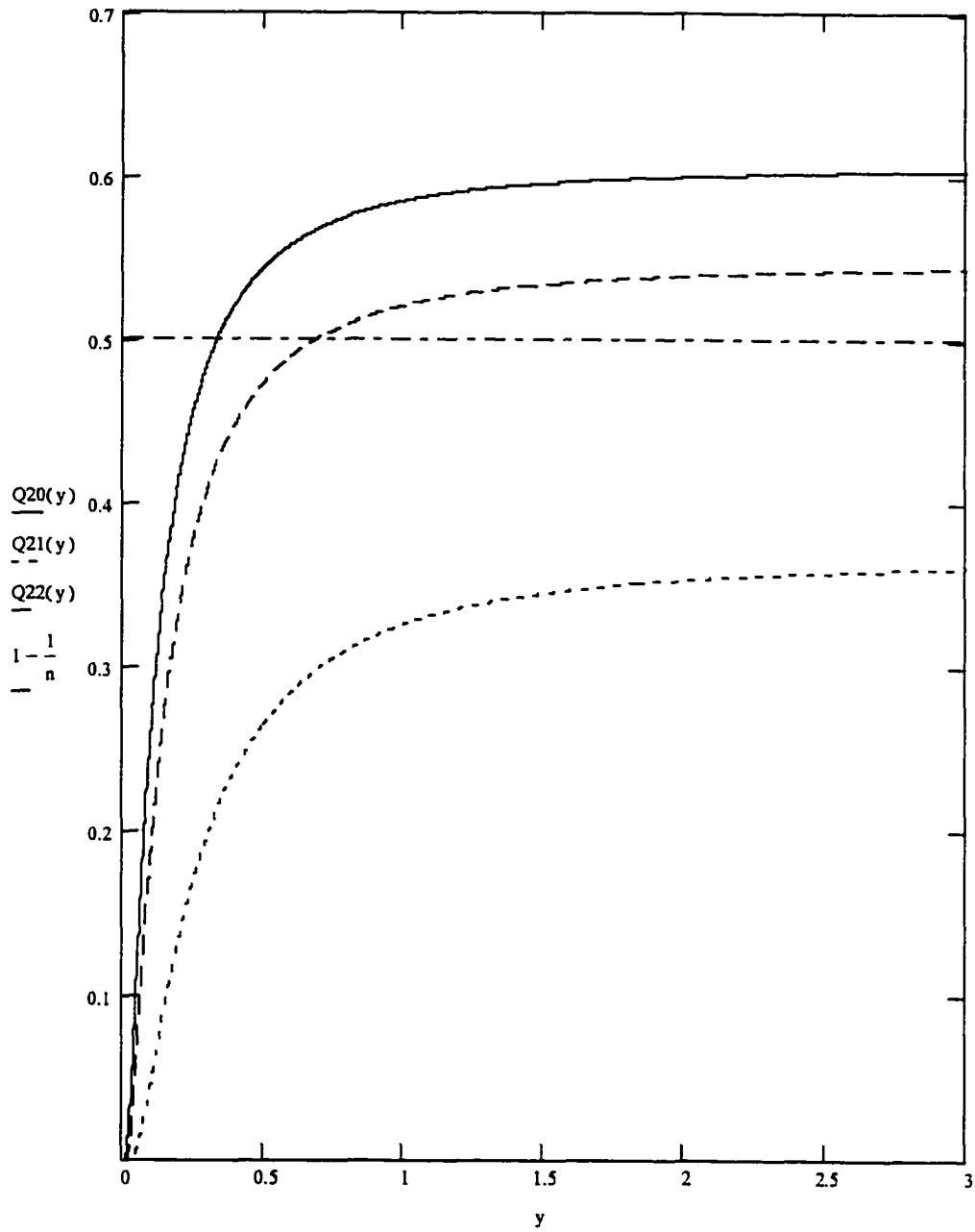

Figure 7: For n = 2, and β a constant multiple of $\epsilon(y)$, $Q_{20}(y)$ represents $\alpha\delta_c$ substituted for ϵ which means $\beta = 1$. For $\beta = 1.2$, $Q_{21}(y)$, by intersecting with 1 - 1/n, exhibits a CSD, and for $\beta = 2$, $Q_{22}(y)$ shows no CSD.

MODEL II: EQUATIONS AND SOLUTIONS

In this model, there is still some tissue in the wound interior for $r < R$. It is merely a passive environment into which GF can diffuse. As before, the ring from the wound edge at R to $R + \delta$ is the domain of GF production. Additional boundary conditions need to be imposed:

continuity of C(r) and $\frac{dC(r)}{dr}$ at R, and $C'(0) = 0$.

The corresponding solutions are:

$$C(r) = AI_0(\alpha r) + BK_0(\alpha r) \qquad \text{for } r < R$$

$$C(r) = MI_0(\alpha r) + NK_0(\alpha r) + \frac{P}{\lambda} \qquad \text{for } R \leq r \leq R + \delta$$

and $$C(r) = GK_0(\alpha r) \qquad \text{for } r > R + \delta.$$

Let $\beta = (I_0K_1 + K_0I_1)(\alpha r)$ and β_δ as before, then

$$C(r) = \frac{P}{\lambda}\left(\frac{K_1(\alpha R)}{\beta} - \frac{K_1(\alpha(R+\delta))}{\beta_\delta}\right)I_0(\alpha r) \quad \text{for } r < R, \tag{13}$$

$$C(r) = \frac{-P}{\lambda}\left(\frac{K_1(\alpha(R+\delta))}{\beta_\delta}\right)I_0(\alpha r) - \frac{P}{\lambda}\left(\frac{I_1(\alpha R)}{\beta}\right)K_0(\alpha r) + \frac{P}{\lambda} \quad \text{for } R \leq r \leq R + \delta \tag{14}$$

and

$$C(r) = \frac{-P}{\lambda}\left(\frac{I_1(\alpha R)}{\beta} - \frac{I_1(\alpha(R+\delta))}{\beta_\delta}\right)K_0(\alpha r) \text{ for } r > R+\delta \quad . \tag{15}$$

A typical graph of C(r) using parameter values P, $\lambda = 1$, $\alpha R = .5$, and $\alpha\delta = 3$ is shown in Figure 8.

The requirement $C(R) \geq \theta$ implies, from equation (14) that

$$\alpha(R+\delta)K_1(\alpha(R+\delta))I_0(\alpha R) + \alpha R I_1(\alpha R)K_0(\alpha R) \leq 1 - \frac{1}{n}.$$

Again if $\epsilon = \alpha\delta$ and $y = \alpha R$ then the above equation becomes

$$Q(\varepsilon, y) = (y+\varepsilon)K_1(y+\varepsilon)I_0(y) + yI_1(y)K_0(y) \leq 1 - \frac{1}{n} \tag{16}$$

the graph of which is given in Figure 9, using parameter values n = 3 and y = .5.

By similar methods to those used in Model I, we can find an approximation for δ_c under the assumption that $\frac{\delta}{R} << 1$. This is $\delta \geq \delta_c = \frac{1}{n\alpha y K_0(y) I_0(y)}$ the graph of

which is given in Figure 10 (for n = 3).

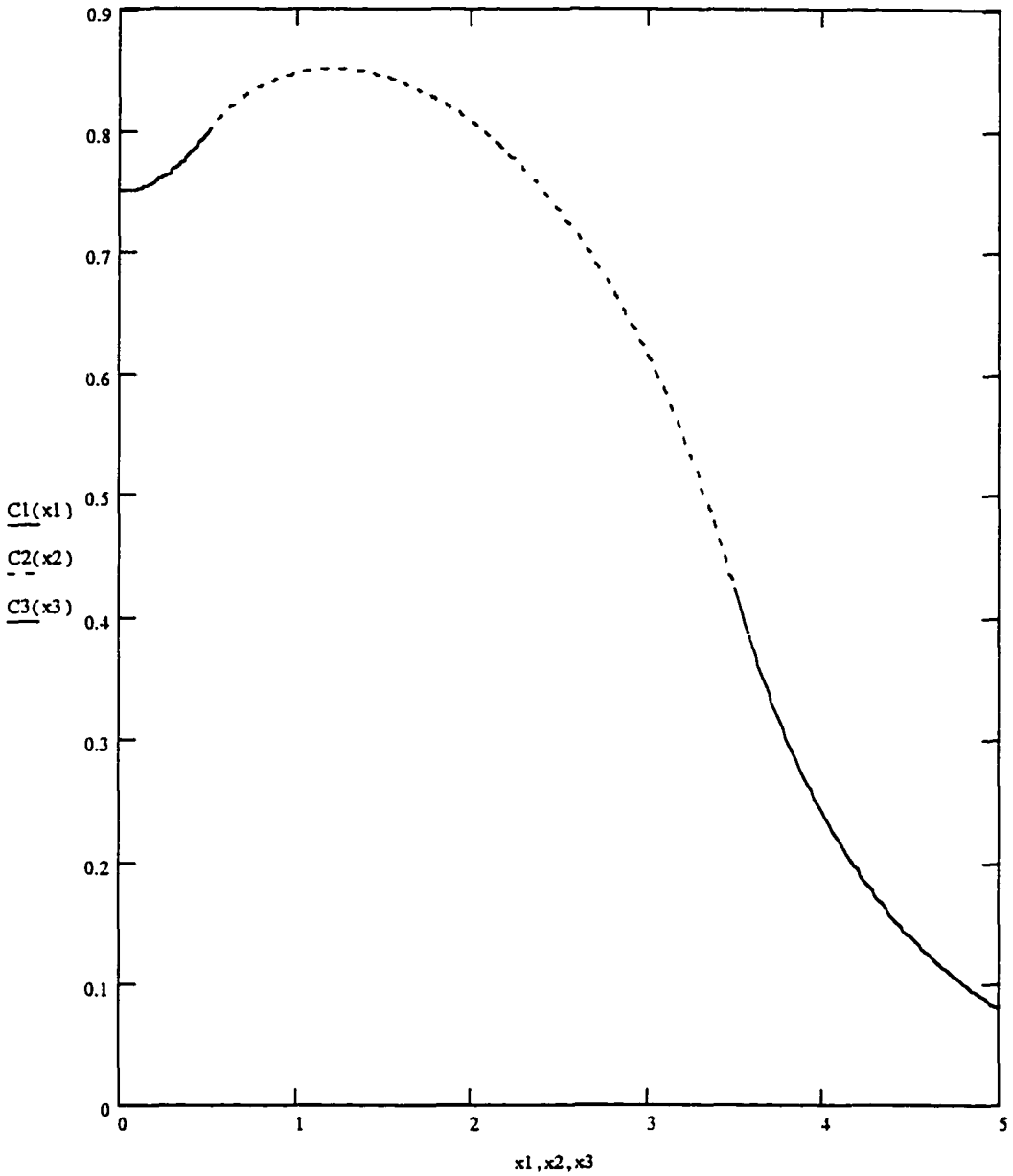

Figure 8: The Growth Factor Concentration C(r) for Model II: (C_1(x1) is defined over [0,R], C_2(x2) is defined over [R,R+δ], and C_3(x3) is defined over [R+δ,∞]).

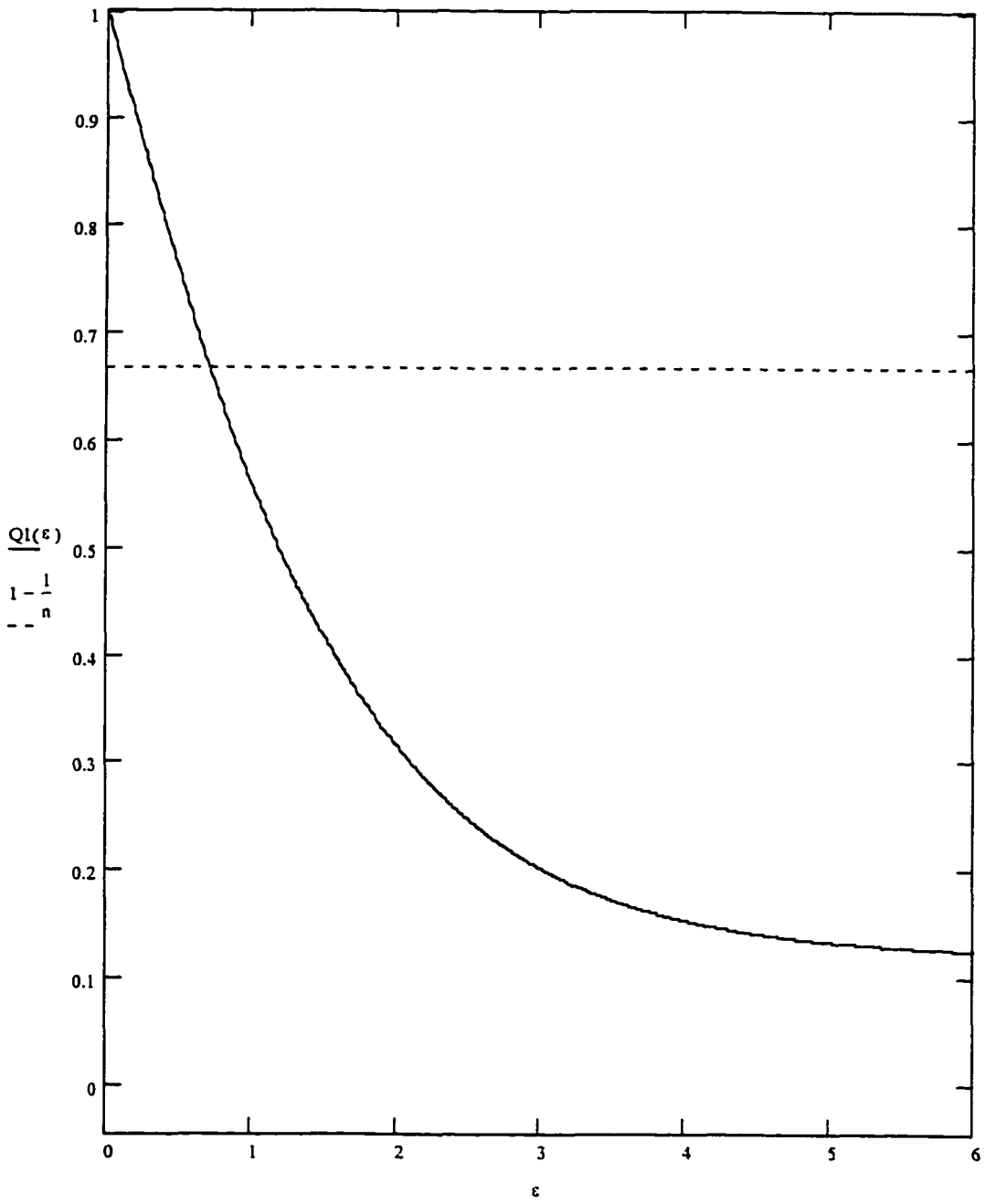

Figure 9: This is the graph of $Q_1(\epsilon)$ from equation 16 with y = .5. The parameter value used is n = 3.

Again substituting ϵ_c from equation (17) for ϵ in $Q(\epsilon,y)$ we obtain the function $Q_2(y)$ whose graph is given in Figure 11 for the parameter value n = 3. The rational function F(y) which closely approximates

$$Q_2(y) = \left(y + \frac{1}{nyK_0(y)I_0(y)}\right)K_1\left(y + \frac{1}{nyK_0(y)I_0(y)}\right)I_0(y) + yI_1(y)K_0(y)$$

with n = 3 is $F(y) = \dfrac{by}{c+y}$ for b = .765 and c = .059 (see Figure 12). As in Model I,

$\lim_{y\to\infty} Q_2(y) = 1$. This guarantees a CSD for all n > 1.

The explicit formula for y from $\dfrac{by}{c+y} \le 1 - \dfrac{1}{n}$ is

$$y \le y_c = \frac{c - cn}{n - 1 - bn} . \qquad (18)$$

(In Table 3 where the $(\alpha\delta_c)_g$ values from the graph show none, the entire graph lay above 1-1/n). Table 4 shows values for αR_c found in like manner as Model I.

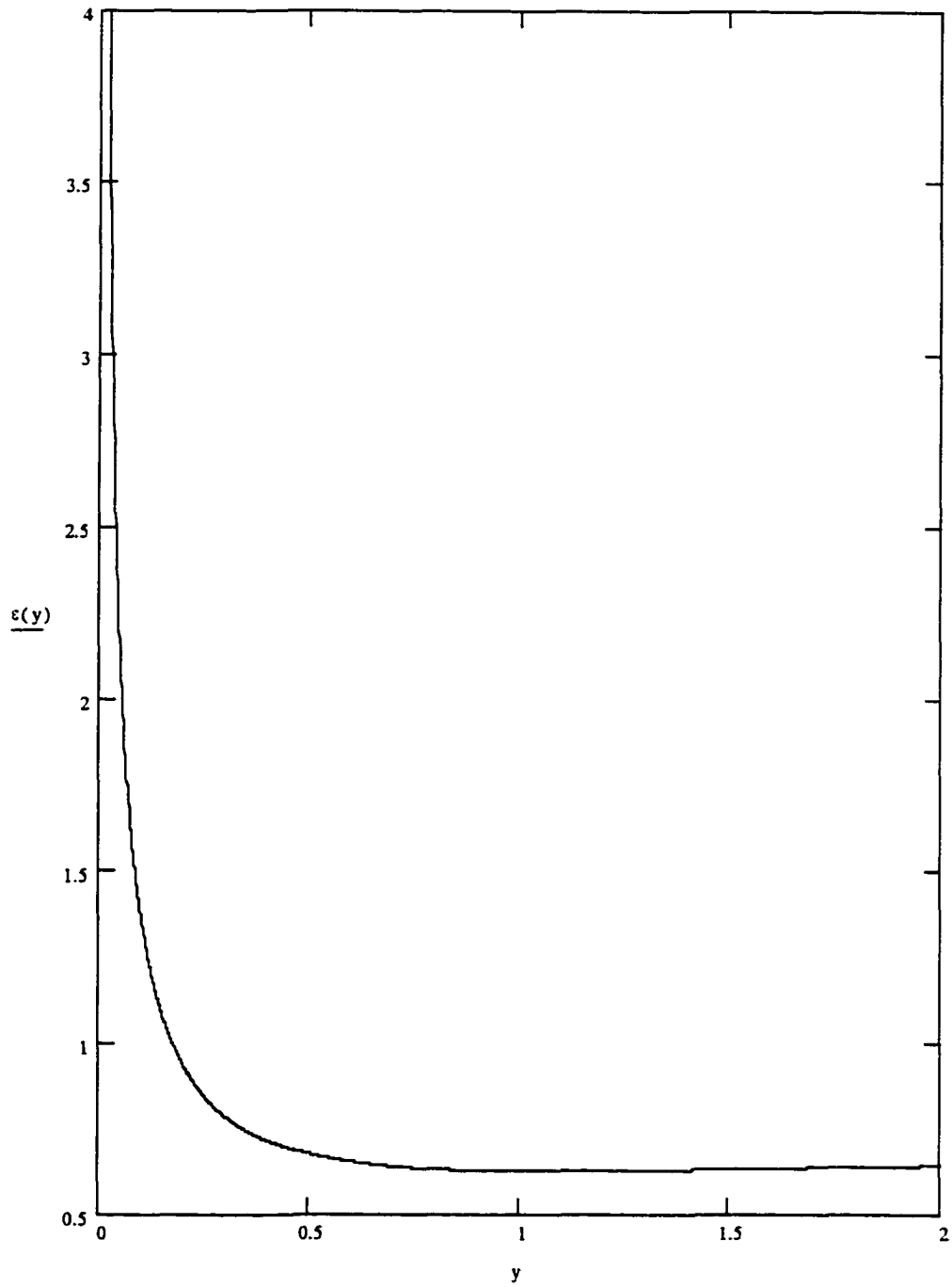

Figure 10: This is the graph of $\epsilon_c(y)$, which represents the δ region of the wound, for $n = 3$.

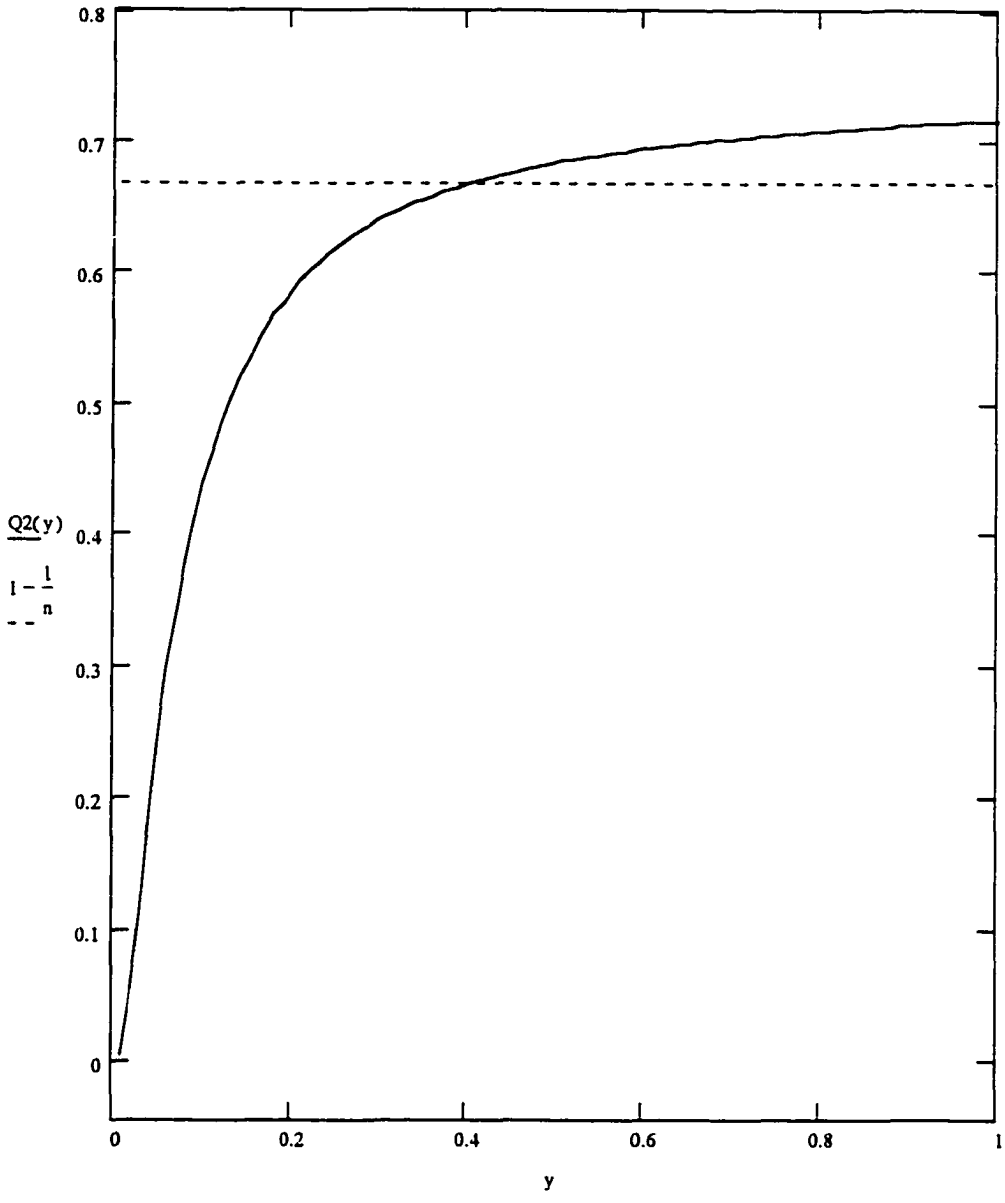

Figure 11: The graph of $Q_2(y)$ for n = 3 which shows the existence of a CSD.

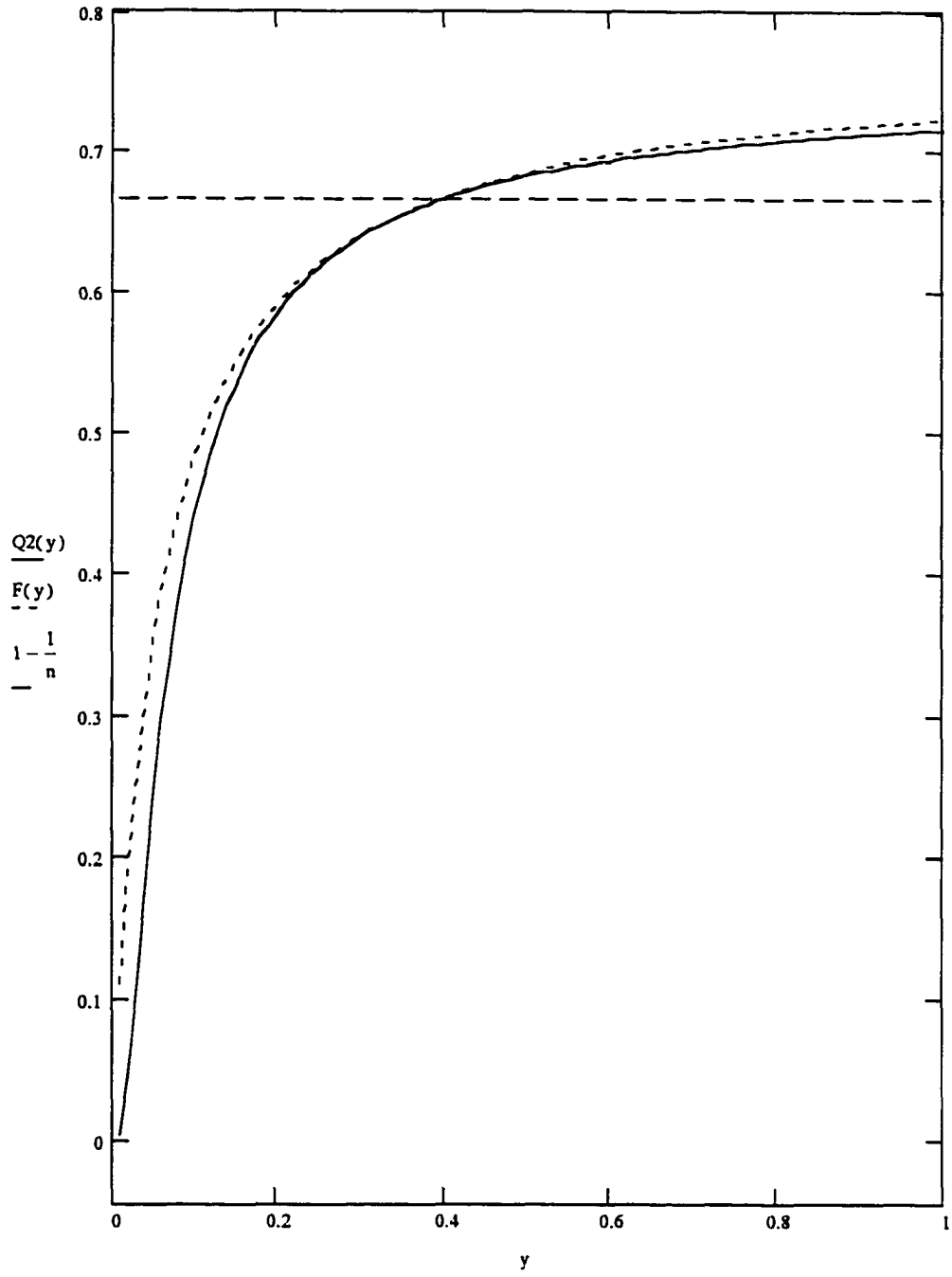

Figure 12: The graph of Figure 11 and its rational approximation function F(y). For this graph n = 3, b = .765, and c = .059.

Table 3. For various values of n and αR, a comparison is made between the approximation for the $\alpha\delta_c$ region and the values found on the graph of $Q(\alpha\delta_c)$.

n	$1-\frac{1}{n}$	αR	$\alpha\delta_c$	$(\alpha\delta_c)_g$	$(\alpha\delta_c)_g - \alpha\delta_c$
1.5	.333	1	1.251	2.58	1.329
1.5	.333	3	1.611	none	
1.5	.333	5	1.326	none	
1.5	.333	7	1.330	none	
1.5	.333	10	1.332	none	
1.5	.333	20	1.333	none	
5.0	.8	1	.3750	.4	.025
5.0	.8	3	.3930	.47	.077
5.0	.8	5	.3980	.49	.092
5.0	.8	7	.3990	.5	.101
5.0	.8	10	.3990	.5	.101
5.0	.8	20	.3990	.5	.101
8.0	.875	1	.2340	.25	.016
8.0	.875	3	.2460	.27	.024
8.0	.875	5	.2490	.28	.031
8.0	.875	7	.2490	.28	.031
8.0	.875	10	.2500	.28	.230
8.0	.875	20	.2500	.29	.040

Table 4. For various values of n, αR_c values are found.

n	$1-\frac{1}{n}$	$(\alpha R_c)_g$	αR_c	b	c
1.1	.091	.116	.072	.597	.4
1.5	.333	.237	.240	.639	.22
3.0	.667	.4	.398	.765	.059
5.0	.800	.480	.466	.845	.026
8.0	.875	.51	.543	.899	.015
10	.900	.53	.585	.909	.006
20	.950	.56	.598	.952	.0015

THE THREE-DIMENSIONAL MODEL

This simple three-dimensional model of wound healing extends earlier work [1] and [2] to three-dimensional spherical geometry, i.e. the case of the entire removal of a spherical portion of bone. However, assuming uniform GF concentration emanating from the wound margins, we will assume an entire sphere in our efforts to find the critical radius beyond which no healing occurs.

As before the time-development of the wound is not addressed. We examine the wound size under which full bone regeneration does not occur under the assumption of diffusive equilibrium (as explained earlier). Thus, in this model we assume the existence of a thin spherical shell of width δ which influences and directs the growth hormone activity up to the wound edge. In the discussion that follows, C(r,t) represents the concentration (i.e. molecules/unit volume) of a generic growth stimulating factor, where $R \leq r < \infty$. R is the wound radius, and t is time, both in appropriate units.

BASIC CONFIGURATIONS:

Centered at the origin a wound sphere of radius R is removed . As indicated earlier we suppose that a generic "growth factor" (GF) is produced as a result of the trauma to the system, and it is the distribution of this growth factor that determines whether or not wound healing occurs in this model.

The differential equation describing the space and time distribution of the growth factor concentration C(r,t) is

$$D\frac{1}{r^2}\frac{d}{dr}\left(r^2\frac{dC}{dr}\right) - \lambda C = -PS(r) \qquad (19)$$

where D, λ, and P are respectively the diffusion coefficient for the GF in the tissue, the decay or depletion rate of the GF, and the production rate of GF by the enhanced mitotically active cells in the vicinity of the wound edges. These are assumed to be constant. As before, S(r) is the source term describing the distribution of GF production throughout the active tissue, assumed to be uniform; thus

$$S(r) = 1 \quad \text{for } R \le r \le R + \delta$$

$$S(r) = 0 \quad \text{elsewhere,}$$

δ being the width of the active layer.

In equation (19), the time rate of change of GF concentration is not included because we are invoking the diffusive equilibrium approximation; full details and the justification for this can be found in [1]. The first term describes the spatial change due to diffusion, and the second term is the depletion or decay rate of GF as it interacts with the system as a whole, and is changed or removed.

EQUATIONS AND SOLUTIONS:

If $\alpha^2 = \frac{\lambda}{D}$ then equation (19) can be written as:

$$\frac{d^2C(r)}{dr^2} + \frac{2}{r}\frac{dC(r)}{dr} - \alpha^2 C(r) = \frac{-P}{D}S(r) \quad . \qquad (20)$$

The boundary conditions are:

- $C(r)$ and $\frac{dC(r)}{dr}$ are both continuous at $R + \delta$
- $\lim_{r \to \infty} C(r) = 0$
- $\frac{dC(r)}{dr} = 0$ at $r = R$

Writing $C(r) = Y(r)r^{-1}$, equation (20) simplifies to

$$\frac{d^2Y(r)}{dr^2} - \alpha^2 Y(r) = \frac{-P}{D} S(r) \tag{21}$$

The homogeneous solutions can be written in terms of hyperbolic function, i.e.

$$C(r) = A\frac{\sinh(\alpha r)}{r} + B\frac{\cosh(\alpha r)}{r} + \frac{P}{\lambda} \quad \text{for } R \le r \le R + \delta \tag{22}$$

where

$$A = \frac{\sinh(\alpha(R+\delta)) - \cosh(\alpha(R+\delta))(\alpha(R+\delta)+1)}{\alpha(1-\Delta)}$$

with $\Delta = \frac{\alpha R\cosh(\alpha R) - \sinh(\alpha R)}{\alpha R\sinh(\alpha R) - \cosh(\alpha R)}$ and $B = -\Delta A$. Also,

$$C(r) = F\frac{\sinh(\alpha R)}{r} + G\frac{\cosh(\alpha R)}{r} \tag{23}$$

for $r > R + \delta$ where,

$$F = \frac{-P}{\lambda}\left[\frac{\cosh(\alpha(R+\delta))(\alpha(R+\delta)+\Delta) - \sinh(\alpha(R+\delta))(\alpha(R+\delta)\Delta + 1)}{\alpha(1-\Delta)}\right]$$

and $G = -F$.

For the parameter values $P,\lambda = 1$, $\alpha R = 2$, and $\alpha\delta = .5$ the graph of $C(r)$ is shown in Figure 13. (C1(r1) represents equation (23)).

Using equation (22), we apply the criterion that $C(R) \geq \theta$ where θ represents a threshold value above which wound healing will occur for values of r satisfying this condition. For $n = \frac{\theta\lambda}{P}$, and using the non-dimensionalized variables $y = \alpha R$ and

$\epsilon = \alpha\delta$, the resulting equation is

$$\frac{[\cosh(y+\varepsilon) - \sinh(y+\varepsilon)](y+\varepsilon+1)}{(y+\varepsilon)[\sinh(y) - \cosh(y)]} \geq \frac{\theta\lambda}{P} - 1 = \frac{1}{n} - 1 \tag{24}$$

which simplifies to

$$Q_1(\varepsilon) = e^{-\varepsilon}\left[\frac{y+\varepsilon+1}{y+1}\right] \leq 1 - \frac{1}{n} \tag{25}$$

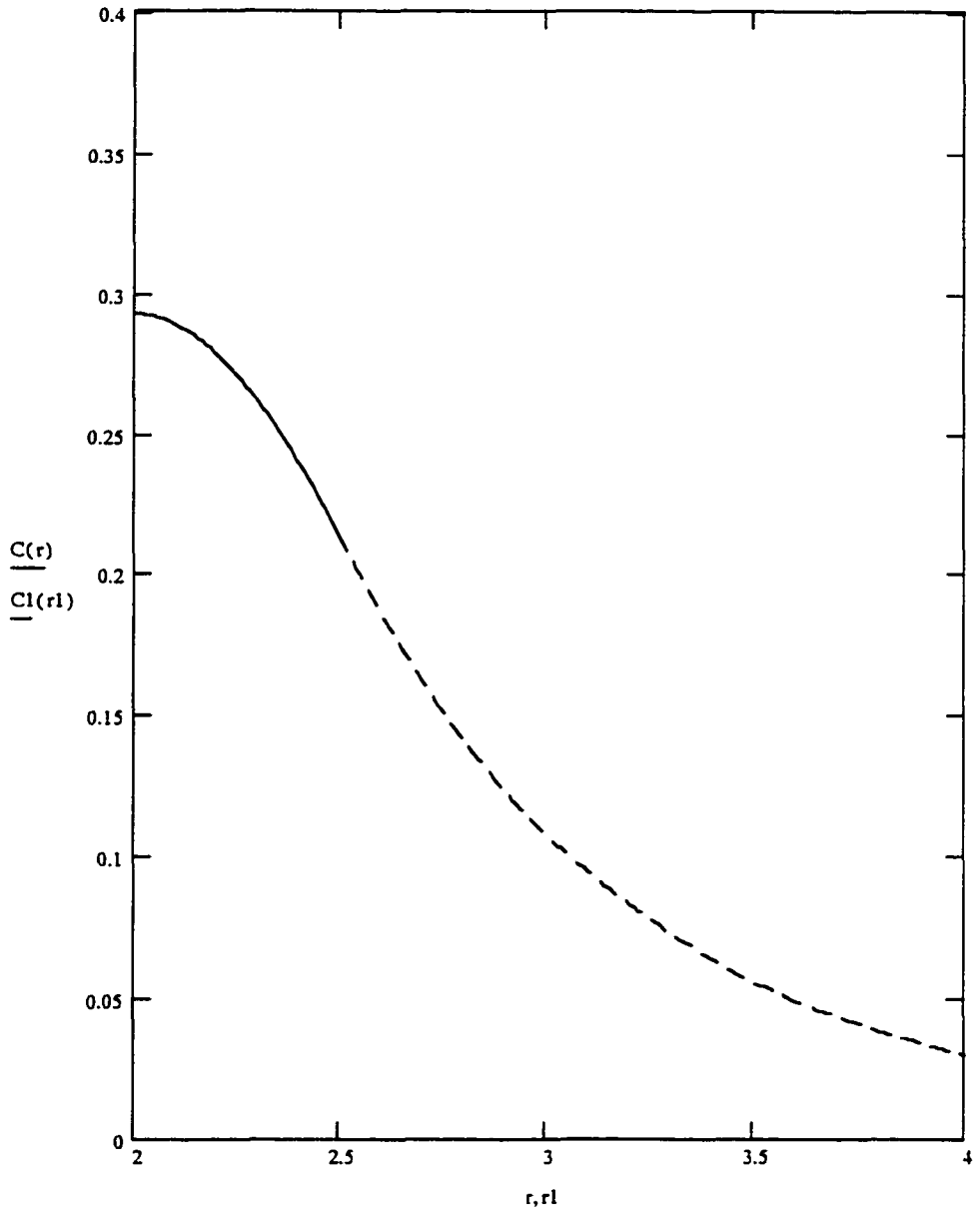

Figure 13: The Growth Factor Concentration C(r), for parameter values P, λ =1, $\alpha R = 2$ and $\alpha\delta = .5$. C(r) is defined over $[R, R + \delta]$ and C1(r1) is defined over $[R + \delta, \infty]$.

whose graph is given in Figure 14 for the values y = .5 and n = 3.

Approximating $e^{-\varepsilon}$ to $O(\varepsilon^1)$ results in the inequality

$$\varepsilon \geq \varepsilon_c = \frac{y+1}{ny} \quad . \tag{26}$$

The graph of $\epsilon_c(y)$ is given in Figure 15 for n = 3.

Note that if $\epsilon = \alpha\delta_c$ satisfies inequality (25), i.e. $Q_1(\epsilon) \leq 1 - \frac{1}{n}$, then $\epsilon \geq \epsilon_c$

satisfies $Q(\epsilon) \leq 1 - \frac{1}{n}$. This follows despite the fact that $e^{-\epsilon}$ is monotone decreasing in

ϵ while $\frac{y+\varepsilon+1}{1+y}$ is monotone increasing in ϵ. The derivative of $e^{-\epsilon}\left[\frac{y+\varepsilon+1}{1+y}\right]$ is

$-(y+\varepsilon)\frac{e^{-\varepsilon}}{1+y}$, hence $e^{-\epsilon}\left[\frac{y+\varepsilon+1}{1+y}\right]$ is monotone decreasing in ϵ. Thus $Q(\epsilon_c) \geq Q(\epsilon)$

since $\epsilon_c \leq \epsilon$.

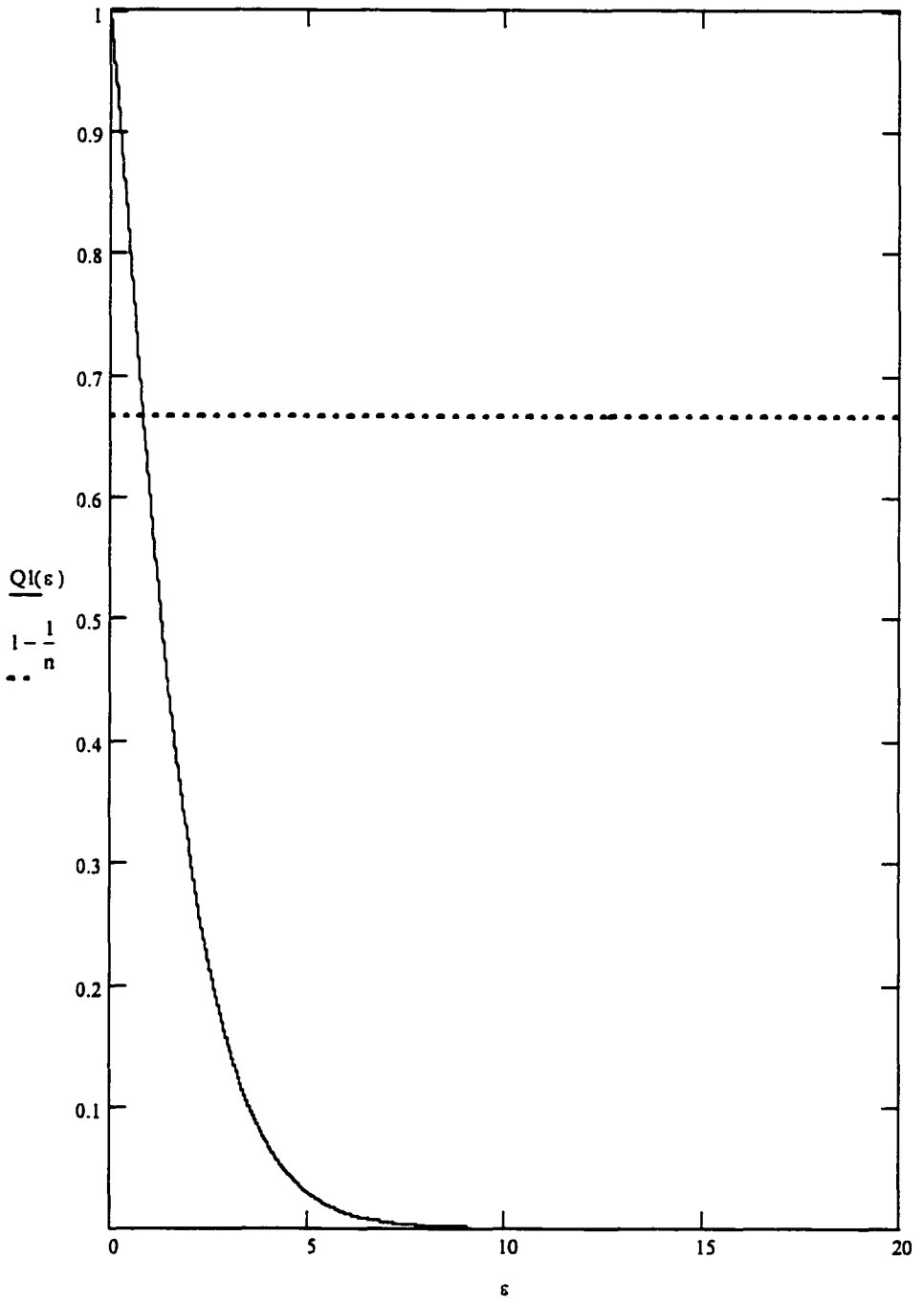

Figure 14: This is the graph of $Q_1(\epsilon)$. The parameter values used are y = .5 and n = 3.

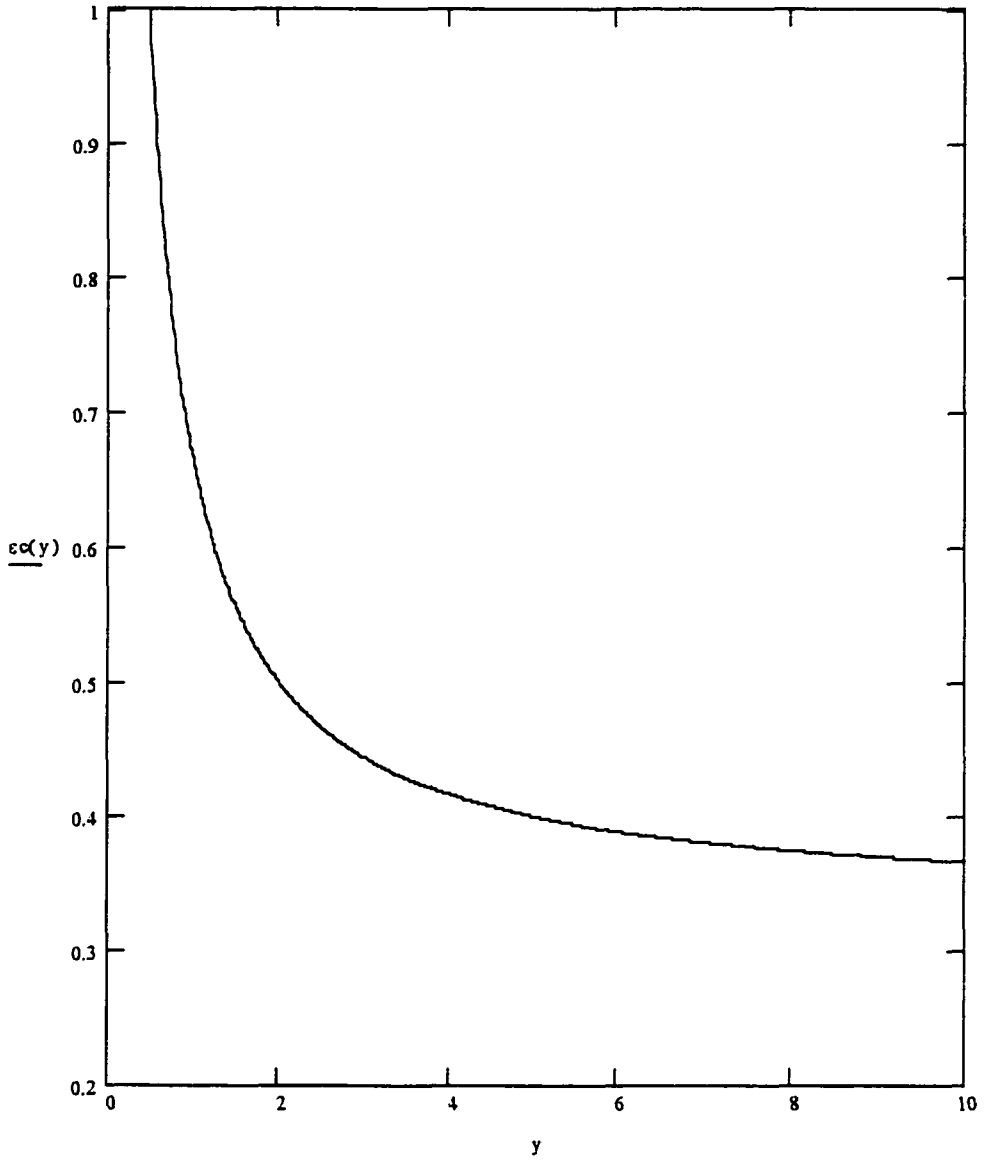

Figure 15: The graph of the approximation function $\epsilon_c(y)$. In this graph n = 3.

A comparison of the values from the graph of equation (25) referred to as $(\alpha\delta_c)_g$ (with no approximation except rounding) and the values from equation (26) referred to as $\alpha\delta_c$ are given in Table 5.

In Figure 16 the graph of $Q_2(y)$ is formed by replacing ϵ in equation (25) with the approximation for ϵ_c given in equation (26). The parameter value used for Figure 16 is n = 3.

Using this value of ϵ_c, a representative for αR_c (which is yc) can be sought. Using equation (26). We can write

$$Q_2(y) = e^{-\frac{y+1}{ny}}\left[1+\frac{1}{ny}\right] \le 1-\frac{1}{n} \quad . \tag{27}$$

Approximating $e^{-\epsilon}$ to $O(\epsilon^3)$ and substituting $\frac{y+1}{ny}$ from equation (26), resulted in the rational expression

$$F(y) = \frac{(y+1)[(3n^2-n)y^3+(3n^2+n-1)y^2+(2n-2)y-1}{6y^4n^4} \le 0 \tag{28}$$

whose positive solution is

$$y \le y_c = \frac{\frac{-2(n-1)}{3a_1}+\left(\frac{a_2}{3a_1}\right)^2}{A^{\frac{1}{3}}} + A^{\frac{1}{3}} - \frac{a_2}{3a_1} \tag{29}$$

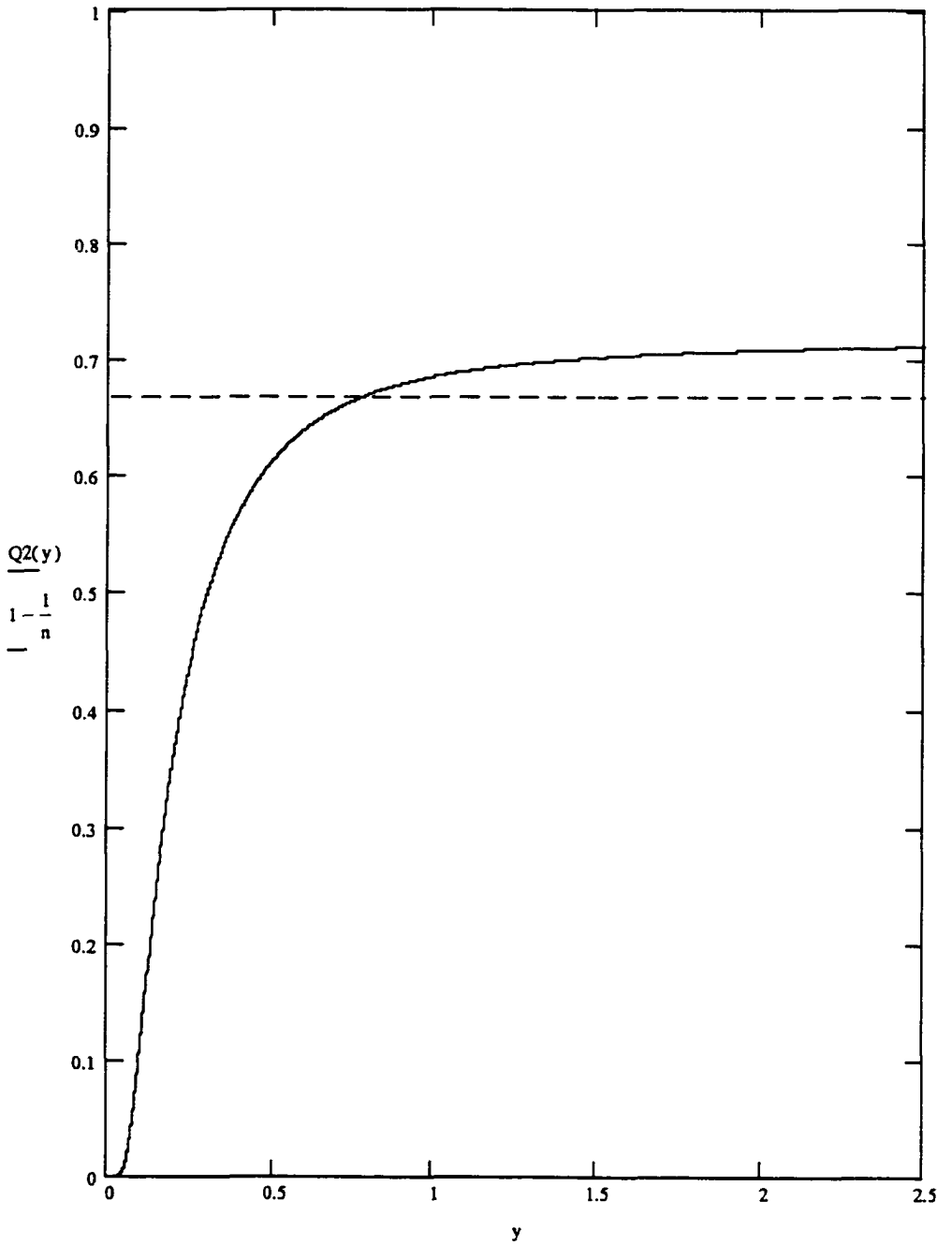

Figure 16: The graph of $Q_2(y)$ for n = 3 showing the existence of a CSD.

Table 5. A comparison is made between the approximation for the $\alpha\delta_c$ region and the values found on the graph of $Q(\alpha\delta_c)$ for various values of n and αR.

n	1 - 1/n	αR	$\alpha\delta_c$	$(\alpha\delta_c)_g$	$(\alpha\delta_c)_g - \alpha\delta_c$
1.5	.3	1	1.333	1.72	.39
1.5	.3	3	0.889	1.41	.53
1.5	.3	5	0.800	1.35	.55
1.5	.3	7	0.762	1.23	.47
1.5	.3	10	0.733	1.20	.47
1.5	.3	20	0.700	1.23	.53
5.0	.8	1	0.400	.410	.01
5.0	.8	3	0.300	.310	.01
5.0	.8	5	0.240	.250	.01
5.0	.8	7	0.229	.250	.021
5.0	.8	10	0.220	.240	.02
5.0	.8	20	0.210	.230	.02
8.0	.9	1	0.250	.252	.002
8.0	.9	3	0.166	.177	.011
8.0	.9	5	0.150	.160	.001
8.0	.9	7	0.143	.152	.009
8.0	.9	10	0.137	.140	.0105
8.0	.9	20	0.131	.140	.009

where $a_1 = 3n^2 - n$; $a_2 = n - 3n^2 - 1$; $a_3 = 24n^4 - 80n^3 + 165n^2 - 42n + 5$

and $$A = \frac{2(n-1)a_2}{6a_1^2} + \frac{1}{2a_1} - \left(\frac{a_2}{3a_1}\right)^3 + \frac{\sqrt{a_3}}{6n(3n-1)^2}.$$

(See Appendix B for a detailed explanation of the choice of $O(\epsilon^3)$.)

The two graphs, $Q_2(y)$ and $F(y)$ are shown in Figure17. The graph of $F(y)$ reveals only one positive y value at $1 - \frac{1}{n}$. The parameter value used was n = 3.

Some additional comparisons are given in Table 6. Since $\lim_{y\to\infty} Q_2(y) = e^{\frac{-1}{n}}$ and

$\lim_{n\to\infty} e^{\frac{-1}{n}} = 1$, it follows that $Q_2(y)$ will always intersect $1 - \frac{1}{n}$, for all $n > 1$, and thus

there will always exist a CSD. This follows from the fact that $e^{\frac{-1}{n}} \geq 1 - \frac{1}{n}$ for $n > 1$.

Table 6. For various values of n, αR_c values are found by graphical and approximation methods.

n	1 - 1/n	$(\alpha R_c)_g$	(αR_c)
1.1	.091	.32	1.515
1.5	.333	.54	1.167
3.0	.667	.78	.909
5.0	.800	.86	.905
8.0	.875	.92	.93
10	.900	.93	.941
15	.933	.96	.959
20	.950	.96	.969

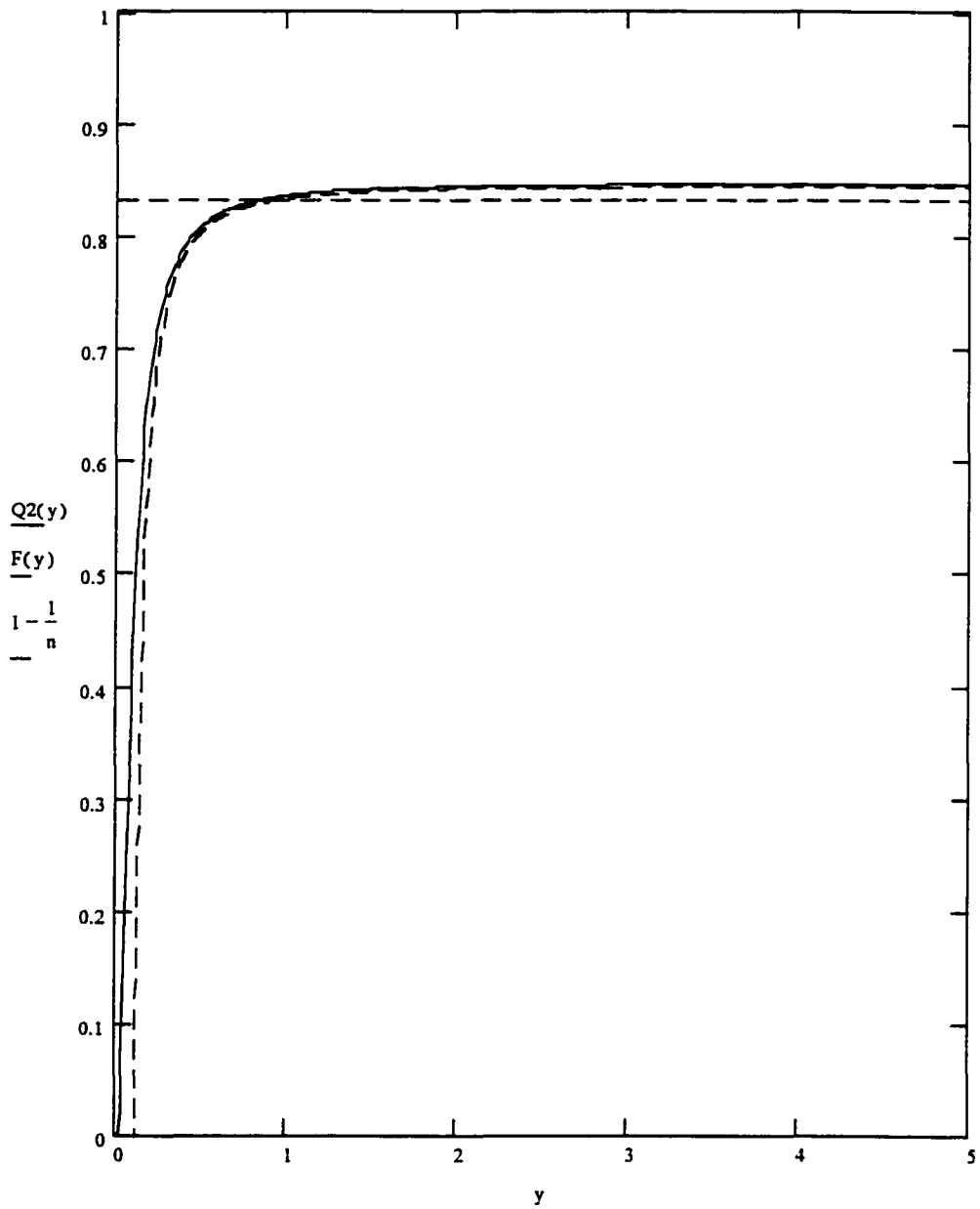

Figure 17: This shows the comparison of $Q_2(y)$ and the approximation function F(y) for n = 6.

CHAPTER III

PARAMETER ESTIMATES

Some reasonable values for the parameters P, λ, θ were found in [1] to be as follows: $\lambda = 1.6 \times 10^{-5}$ sec^{-1} (based on Sherratt and Murray's [24, 25] work that the estimated half-life of chemical decay is about 12 hours and thus, $\lambda = \frac{\ln 2}{12}$ hr^{-1} which yields the preceding value). The value for D, the diffusion parameter, depends on the particular GF or enzyme in general and the medium in which it is diffusing. The higher the molecular weight, the smaller is D. However some indication of this can be found by considering the diffusion of oxygen and sucrose in water. At a temperature of 25°C, D $\approx 2.4 \times 10^{-5}$ cm^2 sec^{-1}, while for sucrose at 20°C, D $\approx 4.6 \times 10^{-6}$ cm^2 sec^{-1} [8]. Sheratt and Murray [24, 25] carried out a best fit analysis from data on epidermal wound healing and estimated that for epidermal GF, D $\approx 3.1 \times 10^{-7}$ cm^2 sec^{-1}, which is considerably smaller because of the high molecular weight (about 6000, see Ruddon [22]). In their papers they also considered growth inhibitors, for which D $\approx 2.4 \times 10^{-5}$ cm^2 sec^{-1}. Thus it seems not unreasonable to take a value of D $\approx 5 \times 10^{-7}$ cm^2 sec^{-1} for GF [1,2].

In earlier work [1] a value for α was estimated from entirely phenomenological considerations for illustrative purposes. The basis for this estimate was soft tissue data, and yielded $\alpha \approx 6$ cm^{-1}. Clearly the CSD phenomenon is confined to bone, and it is reasonable to ask what range of α-values might be appropriate. Since $\alpha = \sqrt{\frac{\lambda}{D}}$ this is

equivalent to asking how both λ and D change from soft to hard tissue environments. Unfortunately, this data, if known at all, is difficult to come by. The best that can be done at this stage is to make some plausible estimates of their orders of magnitude.

Diffusion processes alone will not suffice in bone to provide nourishment for the osteocytes, but capillaries are never far away: the osteocytes are arranged around central capillaries in concentric layers, which form spindle-shaped units known as osteons. Thus pure diffusion is facilitated by the efficient capillary transport system, and we might expect that the effective diffusion coefficient is enhanced compared with the standard value used in [1] (at least for growth factors of the same molecular weight). Concerning the decay coefficient λ it is even harder to speculate. Given the increased average density of bone compared with soft tissue, the effective decay of GF *may* be hindered somewhat (i.e. λ reduced). It is difficult to be more precise at this stage, but again, for the purposes of illustration, we suppose that, compared with the values used in [1], λ is halved and D is increased by a factor of five. Thus we take $\lambda \approx 8 \times 10^{-6}$ sec^{-1} and $D \approx 2.5 \times 10^{-6}$ cm^2 sec^{-1}. This results in a value of $\alpha \approx 1.8$ cm^{-1} It can be seen from column 4 in Table 2 and 4 in this chapter that the dimensionless quantity αR_c ranges from about 0.04 to 0.37; for the above value of α this corresponds to R_c in the range 0.8 mm to 7.4 mm which is certainly of the right order of magnitude for the lower end of the CSD sizes quoted above corresponding to a diameter range of 1 mm - 1 cm. Similarly, for the three-dimensional case, the values of αR_c from Table 6 column 3 range in value from .32 to .96. Using the value 1.8 for α,, R_c ranges from .18 cm to .53 cm or diameter range of 3.6 mm to 10.6 mm. It must be emphasized however that our values for α are only as

valid as the values for λ and D, and these are estimated. Clearly, quantitative validation of the consistency of the models in this chapter must await measurement of these parameters based on experimental data.

CHAPTER IV

RELEVANT EXPERIMENTAL DETAILS

According to Frame, [12] bony healing was studied in skull cavities with diameters of 5, 10, 15, and 20 mm on a crossbreed rabbit of New Zealand reds and half lops. The age of the rabbits used ranged from 6 to 10 months. Weights of the rabbits were between 3 to 4.8 kg. The rabbits underwent a surgical procedure, where using a dental handpiece called a trephine, a spherical hole was removed from the skull of the rabbits. Four groups were formed with four animals in each group. The group was determined by the diameter of the wound (i.e. 5, 10, 15, and 20 mm diameters). The animals recovered without problems from their operation. The experimenters were not concerned with the rate of healing, but whether bony bridging of the defect would occur. Only one time interval of 24 weeks was chosen, after which the animals were killed and their skull removed. The 5 mm holes were filled with new bone that bridged the gap, with loss of definition of the original margin. In some, the new bone was the same thickness as the adjacent skull. Marrow spaces were present in the new bone. The 10 mm group had bone filled cavities and only a few uncalcified areas. The new bone formed at the margins was thinner than the adjacent skull, and several isolated spicules were present. The bony bridge was incomplete in places, the gaps being filled with a layer of dense fibroconnective tissue. Marrow spaces were seen. The 15 mm group had ill defined growth. New bone had formed at the periphery and on isolated islands. The

new bone was thinner at the margins than the surrounding skull. Fibrous connective tissue filled the gap and some spaces were filled with marrow. In the 20 mm group, all specimens showed no bony bridging and a central uncalcified area. Some bone had formed at the margins, and as isolated islands. They concluded that the most suitable size of osseous defect was the 15 mm diameter. Another four rabbits with 15 mm defects were followed up after 36 weeks and compared with the 24 week group. The result was very similar. New bone had formed mainly at the margins of the defect, often as isolated islands, and the gap was filled with dense fibrous tissue. Radiographs showed no significant amount of new growth formed.

Another experiment using the trephine in the Rhesus monkey was detailed in Ferguson et all [9]. Cranial defects measuring 14 - 20 mm in diameter were created in Rhesus monkeys. In the experiment, there was one control defect and one experimental defect. The control defect was implanted with bovine serum albumin (BSA), and the experimental defect was implanted with 100 - 200 mg of a partially purified bovine bone morphogenetic protein (bBMP). After 16 weeks, the control defect consistently showed only fibrous connective tissue in the wound, while the BMP defect had progressive growth of new bone which filled the defect. Hollinger et al [16] also did experiments with bony repair materials on 15 mm baboon calvaria. They invaded the control sites after 2 months to find bone being made althought not completely healed. Hollinger concluded that this was not necessarily a CSD since a longer interval than 2 months might have showed different results.

Prolo et al [21] found 20-mm defects in the calvaria of mongrel dogs. Urist [29]

agrees with this finding. Pigs have been used in some studies [16]. Lange et al [18] used a volume defect of 6, 8, and 12-cc size in the femora of adult formed pigs. There were two groups, a control group and a group whose defect was filled with tricalcium phosphate. After 9 months, the defect had healed but with only half the amount of bone as the group that had the tricalcium phosphate.

The one group for which their is little data is humans. According to Hollinger et al [16], a German group is trying to incorporate humans in the testing of bone repair materials. Hollinger sites that neurosurgeons routinely make defects when entering the skull. Either the defect is left alone, or a bone repair material, such as ceramic or plastics is used to fill the space, - no bony healing occurs in this case. Prolo et al [20] showed that freeze-dried allograft plugs aided the hole in filling with new bone. In this article no data was given on the size of the defect. However, reference was made to the tooth socket as being a possible place to test bony repair materials. This gives us an idea of the size and shape of the defect which could be under consideration. Thus a laterial incisor (an average size tooth) when extracted would leave a hole approximately .32 cm with a diameter of roughly .75cm.

Many experiments on wound healing have been done on rats, rabbits, and dogs, but not much literature has been written on experiments for monkeys or humans. From the literature which we do have, the wound was created in the calvaria, which is the bony part of the cranium from the base of the skull to the forehead. In [21], Prolo implies that humans do not react the same as other animals to calvaria wounds because of a poorer blood supply in the calvaria and some deficiency of bone marrow. This

seems to imply that the experiments on the lower mammals may not extend in the same manner to humans. Freeman and Turnbull [13, 28] were the first to attempt the study of CSD's in rat calvaria. In a 500 mg Wilstar albino rat they studied a 2 mm-diameter CSD, which failed to heal in 12 weeks. Mulliken and Glowacki [19] and Glowacki et al [15] found 4 mm-diameter to be the CSD in young (28 days old) Charles River rats. Tagaki and Urist [26] found 8 mm-diameter to be the CSD in 6 month old Sprague-Dawley rats. It did reduce to 5 mm-diameter in four weeks, but no further healing was noticed at the end of 12 weeks. Kramer et al [17] experimented on the calvaria of 6 to 10 pound New Zealand White rabbits. They found 8 mm-diameter CSD's occurred at various periods up to 16 weeks. Frame [12] worked with a crossbreed of New Zealand White and Half Lop rabbits. He made 5, 10, 15, and 20 mm-diameter wounds in the calvaria of these 6.6 to 10.5 pound rabbits. At 24 and 36 weeks, the 15 mm-diameter wound had created the fibrous connective tissue but continued to retain a central uncalcified area. Friedenberg and Lawrence [14] described the wound healing experiments with mongrel dogs. A 17 mm-diameter had less than 40% osseous repair at 20 weeks. Prolo et al [21] found that a 20 mm-diameter in mongrel dogs healed 20% by 6 months. Urist [29] also suggested that 20 mm-diameter was a reasonable CSD in dogs. These experiments show us that there is a critical size defect, in the general range of 2 mm - 2 cm. A summary of the experiments is given in Table 7.

Table 7. Summary of research experiments on Critical Size Defect taken in part from Schmitz and Hollinger [23].

ANIMAL	Weight of Animal	Estimated CSD	Time Interval of Study
Rat calvaria	500 mg	8 mm	9-12 weeks
Rabbit calvaria	8 lbs	15 mm	24 weeks
Dog calvaria	60 lbs	20 mm	24 weeks
Dog mandible		greater than 20 mm	24 weeks
Monkey calvaria		20 mm suggested	??????
Monkey mandible		greater than 20 mm suggested	??????

CHAPTER V

CONCLUSIONS ON WOUND HEALING

When a bone wound occurs, the body produces electrical signals that stimulate growth hormones in the bone. These growth hormones, which we have called growth factors, trigger the natural healing process. For reasons which are poorly understood, sometimes bone wounds fail to heal properly. Our mathematical model demonstrates why this may occur. Obviously there are many factors affecting these nonunions, but one observation relating to human subjects is that older subjects may not heal as well as younger subjects because older subjects may have other health challenges, which complicate the healing process [5]. The mathematical model indicates that there exists a lower bound value for the width of the growth hormone region, and if that width is no less than this value then the GF concentration is such that healing may ensue. This by itself does not ensure complete healing, but that some healing will occur. In this model we have shown the dependence of the GF region on the original size of the wound. This region is limited in size by the calvaria of the animal available to stimulate the GF region. Large wounds may not have enough GF to stimulate complete healing, (i.e. $C(R) < \theta$). It may also be the case that due to the long time interval (several weeks to years) needed to complete the healing process, the GF region may not be stimulated adequately. According to both models I and II, sufficiently large wounds do not have enough GF in proximity to the wound center and to the edge to stimulate and maintain healing growth,

and thus complete the healing process. This creates the CSD.

CHAPTER VI

TUMOR IMMUNITY

In these next two chapters the focus is shifted to an analysis of some simplified models of cancer growth and the part the immune system plays in inhibiting that growth.

THE SCIENCE OF IMMUNOLOGY

The word immunity originally meant that an individual was free from infection. At present the science of Immunology encompasses such a broad area that sub-classifications such as tumor immunity, transplantation immunity, clinical immunology, autoimmunity and immunohematology are commonly used. In this paper, the focus is on tumor immunity i.e. how the immune system responds to tumor invasion.

HOW THE IMMUNE SYSTEM WORKS

In the paper *The Immune System-How It Works,* published by the National Institute of Health and the National Cancer Institute [32], it is pointed out that the organs of the immune system consist of not only the white blood cells, located in the bone marrow, but also the lymphoid organs such as, the tonsils and adenoids, the thymus where lymphocytes (small white blood cells) known as T cells mature, the spleen, the appendix, the lymph nodes located in the neck, armpits, abdomen and groin, and lymphatic vessels (similar to blood vessels). The immune system stockpiles, in the

various above locations, larger groups of lymphocytes and also cell-devouring phagocytes. In order to have enough room for all the cells needed to attack the million or so types of enemy cells, the immune system stores just a few of each kind. When an antigen (any cell which triggers an immune response) appears, those few matching cells replicate until their job is done.

According to the U.S. Department of Health and Human Services publication on *Immunology And Its Role In Disease And Health* [31], the immune system is very complex. There is strong evidence that effector cells or lymphocytes (small white cells that are normally present in the blood and in lymphoid tissue) react not only against established tumors but that they play a major role in eliminating many tumors before they are able to get established. The lymphocytes eliminate thousands of cells daily which have undergone mutation within our bodies. Why then do individuals develop cancer? One answer may be that while the lymphocytes are there and able to destroy tumor cells, cancer patients have within their blood elements called "blocking factors" which contain antibodies containing tiny fragments of the tumor cell. Thus the patient has two competing forces at work: the lymphocytes which have the ability to kill the cancer tumor and blocking factors which prevent the lymphocytes from doing their job.

In the book *Genes And The Biology of Cancer* [35], the statement is made that "Cancer is a single disease and it is a hundred diseases. The unifying aspect of cancer is uncontrolled growth - the appearance of disorganized tissues that expands without limit, compromising the function of organs and threatening the life of the organism". Different types of cells can produce different types of cancer with their own growth rate. In I

Immunology [31], it states that research shows it is possible for the immunological system of a mouse to destroy millions of tumor cells in less than 48 hours. Thus, the more tumor cells present, the more expeditious the destruction process. A similar example in humans is the swiftness with which multiple warts on the hands or feet vanish once one of the warts is successfully attacked.

WHY DOES THE IMMUNE SYSTEM SOMETIMES FAIL TO PREVENT CANCER?

There are several possibilities which may prevent the immune system from completely assaulting tumor cells in humans. According to Immunology [31] they are:

- Blocking antibodies or antibody antigen complexes in serum prevent the lymphocytes from bombarding the tumor. (An antigen is any substance which provokes an immune response when introduced into tissue. Antibodies recognize antigens through surface characteristics of the foreign substance, especially by the electric charge, or by the pattern or shape. To unite with the antigen, the antibody must be exactly the right kind or specific - a term referring to the selective reaction which occurs between an antigen and its corresponding antibody or lymphocyte.)
- The patient with an antigenic tumor does not have the applicable immune response genes, i.e. he lacks the genetic capacity to react against his own tumor antigens.
- The tumor liberates substances (e.g., viruses or enzymes) which interfere with

the immunological system.

- The patient has made the wrong kind of immune response, i.e. a humoral response (production of antibody molecules which bind the foreign substance) instead of a cellular response (mobilizing cells which can specifically react with and destroy the invader).
- The patient may be unable to mobilize his effector cells, so that they remain locked up or sequestered in the lymphoid organs, never reaching the cancer site.
- The patient may be tolerant to the tumor antigen.

Experimental evidence is available to support each of these possibilities and it is suspected that each of these factors may be acting within the patient to different degrees.

THE MATHEMATICAL MODEL

Following Edelstein-Keshet [8], we utilize a one-dimensional reaction-diffusion partial differential equation to mimic the tumor/immune system interaction for our model, because populations of tumor cells are rarely distributed uniformly within their environment. Their motion, migration, and redistribution are of primary interest. Normally we assume a continuous function and distribution to depict discrete cells which leads to partial differential equation models that are similar to classical models for molecular diffusion.

Historically, biological models involving partial differential equations date back to the early 1900's with work done by K. Pearson and J. Blakeman. In the1930s R. A. Fisher applied partial differential equations to the spatial spread of genes and diseases.

Many partial differential equation models cannot be solved analytically in closed form. This is especially true of the nonlinear equations. A standard first approach is to reduce the problem to one that can be solved, generally by converting the partial differential equation to ordinary differential equations that describe some simpler situation. Two types of solutions are then possible: steady-state distributions and traveling waves.

The mathematical model under investigation is one based on a model in an entirely different context, namely the spruce-budworm model in ecology [39]. In this model we include both the tumor growth of cancer and the attack on the tumor by the immune system. Let us consider the one dimensional problem of a long narrow tube through which the cancer cell concentration C travels i.e. $[0,\infty]$. In Strogatz [39], the problem of the population dynamics for the spruce budworm has been analyzed from which we wish to adopt his findings to the cancer-immune problem. We will consider the partial differential equation

$$\frac{\partial C}{\partial t} = D\frac{\partial^2 C}{\partial x^2} + \alpha C\left(1 - \frac{C}{\beta}\right) - \frac{\gamma C^2}{\psi^2 + C^2} \tag{30}$$

where the first term is the time rate of change of cancer cell concentration C. The second term is the diffusion coefficient and spatial change. The third term is the logistic term representing cancer growth and the last term is the immune response term which models the destruction of cancer cells. The parameters α, β, represent the growth rate of the cancer cells, and the carrying capacity of the population respectively. The

parameter γ is the rate of mortality due to predation by the immune system, while Ψ represents the speed with which the immune system reaches its maximum rate of mortality. All of the parameters are positive. We will nondimensionalize equation (30) by letting $Y(x,t) = \frac{C(x,t)}{\psi}$ and dividing by γ. Thus,

$$\frac{\partial C}{\partial Y}\frac{\partial Y}{\partial t} = \psi \frac{\partial Y}{\partial t} \qquad \text{and} \qquad \psi \frac{\partial^2 Y}{\partial x^2} = \frac{\partial^2 C}{\partial x^2}$$

Substituting in (30) we obtain

$$\psi \frac{\partial Y}{\partial t} = D\psi \frac{\partial^2 Y}{\partial x^2} + \alpha \psi Y\left[1 - \frac{\psi Y}{\beta}\right] - \frac{\gamma Y^2 \psi^2}{\psi^2 + \psi^2 Y^2}$$

Dividing by γ yields

$$\frac{\psi}{\gamma}\frac{\partial Y}{\partial t} = D\frac{\psi}{\gamma}\frac{\partial^2 Y}{\partial x^2} + \alpha \frac{\psi}{\gamma} Y\left[1 - \frac{\psi Y}{\beta}\right] - \frac{Y^2}{1+Y^2} \tag{31}$$

Let $\tau = \frac{\gamma t}{\psi}$, $\overline{D} = D\frac{\psi}{\gamma}$, $\overline{\alpha} = \frac{\alpha\psi}{\gamma}$, and $\overline{\beta} = \frac{\beta}{\gamma}$

then (31) becomes

$$\frac{\partial Y}{\partial \tau} = \overline{D}\frac{\partial^2 Y}{\partial x^2} + \overline{\alpha} Y\left[1 - \frac{Y}{\overline{\beta}}\right] - \frac{Y^2}{1+Y^2} \tag{32}$$

Let $$g(Y) = \overline{\alpha} Y\left(1 - \frac{Y}{\overline{\beta}}\right) - \frac{Y^2}{1+Y^2} \tag{33}$$

In a first analysis we focus on g(Y). The idea in the first instance is to replace g(Y) by its linear Taylor approximation about each fixed point (or equilibrium point).

ANALYSIS OF THE FIXED POINTS

g(Y) has a fixed point at Y = 0 which is unstable because $g'(Y) > 0$ (see Figure 18). Intuitively the cancer population is so small that it seems non-threatening and so the cancer grows exponentially for Y near zero. $g(Y) = 0$ also yields either 3 or 1 real positive root upon solving the expanded and simplified version of equation (33), (see Figure 18), which is

$$\overline{\alpha} Y^3 - \overline{\alpha}\overline{\beta} Y^2 + (\overline{\alpha} + \overline{\beta})Y - \overline{\alpha}\overline{\beta} = 0 \,. \tag{34}$$

Let $k_0 = 0$, and k_i, for i = 1, 2, 3 be the possible 3 roots of equation (34). They are found to be

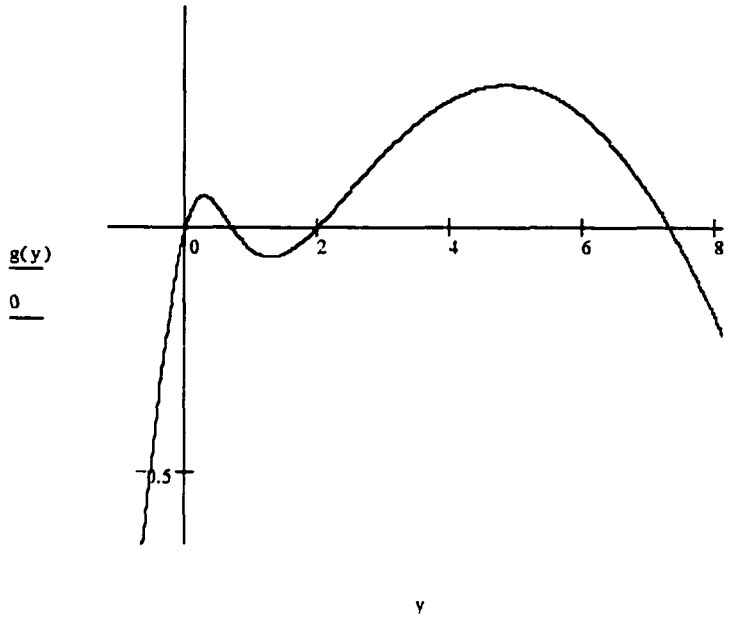

Figure18: This graph shows the four roots of g(Y). We can see that the derivative of g(Y) is positive at Y = 0 and at the second positive root which is the definition of unstable fixed points. In this figure $\bar{\alpha} = .5$ and $\bar{\beta} = 10$.

$$k_3 = P + \frac{1}{3}\bar{\beta}$$

$$k_1 = -.5\left[P - i\sqrt{3}\left(M + \frac{\frac{1}{3}\frac{(\bar{\alpha}+\bar{\beta})}{\bar{\alpha}} - \frac{1}{9}\bar{\beta}^2}{M}\right)\right] + \frac{1}{3}\bar{\beta}$$

and

$$k_2 = -.5\left[P + i\sqrt{3}\left(M + \frac{\frac{1}{3}\frac{(\bar{\alpha}+\bar{\beta})}{\bar{\alpha}} - \frac{1}{9}\bar{\beta}^2}{M}\right)\right] + \frac{1}{3}\bar{\beta} \quad , \text{ where}$$

$$N = \sqrt{4\bar{\alpha}^3 + 12\bar{\alpha}^2\bar{\beta} + 8\bar{\alpha}^3\bar{\beta}^2 + 12\bar{\alpha}\bar{\beta}^2 - 20\bar{\alpha}^2\bar{\beta}^3 + 4\bar{\alpha}^3\bar{\beta}^4 + 4\bar{\beta}^3 - \bar{\alpha}\bar{\beta}^4}$$

$$M = \left[\frac{-1}{6}\frac{(\bar{\alpha}+\bar{\beta})}{\bar{\alpha}}\bar{\beta} + \frac{1}{2}\bar{\beta} + \frac{1}{27}\bar{\beta}^3 + \frac{1}{18}N\frac{\sqrt{3}}{\bar{\alpha}^{\frac{3}{2}}}\right]^{\frac{1}{3}} \qquad \text{and}$$

$$P = M - \frac{\frac{1}{3}\frac{(\bar{\alpha}+\bar{\beta})}{\bar{\alpha}} - \frac{1}{9}\bar{\beta}^2}{M} \quad . \quad \text{For } g(Y) = \bar{\alpha}Y\left[1 - \frac{Y}{\bar{\beta}}\right] - \frac{Y^2}{1+Y^2},$$

$$g'(Y) = \frac{-2\bar{\alpha}}{\bar{\beta}}Y + \bar{\alpha} - \frac{2Y}{(1+Y^2)^2}. \quad \text{At } Y = 0 \text{ an approximation for } g(Y) \text{ using Taylor}$$

polynomials is $g'(0)(Y-0) = \bar{\alpha}Y$ and at each real root k_i, $g'(k_i)(Y-k_i)$ for $i = 1,2,3$ represents the other three approximations. If all three roots are real, we have two unstable fixed points and two stable fixed points, (see Figure 18). If we define the four

real roots as 0, k_1, k_2, and k_3 then according to Strogatz [39], k_2 and k_3 approach each other and eventually coalesce in a saddle-node bifurcation when $k_2 = k_3$. After the bifurcation, the only remaining fixed point is k_1 (in addition to 0 of course). Similarly k_1 and k_2 can collide and annihilate as $\overline{\alpha}$ is increased. Thus, for three positive fixed points, the smaller stable fixed point k_1 is called the refuge level of the budworm population or in our case the cancer population, while the larger stable point k_3 is the outbreak level. From the point of view of pest control i.e. cancer control, we would like to keep the population at k_1 and away from k_3. The fate of the system is determined by the initial condition Y_0. Thus an outbreak occurs if and only if $Y_0 > k_2$. In this sense the unstable equilibrium k_2 plays the role of a threshold. An outbreak can also be triggered by a saddle-node bifurcation. If the parameters $\overline{\alpha}$ and $\overline{\beta}$ drift in such a way that the fixed point k_1 disappears, then the population will jump suddenly to the outbreak level k_3. The situation is made worse by the hysteresis effect-even if the parameters are restored to their values before the outbreak, the population will not drop back to the refuge level.

The condition for a saddle-node bifurcation is that k_2 coalesce with k_3. This can also be described as that condition where the line $\overline{\alpha}\left(1-\frac{Y}{\overline{\beta}}\right)$ intersects the curve $\frac{Y}{1+Y^2}$ tangentially (see Figure 19 and Figure 20). Thus both $g(Y) = 0$ and $\frac{dg}{dY} = 0$.

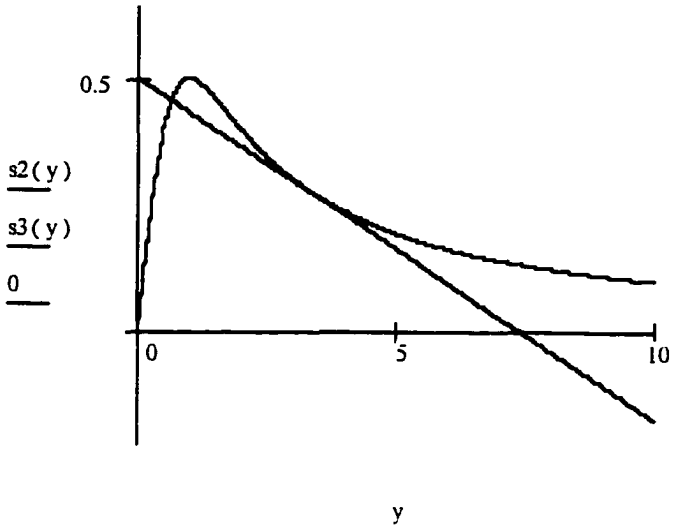

Figure 19: Tangential intersection of g(Y) = 0 i.e. $k_2 = k_3$.

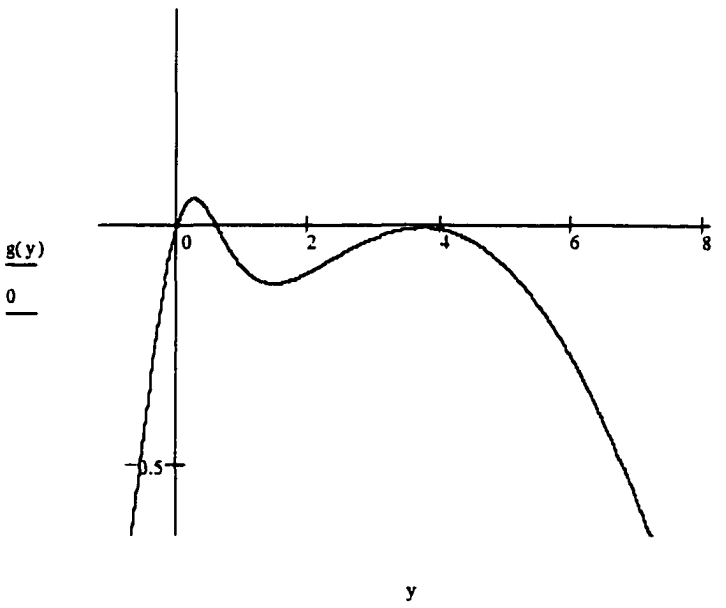

Figure 20: $k_2 = k_3$ which creates the tangential effect in Figure 19. The parameter value used in both Figures 19 and 20 are $\overline{\alpha} = .465$ and $\overline{\beta} = 8$.

$$\frac{-\bar{\alpha}}{\bar{\beta}} = \frac{1 - Y^2}{(1 + Y^2)^2}. \tag{35}$$

Substitution of $\bar{\alpha} / \bar{\beta}$ into g(Y) = 0 results in the expression

$$\bar{\alpha} = \frac{2Y^3}{(1 + Y^2)^2} \tag{36}$$

Substituting equation (36) into equation (35) yields

$$\bar{\beta} = \frac{2Y^3}{Y^2 - 1}. \tag{37}$$

Thus $\bar{\beta} > 0$ implies that Y is restricted to $Y > 1$. Together equations (36) and (37) define the bifurcation curves. For each $Y > 1$, we can plot the corresponding point $\bar{\beta}$ and $\bar{\alpha}$ in the $(\bar{\beta}, \bar{\alpha})$ plane (see Figure 21).

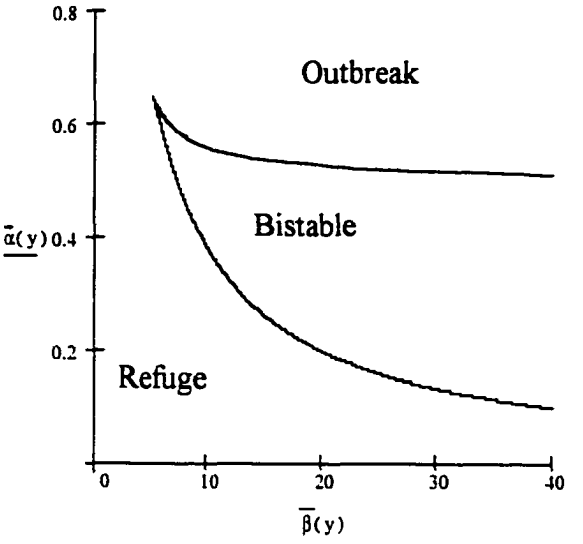

Figure 21: Together equations (36) and (37) define the bifurcation curves. For each $Y > 1$, we can plot the corresponding point $\bar{\beta}$ and $\bar{\alpha}$ in the $(\bar{\beta}, \bar{\alpha})$ plane.

The different regions in Figure 21 are labeled according to the stable fixed points that exist. The refuge level k_1 is the only stable state for low $\bar{\alpha}$, and the outbreak level k_3 is the only stable state for large $\bar{\alpha}$. In the bistable region, both stable states exist. The stability diagram can be regarded as the projection of a cusp catastrophe surface, as seen in Figure 22.

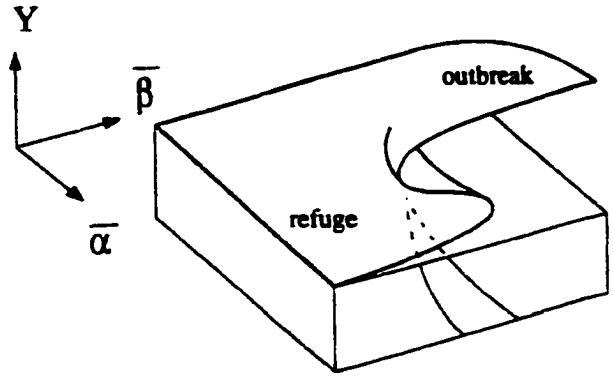

Figure 22: Cusp catastrophe surface.

TRAVELING WAVE SOLUTION

Again let us begin with equation (30) this time on the whole real line and approximate g(Y) defined by equation (33) to $O(Y^2)$. Simplifying we obtain

$$\frac{\partial Y}{\partial \tau} = \overline{D}\frac{\partial^2 Y}{\partial x^2} + \overline{\alpha} Y\left[1 - \left(\frac{1}{\overline{\alpha}} + \frac{1}{\overline{\beta}}\right) Y\right] \tag{38}$$

In 1937 Fisher considered a population of individuals carrying an advantageous allele of some gene a and migrating randomly into a region in which only the allele A is initially present. I would like to adapt his equation from Edelstein-Keshet [8] in which she gave an analysis of his equation. In this framework we assume Y to be the frequency of cancer cells in the population of cells and $\left[1 - \left(\frac{1}{\overline{\alpha}} + \frac{1}{\overline{\beta}}\right) Y\right]$ the frequency of immune cells.

Assume a traveling wave solution $Y(x,\tau) = Y(w)$ where $w = x - v\tau$ and $w \in (-\infty, \infty)$.

We can then write an ordinary second order differential equation

$$\frac{dY}{dw} = \frac{-\overline{D}}{v}\frac{d^2 Y}{dw^2} - \frac{\overline{\alpha}}{v} Y\left[1 - \left(\frac{1}{\overline{\alpha}} + \frac{1}{\overline{\beta}}\right) Y\right] \tag{39}$$

Define

$$\frac{dY}{dw} = -Q \tag{40}$$

then, equation (39) becomes

$$\frac{dQ}{dw} = \frac{\bar{\alpha}}{\bar{D}} Y\left[1 - \left(\frac{1}{\bar{\alpha}} + \frac{1}{\bar{\beta}}\right) Y\right] - \frac{v}{\bar{D}} Q \tag{41}$$

Consider a YQ plane corresponding to the system of equations (40) and (41). First we deduce the nullclines.

$$Q = 0 \qquad \text{(Y nullcline)} \tag{42}$$

$$Q = \frac{\bar{\alpha}}{v} Y\left[1 - \left(\frac{1}{\bar{\alpha}} + \frac{1}{\bar{\beta}}\right) Y\right] \qquad \text{(Q nullcline)} \tag{43}$$

Next we find their intersection (i.e. the steady states). These are $(Y_1, Q_1) = (0,0)$ and $(Y_2, Q_2) = \left(\frac{\bar{\alpha}\bar{\beta}}{\bar{\alpha} + \bar{\beta}}, 0\right)$. The Jacobian of equations (40) and (41) is

$$\begin{bmatrix} \frac{\bar{\alpha}}{\bar{D}} - \frac{2\bar{\alpha}}{\bar{D}}\left(\frac{1}{\bar{\alpha}} + \frac{1}{\bar{\beta}}\right) Y & \frac{-1}{\bar{D}} \\ 0 & \frac{-v}{\bar{D}} \end{bmatrix}$$ which at (0,0) is $\begin{bmatrix} \frac{\bar{\alpha}}{\bar{D}} & \frac{-1}{\bar{D}} \\ 0 & \frac{-v}{\bar{D}} \end{bmatrix}$ and at $\left(\frac{\bar{\alpha}\bar{\beta}}{\bar{\alpha} + \bar{\beta}}, 0\right)$ is

$\begin{bmatrix} \frac{-\bar{\alpha}}{\bar{D}} & \frac{-1}{\bar{D}} \\ 0 & \frac{-v}{\bar{D}} \end{bmatrix}$. This makes (Y_1, Q_1) a stable node and (Y_2, Q_2) a saddle point provided

$v > 2(\bar{\alpha}\bar{D})^{1/2}$. The YQ phase plane is shown in Figure 23. On this figure arrows

correspond to increasing w values, since w is the independent variable in equations (40) and (41). A single trajectory emanates from the saddle point and approaches the node as w increases from - ∞ to ∞. A trajectory that connects two steady states is said to be heteroclinic. Such trajectories have special significance to our analysis, as will presently be shown.

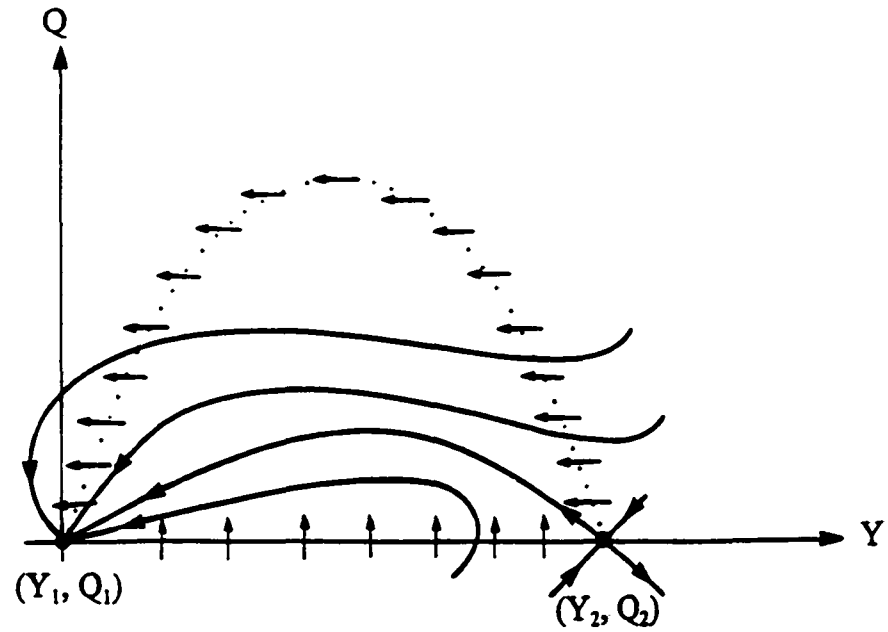

Figure 23: Traveling wave solutions to equation (38) satisfy a set of ODE's (equations (40) and (41)) whose phase-plane diagram is shown here.

Figure 24 shows a traveling-wave solution to Fisher's equation (38) . The heteroclinic trajectory shown connecting the two steady states $(Y_1,Q_1) = (0,0)$ and $(Y_2,Q_2) = \left(\frac{\bar{\alpha}\bar{\beta}}{\bar{\alpha}+\bar{\beta}},0\right)$ is the only bounded positive trajectory. Since $Y(w) \to \frac{\bar{\alpha}\bar{\beta}}{\bar{\alpha}+\bar{\beta}}$ for

$w \to -\infty$ and $Y(w) \to 0$ for $w \to \infty$.

To interpret Figure 24 in light of propagating waves we must first recall the interpretation given to the functions Y(w) and Q(w). Forfeiting a role previously played by time, the variable w stands for distance along the length of a wave. Any one curve in the YQ plane thus depicts the cancer frequency Y and its spatial variation Q from one end of the wave ($w = -\infty$) to the other ($w = \infty$). We are primarily interested in the former, Y(w). However, not all the phase plane trajectories give reasonable depictions of a biological wave. We consider the heteroclinic orbit mentioned above and observe the following properties of this curve:

$$Y(w) = Y_2 = \frac{\bar{\alpha}\bar{\beta}}{\bar{\alpha} + \bar{\beta}} \qquad (w \to -\infty)$$

$$Y(w) = Y_1 = 0 \qquad (w \to \infty)$$

$$Y_1 < Y(w) < Y_2 \qquad (-\infty < w < \infty)$$

A sketch is given of these qualities in Figure 24. This wave has the shape of a moving front. At large positive w, Y(w) is very small (approaching zero for $w \to \infty$), whereas at large negative w values Y(w) is very close to $\frac{\bar{\alpha}\bar{\beta}}{\bar{\alpha} + \bar{\beta}}$ (approaching $\frac{\bar{\alpha}\bar{\beta}}{\bar{\alpha} + \bar{\beta}}$ for $w \to -\infty$).

This means that the spread of cancer cells has become dominant at the left part of the domain, whereas it has become subdued towards the right.

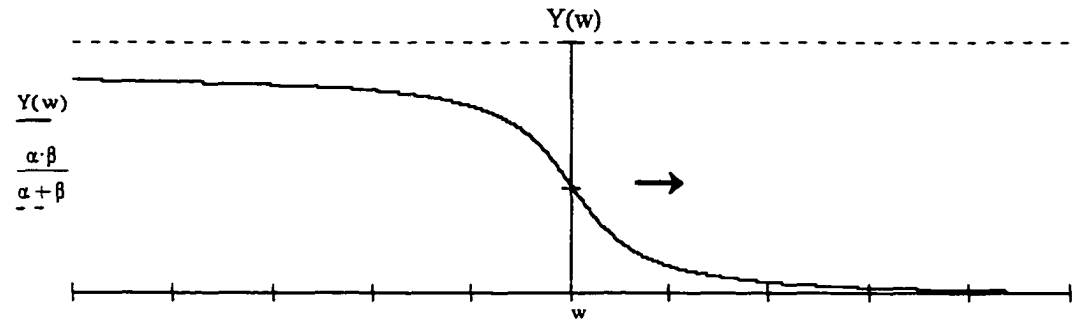

Figure 24: The qualitative shape of the wave. $Y(w) \to \frac{\alpha\beta}{\alpha+\beta}$ for $w \to -\infty$ and $Y(w) \to 0$ as $w \to +\infty$. The direction and speed of the motion is indicated.

If A equals the Jacobean matrix for equations (40) and (41) evaluated at each of the steady states, then the conditions for a stable node are:

$B < 0$ and $\gamma > 0$ where $B = \text{Tr } A$, and $\gamma = \det A$. $\text{Tr } A = -v/D < 0$, thus $B < 0$ and $\text{Det } A = \alpha/D > 0$, thus $\gamma > 0$. Hence (0,0) is a stable node. A saddle point is defined when $\gamma < 0$. In this case $\gamma = -\alpha/D$, and $B = -v/D$. The disc $A = B^2 - 4\gamma$ must be positive for the eigenvalues to be real numbers, thus $B^2 > 4\gamma$ implies $v^2/D^2 > 4\alpha/D$, $v^2 > 4\alpha D$ or $v > 2\sqrt{\alpha D}$. Thus the wave shown in Figure 24 must move at speeds that exceed the minimum velocity $2\sqrt{\alpha D}$.

Adam [40] sites the lower bound on wave speeds for wavefronts linking stable tumoral states to unstable cancer-free states as 2×10^{-7} - 2×10^{-8} cm/sec corresponding to a tumor of size 1 cm being established in 50-500 days (depending on the value of the diffusion coefficient).

CHAPTER VII

TUNNELING

"If an idea is not outrageous to start with, then it probably wasn't a good idea to begin with." Attributed to Albert Einstein

According to Löwden, [37] there is little doubt that many of the fundamental biochemical processes in living systems are directly connected with the transfer of electrons and protons. Since these are fundamental particles which do not obey the laws of classical physics but the laws of modern quantum chemistry, the electronic and protonic structure of biologically interesting molecules and systems has to be treated by quantum chemistry. This has led to the opening of a new field which has been called submolecular biology or "quantum biology". After a DNA replication, the protons are necessarily in nonstationary states which implies that there is a certain probability for "quantum jumps" which will lead to discontinuous changes of the code which will become apparent at the next DNA replication. This mechanism may be responsible for the occurrence of spontaneous mutations, the phenomenon of aging considered as a loss of useful genetic information, and the spontaneous occurrence of tumors (and cancer) as a consequence of somatic (or bodily) mutations depending on the accumulated effects of code changes in a certain direction. We try to understand these ideas by considering a simple model of "tunneling".

Löwden [36] states: In the tunnel-effect discovered by G. Gamow, and Gurney

and Condon, a quantum-mechanical particle having mass m and energy E may penetrate a classical potential barrier V = V(x). From Baym [33] particles can penetrate into regions that are forbidden classically. This means that even though a classical particle would be unable to penetrate a barrier, a quantum mechanical particle incident from the left has a certain probability of being found to the right of the barrier. If we consider a potential barrier of height V over [0,a] and if E represents an energy state such that E < V then a mathematical model illustrating this phenomenon is

$$\psi(x) = \begin{cases} Ae^{ipx/h} + Be^{-ipx/h}, x < 0 \\ Ce^{-kx} + De^{kx}, 0 < x < a \\ AS(E)e^{ip(x-a)/h}, x > a \end{cases}$$

where $\psi(x)$ is derived from the time independent Schrödinger equation

$$\frac{ih}{2\pi}\frac{\partial\psi(x,t)}{\partial t} = \frac{-h^2}{4\pi m}\frac{\partial^2\psi(x,t)}{\partial x^2} + V(x)\psi(x,t)$$ with boundary conditions.

The function S(E) is called the tunneling matrix element or transmission amplitude. It is essentially the probability amplitude for the process that a particle incident on the left with energy E will tunnel through the step. For E <V,

$$S(E) = \frac{4ikph\pi}{4ikph\pi\cosh ka + (4\pi^2p^2 - h^2k^2)\sinh ka}$$ where $p = \sqrt{2mE}$,

$hk = 2\pi\sqrt{2m(V-E)}$ and m represents the mass of the particle, and h is Planck's constant. The probability that a particle striking the barrier from the left will tunnel through to the right, is given by

$$T(E) = |S|^2 = \left[1 + \frac{\sinh^2 ka}{4(E/V)(1-E/V)}\right]^{-1}$$

(as is shown in standard texts on quantum mechanics, e.g. Schiff [41]). In a similar manner, cancer is made up of many "particles" (cells) that obviously would not exist if the immune system were 100% effective. While indeed the immune system may kill some or all of the invading cancer cells, (i.e. by acting as a barrier to the cancer growth), sometimes the cancer evades the immune response mechanism and subsequently prevails. In this light, we borrow the idea of quantum tunneling to examine the cancer/immune system response from a somewhat novel perspective, noting that the cells are macroscopic quantities (compared with atomic particles) and so the relevant mathematical model contains no reference to h and m. Nevertheless, the methodology is similar; an eigenvalue problem can be posed for the effective "transmissivity" of the immune system.

THE MATHEMATICAL MODEL

Let x_c represent the number of cells in a malignant tumor. We would expect that x_c would be no more than $O(10^{13})$ which is the approximate number of cells in a human being. A tumor may be palpable when the number of cells is of $O(10^9)$ (as occurs for example in the breast area). Thus, instead of using x_c as the independent variable, it

would seem more natural to use $\bar{x} = \log x_c$ as our independent variable. Let $\bar{V}(\bar{x})$ be the measure of the host immune response to tumorigenesis, i.e. the beginning of a tumor. Next assume $\bar{x}$ is defined on $[0,x_m]$ where $x_m = 13$ on the log scale or 10^{13} on the original scale. Rescale $[0,x_m]$ onto $[0,1]$ by using a new variable $x = \frac{\bar{x}}{x_m}$. We will

assume a barrier interval [p,q] of width q - p and height V(x) where [p,q] is contained within the interval [0,1]. We might think of the width of the barrier as a measure of the efficiency of the immune system in preventing "leakage" from a state of low cancer cell number to a correspondingly higher (and dangerously so) state. The height of the barrier can be thought of as a measure of the aggression of the cancer, insofar as a higher barrier can contain more " levels" of cancer aggression (i.e. more energy levels). It is as if the cancer interacts with the immune system (which it does) to induce a yet higher level of aggression which may not be present in lower barriers. Of interest would be to take a barrier of given height (such that there are at least two eigenvalues, and progressively widen the barrier, keeping the height constant, to see how the eigenfunctions (and hence probabilities) change across the barrier.

Consider the one-dimensional "Schrödinger-type" equation for the cancer cell population in a steady-state

$$\frac{d^2y}{dx^2} + [\lambda - V(x)]y = 0 \qquad (52)$$

where y(x) is the probability amplitude of cancer being found at location x. Here λ is

an eigenvalue representing the energy or "progression" of the cancer cells towards a highly malignant and dangerous state, while V(x) is the height of the barrier (i.e. V is constant).

The boundary conditions are

- $y(1) = 0$ (no cancer beyond this maximum value of $x = 1$)
- for some parameter α, such that $0 \le \alpha \le 1, \alpha y(0) - (1-\alpha)y'(0) = 0$,and
- y and y' are continuous at p and q

The first two conditions follow from the fact that we are assuming that $|y|^2$ is equal to the probability of the system (host) being found at "location" x. The last condition is required for purposes of continuity. In addition V = 0 outside the interval [p,q] and $\int_0^1 |y|^2 = 1$. The solution of equation (52) is

$$y = \begin{cases} A\sin(\sqrt{\lambda}x) + B\cos(\sqrt{\lambda}x) & \text{for } 0 \le x < p \quad V = 0 \qquad (53) \\ Ne^{\sqrt{V-\lambda}x} + Me^{-\sqrt{V-\lambda}x} & \text{for } p \le x \le q \text{ and } V > \lambda \qquad (54) \\ F\sin(\sqrt{\lambda})x + G\cos(\sqrt{\lambda})x & \text{for } q < x < 1 \quad V = 0 \qquad (55) \end{cases}$$

Let $k = \sqrt{\lambda}$, $h = \sqrt{V - \lambda}$, and $\beta = \frac{1-\alpha}{\alpha}$ then the constants for equation (53) are

$A = (A1 + A2 + A3 + A4 + A5)^{-.5}$ where

$$A1 = \frac{1}{2k}\left[\frac{(k^2\beta^2 - 1)\sin(2kp)}{2} + k(k^2\beta^2 p + 2\beta + p) - 2k\beta\cos^2(kp)\right]$$

$$A2 = \frac{1}{2}\frac{N1^2 e^{(4hq)} - M1^2 + 4N1M1e^{(2hq)}hq}{e^{(2hq)}h}$$

$$A3 = -\frac{1}{2}\frac{\left(N1^2 e^{(4hp)} - M1^2 + 4N1M1e^{(2hp)}hp\right)}{e^{(2hp)}h}$$

$$A4 = \frac{F1^2}{2k}\left[\frac{(\tan^2 k - 1)\sin 2k}{2} + k\tan^2 k + k + 2\tan k\cos^2 k\right]$$

$$A5 = \frac{F1^2}{2k}\left[\frac{(1 - \tan^2 k)\sin 2kq}{2} - kq\tan^2 k - kq - 2\tan k\cos^2 kq\right]$$

and $B = Ak\beta$. The constants for equation (54) are $M = M1 \cdot A$ and $N = N1 \cdot A$,

where $M1 = \frac{-kQ3\cos kp + Q4\sin kp}{2he^{-hp}}$ and $N1 = \frac{kQ1\cos kp + Q2\sin kp}{2he^{hp}}$.

The constants for equation 55 are:

$$F = A\frac{kQ1\cos kp + Q2\sin kp}{(k - h\tan k)\cos kq + (h + k\tan k)\sin kq}e^{h(q-p)}, \qquad (56)$$

where $Q1 = 1+\beta h$, $Q2 = h - k^2\beta$, $Q3 = 1-\beta h$, and $Q4 = h + k^2\beta$.

and $G = -F\tan k$. Also, in solving we find that F must also equal equation (57)

$$F = A\frac{Q4\sin kp - kQ3\cos kp}{(h - k\tan k)\sin kq - (k + h\tan k)\cos kq}e^{h(p-q)} \qquad (57)$$

An eigenvalue problem is a boundary value problem that has nontrivial solutions only when a parameter λ has special values called eigenvalues. In order for this problem to have solutions equation (56) must equal equation (57). Rewriting equation (56) in terms of λ we obtain:

$$f_1(\lambda) = \frac{\sqrt{\lambda}(1-\beta\sqrt{V-\lambda})\cos\sqrt{\lambda}p + (\sqrt{V-\lambda} + \beta\lambda)\sin\sqrt{\lambda}p}{(\sqrt{\lambda} - \sqrt{V-\lambda}\tan\sqrt{\lambda})\cos\sqrt{\lambda}q + (\sqrt{V-\lambda} + \sqrt{\lambda}\tan\sqrt{\lambda})\sin\sqrt{\lambda}q}e^{\sqrt{V-\lambda}(q-p)}$$

and for equation (57) in terms of λ we obtain:

$$f_2(\lambda) = \frac{(\sqrt{V-\lambda} - \beta\lambda)\sin\sqrt{\lambda}p - \sqrt{\lambda}(1-\beta\sqrt{V-\lambda})\cos\sqrt{\lambda}p}{(\sqrt{V-\lambda} - \sqrt{\lambda}\tan\sqrt{\lambda})\sin\sqrt{\lambda}q - (\sqrt{\lambda} + \sqrt{V-\lambda}\tan\sqrt{\lambda})\cos\sqrt{\lambda}q}e^{\sqrt{V-\lambda}(p-q)}$$

Setting $f_1(\lambda) = f_2(\lambda)$ and rewriting, we obtain two functions to be called $f_3(\lambda)$ and $f_4(\lambda)$ defined as follows

$$f_3(\lambda) = e^{\lambda\sqrt{V-\lambda}(q-p)}, \tag{58}$$

$$f^*(\lambda) = \frac{\left(\sqrt{V-\lambda}+\beta\lambda\right)\sin\sqrt{\lambda}\,p - \sqrt{\lambda}\,(1-\beta\sqrt{V-\lambda})\cos\sqrt{\lambda}\,p}{(\sqrt{V-\lambda}-\beta\lambda)\sin\sqrt{\lambda}\,p + \sqrt{\lambda}\,(1+\beta\sqrt{V-\lambda})\cos\sqrt{\lambda}\,p}$$

$$f_4(\lambda) = f^*(\lambda)\frac{(\sqrt{V-\lambda}+\sqrt{\lambda}\tan\sqrt{\lambda})\sin\sqrt{\lambda}\,q + (\sqrt{\lambda}-\sqrt{V-\lambda}\tan\sqrt{\lambda})\cos\sqrt{\lambda}\,q}{(\sqrt{V-\lambda}-\sqrt{\lambda}\tan\sqrt{\lambda})\sin\sqrt{\lambda}\,q - (\sqrt{\lambda}+\sqrt{V-\lambda}\tan\sqrt{\lambda})\cos\sqrt{\lambda}\,q} \tag{59}$$

The parameters needed to graph $f_3(\lambda)$ and $f_4(\lambda)$ are the height V, and position of the width, p and q. For example, for p = .6 and q = .8 with a height of V = 4 the graph of equations (58) and (59) are given in Figure 25.

As observed in Figure 25, for each barrier there always exists at least one eigenvalue namely $\lambda = V$, but there may not exist an eigenvalue $\lambda < V$ for all heights V. As we will see, for some larger values of V it is possible to obtain more than two eigenvalues less than V. A graph of the function y from equations (53), (54) and (55) for $\alpha = .3$, $\lambda = 3.61$, V = 4, p = .6 and q = .8 is given in Figure 26. The graph of the square of the function y is given in Figure 27 for the same barrier values as given above in Figure 26. Following Figure 26 are various other figures depicting different immune/cancer responses. At the conclusion of the figures there is a table of eigenvalues for various values of α, V, p, and q.

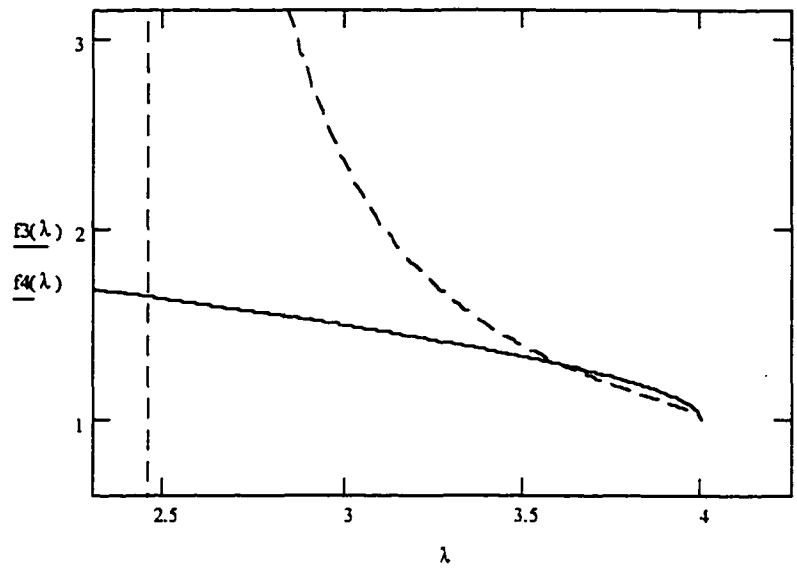

Figure 25: f_3 is represented by the solid line, and f_4 by the dotted line. You can see the intersection at $V = \lambda$. Our interest is in the $\lambda < V$. In this graph $\alpha = .3$, $V = 4$, $p = .6$, and $q = .8$. The intersection of f_3 and f_4 is at $\lambda = 3.61$.

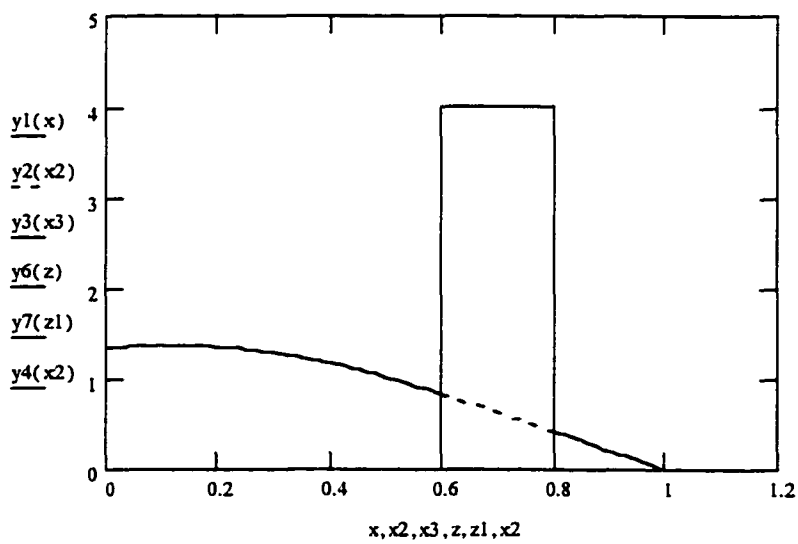

Figure 26: The function y1,y2, and y3 forms the three pieces of the function y from equations (53), (54), and (55). y6, y7,and y4 forms the rectangular barrier. The parameter values are identical to those used in Figure 25.

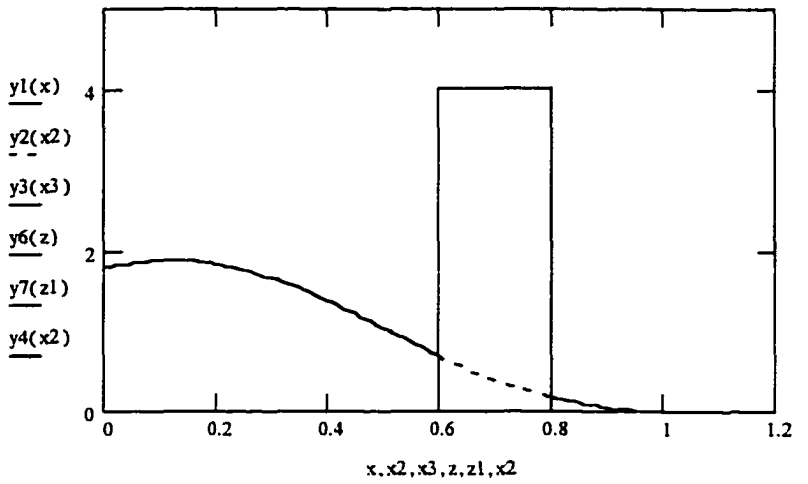

Figure 27: This is the square of the function y of Figure 26.

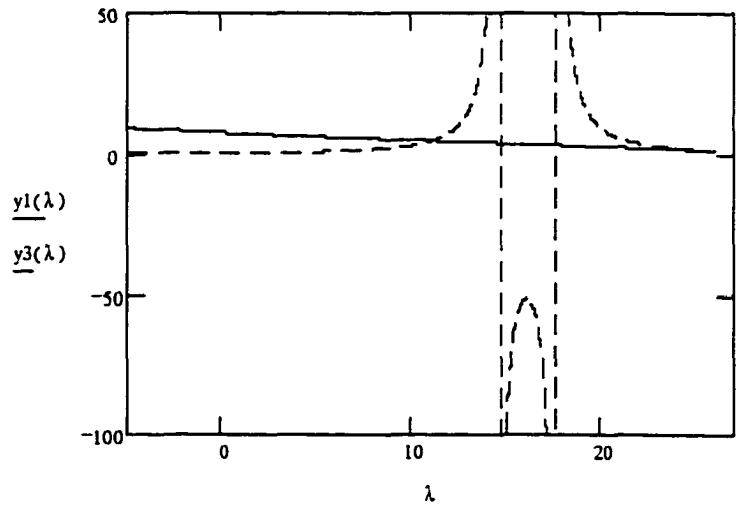

Figure 28: V = 26, α = .5, p = .2 and q = .4. This produces two eigenvalues as shown above. The first λ_1 = 11.1 and the second λ_2 = 25.77.

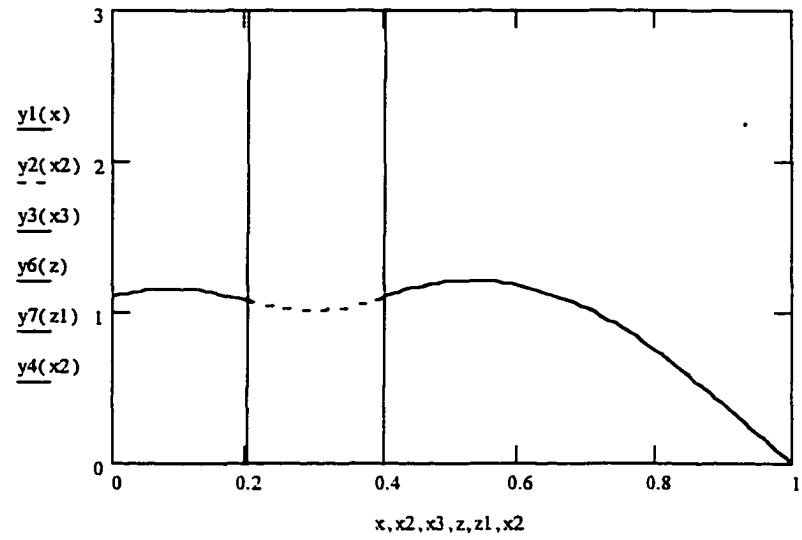

Figure 29: V = 26 and λ_1 = 11.1, p = .2, and q = .4. The immune system does not appear to affect the cancer significantly.

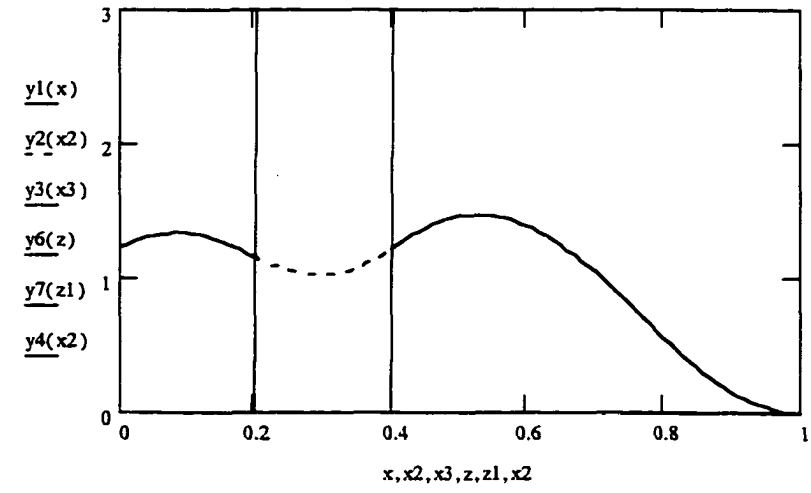

Figure 30: The graph of y^2 corresponding to Figure 29.

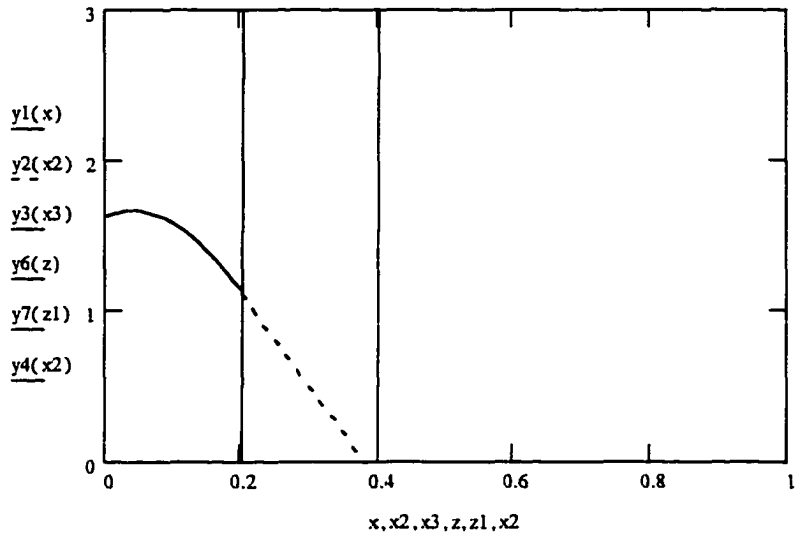

Figure 31: V = 26, and $\lambda_2 = 25.77$, α, p, and q as in Figure 28. Now the immune barrier prevents the cancer from tunneling through.

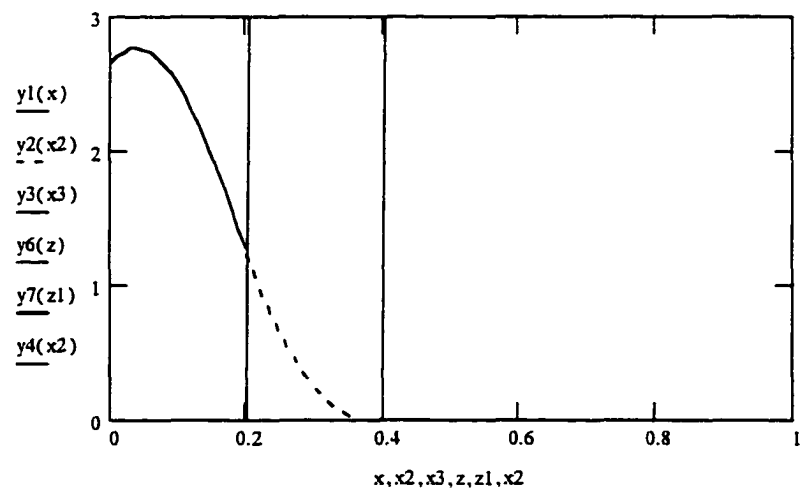

Figure 32: The graph of y^2 corresponding to Figure 31.

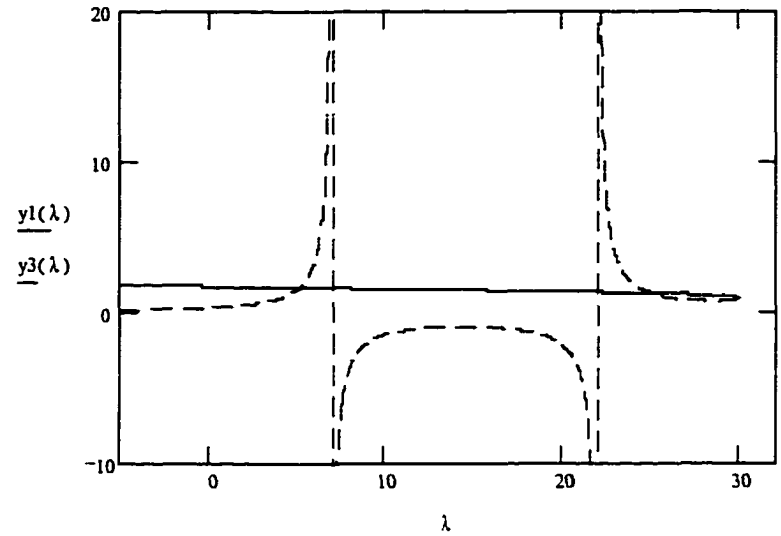

Figure 33: V = 30, α = .4, p = .5 and q = .55. The graph shows two eigenvalues which are $\lambda_1 = 5.03$ and $\lambda_2 = 25.1$.

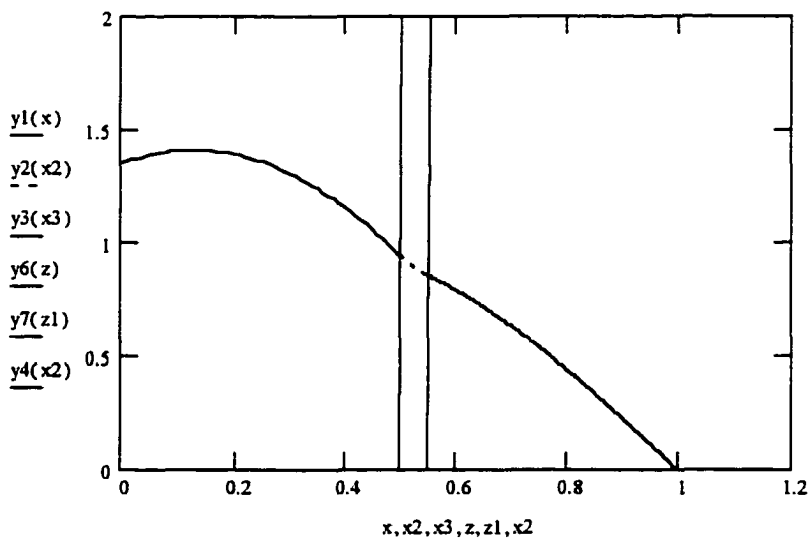

Figure 34: V = 30, α = .4, p = .5 and q = .55. This graph was formed using the eigenvalue $\lambda_1 = 5.03$.

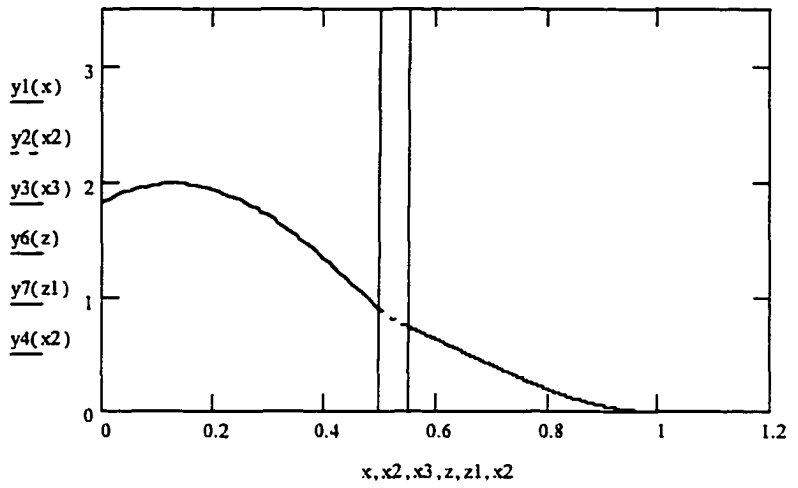

Figure 35: The graph of y^2 corresponding to Figure 34.

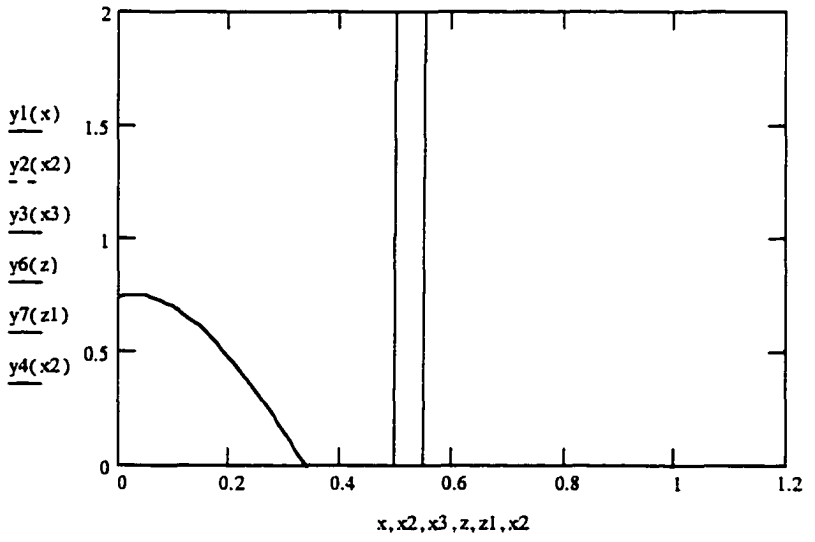

Figure 36: V = 30, α = .4, p = .5 and q = .55. This graph was formed using the eigenvalue $\lambda_2 = 25.1$. It would appear that the cancer tumor was destroyed for reasons other than the presence of the immune barrier.

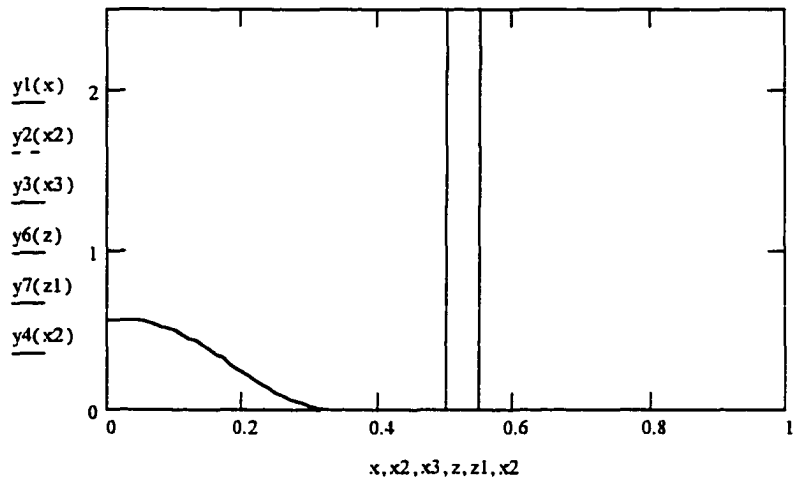

Figure 37: The graph of y^2 corresponding to Figure 36.

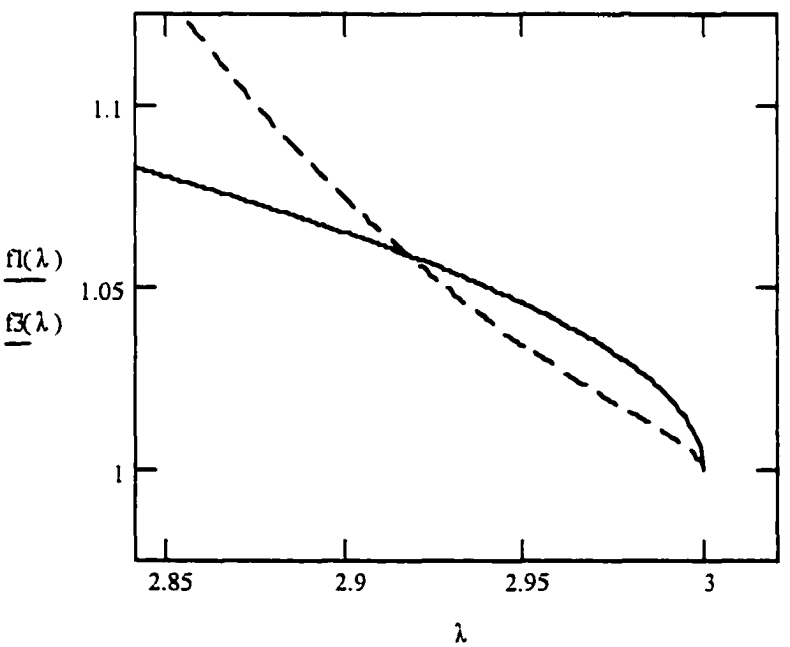

Figure 38: V = 3, α = .01, p = .3, q = .4. The eigenvalue is 2.92.

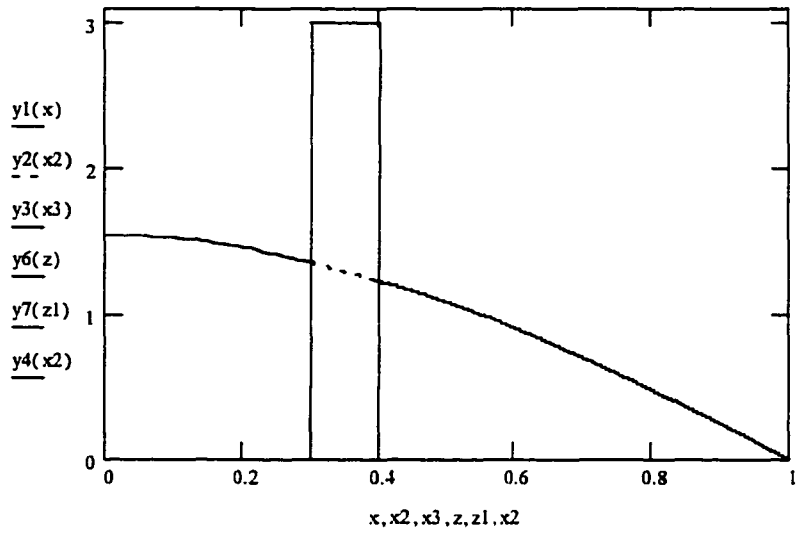

Figure 39: The graph of y for V = 3, α = .01, p = .3, q = .4. The eigenvalue is 2.92

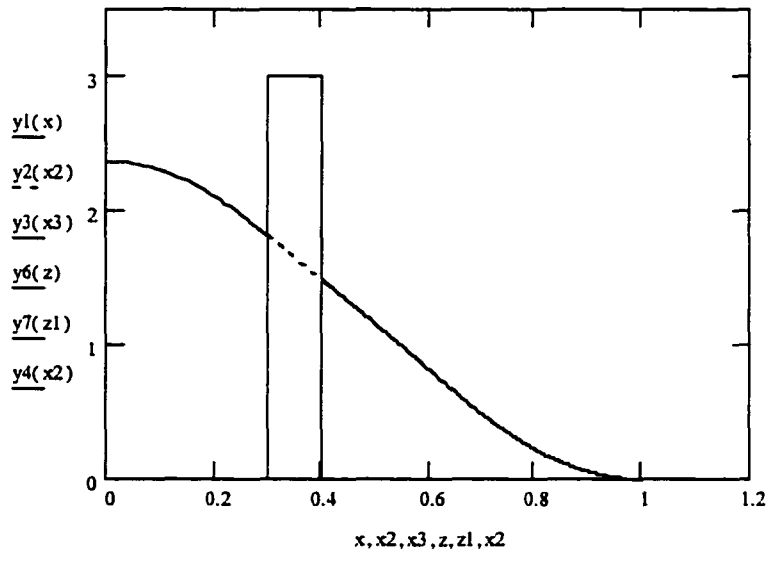

Figure 40: The graph of y^2 corresponding to Figure 39.

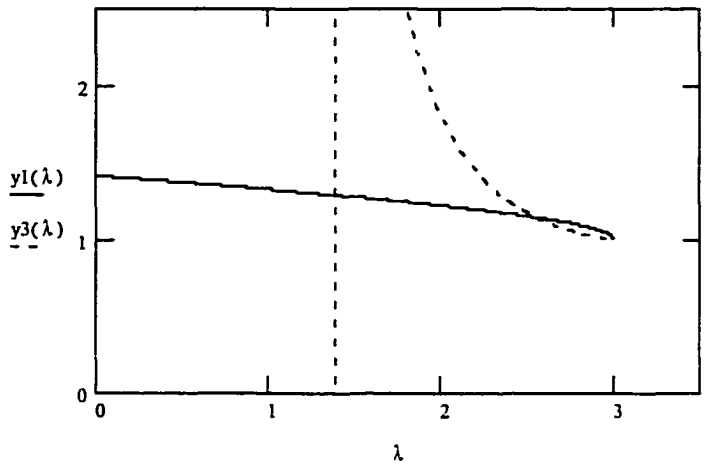

Figure 41: This graph represents the special case when $\alpha = 0$ V = 3 and p = .7 q = .8. The eigenvalue is 2.55.

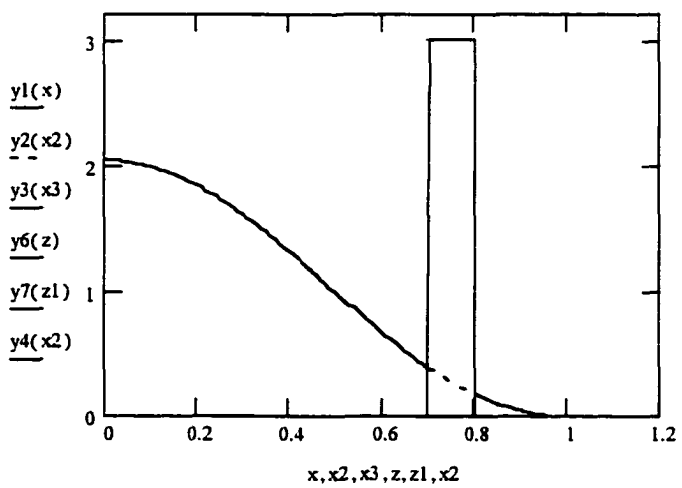

Figure 42: This is the graph of y^2 for $\alpha = 0$, V = 3, p = .7, q = .8 and $\lambda = 2.55$.

Table 8. A Table of Eigenvalues

α	V	p	q	λ
.01	4	.2	.3	3.157
.01	4	.2	.4	3.721
.01	5	.2	.5	4.57
.01	6	.2	.7	6.428
.01	3	.5	.6	2.734
.01	3	.5	.7	2.88
.01	3	.5	.8	2.95
.01	3	.7	.8	2.57
.01	3	.7	.9	2.6
.01	24	.2	.3	6.19, 23.1
.01	24	.2	.4	9, 23.2
.01	27	.2	.5	12.2, 24.42
.01	27	.5	.6	4.26, 26.1
.01	27	.7	.8	3.0843, 26.25
.01	76	.7	.8	3.6255, 31.18, 75.7
.3	4	.2	.3	3.917
.3	5	.2	.4	4.805
.3	6	.2	.5	5.8027
.3	8	.2	.9	8.52
.3	4	.5	.6	3.614
.3	4	.5	.7	3.833
.3	5	.5	.8	4.1
.3	4	.7	.8	3.38

Table 8 Continued

α	V	p	q	λ
.3	4	.7	.9	3.42
.5	6	.2	.3	5.08
.5	6	.2	.4	5.977
.5	8	.2	.5	7.595
.5	11	.2	.7	10.52
.5	13	.2	.9	11.97
.5	5	.5	.6	4.62
.5	6	.5	.7	5.06
.5	6	.5	.8	5.23
.5	5	.7	.1	4.28
.5	5	.7	.9	4.35
1	12	.2	.3	10.95
1	13	.2	.4	12.73
1	17	.2	.5	16.23
1	35	.2	.7	34.72
1	74	.2	.9	73.74
1	13	.5	.6	12.26
1	15	.5	.7	14.6
1	17	.5	.8	16.23
1	12	.7	.8	10.95
1	12	.7	.9	11.32
.8	8	.2	.3	7.72
.8	10	.2	.4	9.498
.8	12	.2	.5	11.886

Table 8 Continued

α	V	p	q	λ
.8	21	.2	.7	20.492
.8	25	.2	.9	24.01
.8	8	.5	.6	7.68
.8	9	.5	.7	8.56
.8	10	.5	.8	9.16
.8	8	.7	.8	7.06
.8	8	.7	.9	7.19
0	4	.2	.3	3.14
0	4	.2	.4	3.7
0	5	.2	.5	4.55
0	7	.2	.7	6.2
0	7	.2	.9	6.4
0	3	.5	.6	2.719
0	3	.5	.7	2.86
0	3	.5	.8	2.93
0	3	.7	.8	2.55
0	3	.7	.9	2.57

CONCLUSION ON TUNNELING

As the table and graphs show, there are many models for the many situations that are possible in the cancer/immune relationship. While we use terms like "aggressive", or "slow" to describe certain types of cancer, at present there is no numerical value associated with cancer progression. In this model, in forming the table, the "minimum" values were sought, i.e. in terms of whole number quantities, which would produce an eigenvalue. For example, for $\alpha = .01$, and $p = .2$ and $q = .3$ a barrier height of 4 was the first whole number which produced an eigenvalue $\lambda < V$. Naturally, we would be interested in knowing more about the circumstances which lead the immune system to triumph over the cancer as in Figure 29. From a mathematical standpoint, Figure 29 seems to occur in similar circumstances, i.e. a large height which permits two eigenvalues less than V and the eigenvalue closest to V being the value producing the result of immune barrier stopping the cancer. Wide barriers, implying the immune system is very effective, also induce a decline in the probability that cancer is present. This is obviously just a beginning in the modeling of cancer and the immune system from this perspective and much more remains to be done. One significant question concerns the validation of this type of model: how can this be done? The present results are suggestive that the "immune barrier" may be a useful metaphor for tumorigenesis, but to bring it down to the level of a model it must be predictive and testable. In this dissertation, a start has been made on the "metaphorical" aspect of the problem. Tumorigenesis is based on the notion that developing tumor cells acquire an ever-

increasing growth advantage through gene mutations. These mutations create genetic variability; the cells with the most growth-favoring mutations proliferate rapidly, outcompete normal cells, and soon dominate. But to survive a tumor cell must also defeat the host's defenses and become an effective parasite. Accomplishing this may depend upon its abilities to evade immune surveillance, to metastasize, and to attract a blood supply. The importance of immune defenses against cancer is a matter of controversy. One school of thought argues that specialized cells of the immune system continuously survey tissues for small nests of tumor cells that, once recognized, are attacked and wiped out. This view is supported by the discovery of natural killer lymphocytes that seem able to identify and destroy many types of tumor cells. Tumor cells may display specific antigens on their surfaces that alert the immune system to their presence. Tumors more than a few millimeters in diameter soon stop growing unless they have a blood supply. If immune surveillance by these and other cell types is indeed important in antitumor defenses, then cancer cells must acquire an ability to elude the immune system [38].

REFERENCES

1. J. A. Adam, A Simplified Model Of Wound Healing (with particular reference to the Critical Size Defect), *Mathematical and Computer Modelling* 30 (5/6), 23-32 (1999).

2. J. Arnold and J. A. Adam, A Simplified Model Of Wound Healing II (The Critical Size Defect In Two Dimensions) , *Mathematical and Computer Modelling*, 30, 47-60, (1999).

3. Bloom and Fawcett, *Histology*, Chapters 8 and 9, 3rd edition.

4. Neil T. Bennett, and Gregory S. Schultz, Growth Factors and Wound Healing: Biochemical Properties of Growth Factors and Their Receptors, *The American Journal of Surgery*, V165, 728-737 (1993).

5. F. Bowman, *Introduction To Bessel Functions*, Dover Publications Inc., New York City, (1958).

6. L. Du Noüy, *Biological Time.,Ch V: Cicatrization Of Wounds (II)-Experimental Technique-Curves-Mathematical Study*, Methuen , London, (1936).

7. EBI Medical Systems: EBI Bone healing Systems, Internet: www.ebimedical.com/normal_boneheal.html.

8. L. Edelstein-Keshet, *Mathematical Models in Biology*, Random House, New York, (1988).

9. D. Ferguson, W. Davis, M. Urist, W. Hurt, E. Allen, Bovine Bone Morphogenetic Protein (bBMP) Fraction-induced Repair of Craniotomy Defects in the Rhesus Monkey (Macaca speciosa), *Clinical Orthopaedics and Related Research*, 251-258, (1984).

10. Fractures Treatment methods are tailored to the break:Mayo Clinic Health Letter, April 1986: Internet: www.mayohealth.org/mayo/9604/htm/fracture.htm, (1986).

11. J. W. Frame, A composite of porous calcium sulfate dihydrate and cyanoacrylate as a substitute for autogenous bone, *J. Oral Surg.* Vol 38, 251, (1980).

12. J. W. Frame, A convenient animal model for testing bone substitute materials, *J. Oral Surg.* Vol 38, 176-180, (1980).

13. E. Freeman, and R.S. Turnbull, The role of osseous coagulum as a graft material, *J. Periodont.* Res. 8, 229, (1973).

14. Z. B. Friedenberg, and R. R. Lawrence, The regeneration of bone in defects of varying size, *Surg. Gynecol. Obstet.* 114, 721, (1962).

15. J. Glowacki, D. Altobelli, and J. B. Mulliken, Fate of mineralized and demineralized osseous implants in cranial defects. *Cacif. Tissue Int.* 33, 71, (1981).

16. J. O. Hollinger, and J. C. Kleinschmidt, The Critical Size Defect as an Experimental Model To Test Bone Repair Materials, *The Journal of Craniofacial Surgery VI*, Number 1, 60-68, January (1990).

17. I. R. H. Kramer, H. C. Kelly, and H. C. Wright, A histological and radiological comparison of the healing of defects of the rabbit calvarium with and without implanted heterogenous anorganic bone. *Arch. Oral Biol.* 13, 1095, (1968).

18. T. A. Lange, J. E. Zerwekh, R. D.Peek,V. Mooney, B. H. Harrison, Granular tricalcium phosphate in large cancellous defects, *Ann Clin Lab Sci*, 16, 467-472, (1986).

19. J. B. Mulliken, and J. Glowacki, Induced osteogenesis for repair and construction in the craniofacial region, *Plast. Reconstr. Surg.* 65, 553, (1980).

20. D. J. Prolo, Gutierrez, DeVine, S. Oklund, Clinical utility of allogenic skull discs in human craniotomy, *Neurosurgery*; 14, 183-186, (1984).

21. D. J. Prolo, P. W. Pedrotti, K. P. Burres, and S. Oklund, Superior osteogenesis in transplanted allogenic canine skull following chemical sterilization, *Clin Orthrop.* 108, 230-242, (1982).

22. R. W. Ruddon, *Cancer Biology*, (second edition) Oxford University Press, New York, (1987).

23. J. P. Schmitz, and J. O. Hollinger, The critical size defect as an experimental model for craniomandibulofacial nonunions, *Clinical Orthopaedics and Related Research*, 205, 299-308, (1986).

24. J. A. Sherratt, and J. D. Murray, Models of epidermal wound healing, *Proc. R. Soc. Lond.*, 241B, 29-36, (1990).

25. J. A. Sherratt, and J. D. Murray, Mathematical analysis of a basic model for epidermal wound healing, *J. Math. Biol.*, 29, 389-404, (1991).

26. K. Takagi, M.R.Urist, The reaction of the dura to bone morphogenetic protein (BMP) in repair of skull defects, *Ann. Surg.* 196, 100-109, (1982).

27. C. J. Tranter, *Bessel Functions With Some Physical Applications*, Hart Publishing, New York, (1969).

28. R.S. Turnbull, and E. Freeman, Use of wounds in the parietal bone of the rat for evaluating bone marrow for grafting into periodontal defects, *J. Periodont. Res.* 9, 39, (1974).

29. M. R. Urist, New advances in bone research, *West. J. Med.* 141, 71, (1984).

30. H. Winet, H., The Role Of Microvasculature In Normal And Perturbed Bone Healing As Revealed By Intravital Microscopy, *Bone Vol. 19* No.1,39S-57S, Supplement July (1996).

31. U.S. Department of Health and Human Services; *Immunology its role in disease and health*, April (1980).

32. U.S. Department of Health and Human Services; *The Immune System-How It Works*, December (1993).

33. G. Baym, *Lectures On Quantum Mechanics*, New York, (1969).

34. R. W. Gurney, and E. U. Condon, Quantum mechanics and radioactive disintegration, *Physics Rev.*, 33, 127-140, (1929).

35. Harold Varmus and Robert A. Weinberg, *Genes And The Biology Of Cancer*, New York, (1993).

36. Per-Olov Löwden, Isotope Effect In Tunneling And Its Influence On Mutation Rates, *Mutation Research* 2, 218-221, (1965).

37. Per-Olov Löwden, Proton Tunneling in DNA and its Biological Implications, *Reviews of Modern Physics* Vol 35, Number 3, July (1963).

38. Scientific American Special Issue: *What You Need To Know About Cancer*; September (1996).

39. Strogatz, Steven H, *Nonlinear Dynamics and Chaos*, Addison-Wesley, Maine, (1994).

40. J. A. Adam, The Dynamics Of Growth-Factor-Modified Immune Response To Cancer Growth: One Dimensional Models, *Mathematical and Computer Modelling*, Vol. 17, (1993).

41. L.I. Schiff, *Quantum Mechanics*, 3rd edition, New York, (1968).

APPENDIX A

COMPARISONS OF THE AREAS OF THE δ-WIDTHS AND THE RADIUS OF THE WOUND

In Model I and II of the two-dimensional case in wound healing, and in the three-dimensional case, the critical δ-region is found by approximation, and in each case is found to be dependant on the original wound size R. Figure 2, Figure 10, and Figure 15 show monotone decreasing functions which imply that as the wound size R increases the δ-values decrease. At first this may seem to be a contradiction to logic, i.e. that large wounds require smaller δ-band widths. However, by comparing the area of the δ band width with the radius of the wound size we obtain the following formula

$$\delta\text{-Area}(R) = \pi(2R\,\delta + \delta^2).$$

After non-dimensionalizing the area formula and substituting the minimum δ values found we have the following equations.

For the two-dimensional Model I

$$\text{Area}(Y) = \pi\left(2Y\frac{K_1(Y)}{nK_0(Y)} + \left(\frac{K_1(Y)}{nK_0(Y)}\right)^2\right)$$

whose graph is Figure 43 for n = 3.

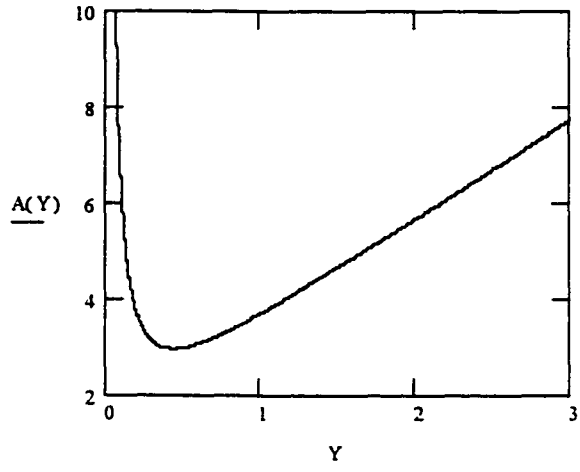

Figure 43: The graph of the area function for the two-dimensional model I and n = 3.

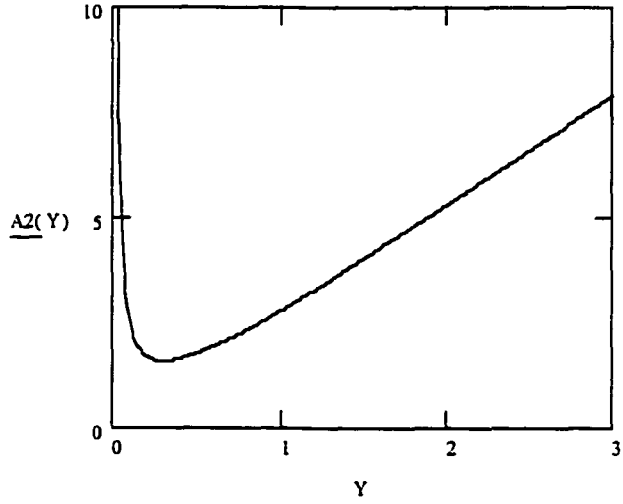

Figure 44: The graph of the area function for the two-dimensional model II and n = 3.

For the two-dimensional model II the area equation is

$$\text{Area}(Y) = \pi\left(2Y\frac{1}{nYK_0(Y)I0(Y)} + \left(\frac{1}{nYK_0(Y)I0(Y)}\right)^2\right)$$

and the graph is given in Figure 44. For the three-dimensional model the equation is

$$\text{Area}(Y) = \pi\left(2\frac{Y+1}{n} + \left(\frac{Y+1}{nY}\right)^2\right)$$

and the graph is given in Figure 45.

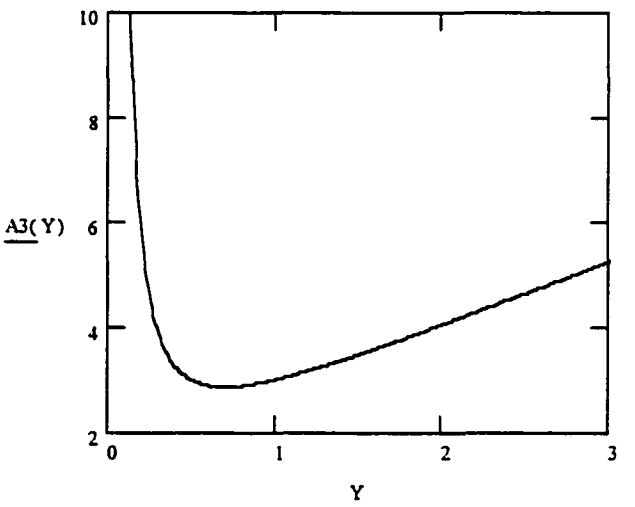

Figure 45: The graph of the area function for the three-dimensional model and n = 3.

The graphs of these three functions are all similar showing an almost parabolic shape with a relative minimum value beyond which the area of the δ-region is increasing as Y gets larger.

APPENDIX B

JUSTIFICATION FOR THE CHOICE OF THE APPROXIMATION FUNCTION OF $O(\epsilon^3)$

In the three -dimensional model $e^{-\epsilon}$ was approximated to $O(\epsilon^1)$ but the approximation yielded no useful information. Even approximations (i.e. $O(\epsilon^2)$ etc.) yield functions which are monotonically decreasing and thus do not give the information needed (see Figure 46).

The approximations for $e^{-\epsilon}$ are as follows:

$$O(\epsilon^1):\ 1-\frac{Y+1}{nY} \quad ; \quad O(\epsilon^2):\ 1-\frac{Y+1}{nY}+\frac{1}{2}\left(\frac{Y+1}{nY}\right)^2 \text{ and}$$

$$O(\epsilon^3):\ 1-\frac{Y+1}{nY}+\frac{1}{2}\left(\frac{Y+1}{nY}\right)^2-\frac{1}{6}\left(\frac{Y+1}{nY}\right)^3.$$

The graph of $O(\epsilon^2)$ is given in Figure 46.

Since these are only approximations and for m a positive integer $O(\epsilon^{2m})$ gives rise to monotonically decreasing functions while $O(\epsilon^{2m+1})$ produces monotonically increasing functions (the kind of approximation needed for our study) the choice $O(\epsilon^3)$

was made because it was also solvable and higher odd orders would have been more difficult or impossible to obtain explicitly.

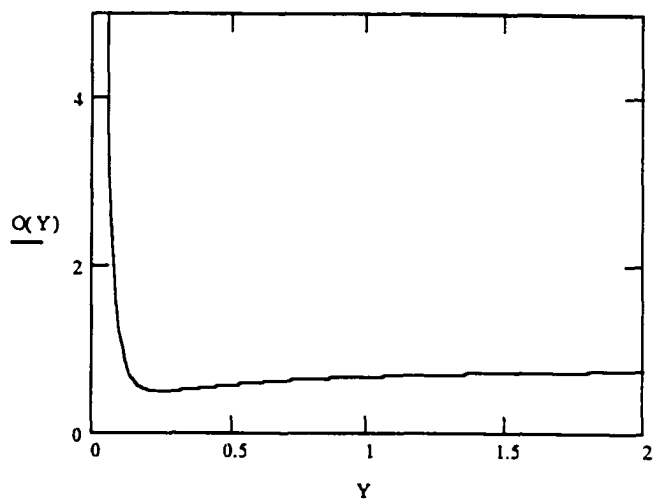

Figure 46: The graph of the approximation function to $O(\epsilon^2)$.

APPENDIX C

DETAILS ON MODIFIED BESSEL FUNCTIONS AND DERIVATION OF SELECTED FORMULAS WITHIN THE TEXT

The modified Bessel functions used in the text were I_0, I_1, K_0, and K_1. These functions are defined as follows:

$I_0(x) = J_0(ix)$ where J_0 is a Bessel function. . $\frac{d(I_0(x))}{dx} = I_1(x)$

$$K_0(x) = \lim_{p \to 0} \frac{\pi}{2}\left[\frac{I_{-p}(x) - I_p(x)}{\sin(p\pi)}\right] \text{ and } \frac{d(K_0(x))}{dx} = -K_1(x).$$

These functions satisfy the differential equation $x^2y'' + xy' - (x^2 + n^2)y = 0$

for n = 0 or 1.

The Asymptotic Expansions (which were used to find the limits for large y values in Model I and Model II) for each of the four functions are as follows:

$$I_0(x) \approx \frac{e^x}{\sqrt{2\pi x}}\left\{1 + \frac{1}{8x} + \frac{9}{128x^2} + \frac{75}{1024x^3}\cdots\right\}$$

$$I_1(x) \approx \frac{e^x}{\sqrt{2\pi x}}\left\{1 - \frac{3}{8x} - \frac{15}{128x^2} - \frac{105}{1024x^3}\cdots\right\}$$

$$K_0(x) \approx \sqrt{\frac{\pi}{2x}}e^{-x}\left\{1 - \frac{1}{8x} + \frac{9}{128x^2} - \frac{75}{1024x^3}\cdots\right\} \quad \text{and}$$

$$K_1(x) \approx \sqrt{\frac{\pi}{2x}}e^{-x}\left\{1 + \frac{3}{8x} - \frac{15}{128x^2} + \frac{105}{1024x^3}\cdots\right\}$$

The graphs of the four functions are below.

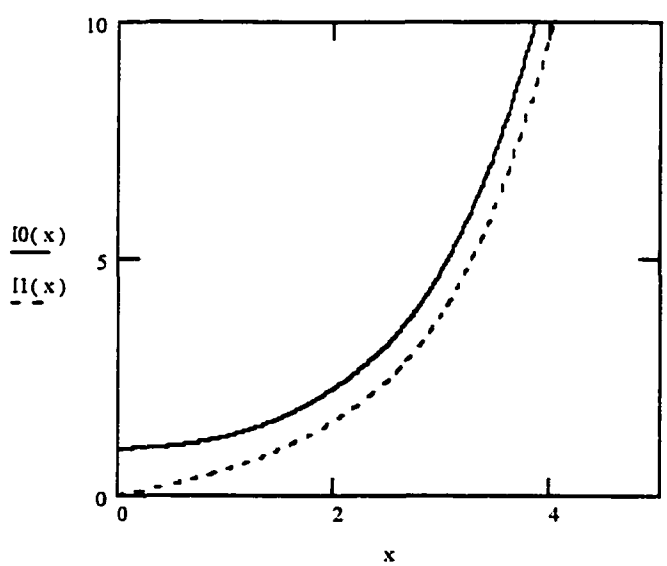

Figure 47: The top graph is $I_0(x)$ and the bottom graph is $I_1(x)$.

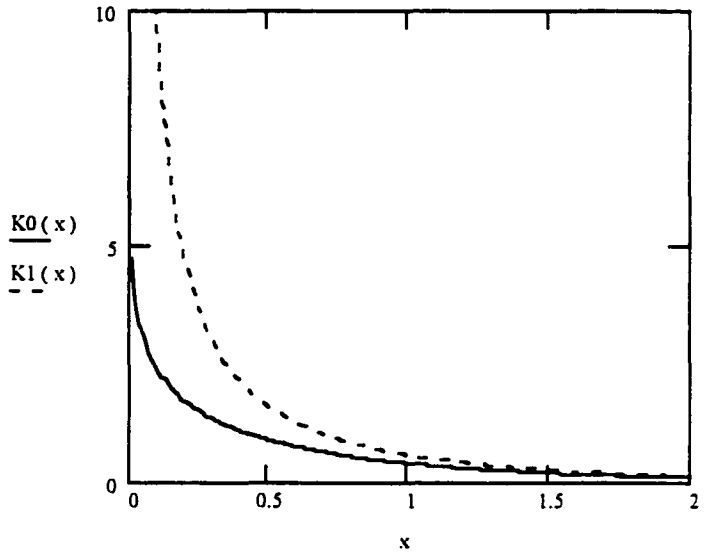

Figure 48: The top graph is $K_1(x)$ and the bottom graph is $K_0(x)$.

The wronskian identity is $I_0(x)\,K_1(x) + I_1(x)\,K_0(x) = 1/x$.

DETAILS OF THE ONE-DIMENSIONAL MODEL

In the one-dimensional model, the solutions were hyperbolic functions. In this model the wound edge is L/2. Thus $C\left(\frac{L}{2}\right) \geq \theta$ was examined for Model I which assumes no bone remains in the wound area. The δ-region was found to be only dependant on n, i.e. $\delta_c = \ln\left(\frac{n}{n-1}\right)$ where n is defined in the same manner as the two and three dimensional models. No result was given for L-critical in Model I. In

Model II, a solution for L-critical is obtained in terms of the width of the growth factor region, δ, namely $L_c = \alpha^{-1} \ln\left\{\frac{n(1-e^{-\alpha\delta})}{2-n(1-e^{-\alpha\delta})}\right\}$.

DERIVATION OF C(r) FOR THE TWO-DIMENSIONAL CASE MODEL I

Since $x = \alpha R$, we can write the solution in terms of αR. Thus,

$C_1(r) = AI_0(\alpha r) + BK_0(\alpha r) + \frac{P}{\lambda}$ for $R \le r \le R + \delta$ and

$C_2(r) = FI_0(\alpha r) + GK_0(\alpha r)$ for $r > R + \delta$.

The boundary condition $\frac{dC(r)}{dr} = 0$ gives us $B = A\frac{I_1(\alpha R)}{K_1(\alpha R)}$. The boundary condition

$\lim_{r\to\infty} C(r) = 0$ tells us that $F = 0$ since $I_0(\alpha R)$ is an increasing function. $K_0(\alpha R)$

approaches zero for large x. Thus $C_2(r) = GK_0(\alpha r)$. The last boundary condition

(continuity at $R + \delta$ for C and $\frac{dC(r)}{dr}$) will allow us to find A and G.

$$AI_0(\alpha(R+\delta)) + BK_0(\alpha(R+\delta)) + \frac{P}{\lambda} = GK_0(\alpha(R+\delta)) \text{ and}$$

$AI_1(\alpha(R+\delta)) - BK_1(\alpha(R+\delta)) = GK_1(\alpha(R+\delta))$. Rearranging the terms

and substituting our solution for B, we obtain the system

$$A\left(I_0(\alpha(R+\delta)) + \frac{I_1(\alpha R)}{K_1(\alpha R)}K_0(\alpha(R+\delta)\right) - GK_0(\alpha(R+\delta)) = -\frac{P}{\lambda} \quad \text{and}$$

$$A\left[I_1(\alpha(R+\delta)) - \frac{I_1(\alpha R)}{K_1(\alpha R)}K_1(\alpha(R+\delta)\right] + GK_1(\alpha(R+\delta)) = 0 .$$

Using determinants $A = \dfrac{\frac{-P}{\lambda}K_1(\alpha(R+\delta))}{(I_0K_1 + I_1K_0)(\alpha(R+\delta))}$ and

$$G = \frac{\frac{P}{\lambda}\left[I_1(\alpha(R+\delta)) - \frac{I_1(\alpha R)}{K_1(\alpha R)}K_1(\alpha(R+\delta))\right]}{(I_0K_1 + I_1K_0)(\alpha(R+\delta))}$$. Similar method were used to

derive Model II and the three-dimensional model .

VITA

JULIA SUZANNE ARNOLD
Old Dominion University
Department of Mathematics and Statistics
BAL 500, Hampton Blvd.
Norfolk, VA 23529-0077

EDUCATION:

- PhD degree May, 2000 - Old Dominion University
- MS degree Applied Mathematics 1996 - Old Dominion University
- MA degree Mathematics 1967- University of Georgia
- BA degree in Mathematics and Education 1964- University of South Florida

TEACHING EXPERIENCE FULL-TIME

- 1999 accepted position as Assistant Professor for the Thomas Moss Campus of Tidewater Community College
- 1994-1999 Graduate Teaching Assistant, Old Dominion University
- 1993-1994 Visiting Instructor, Virginia Wesleyan College
- 1985-1987 Math Instructor, Suffolk Christian High School
- 1970-1981 Assistant Professor , Tidewater Community College, Portsmouth, VA
- 1964-65 Teacher, King High School , Tampa, Florida

PART-TIME TEACHING EXPERIENCE

- 1998-1999, Tidewater Community College Portsmouth Campus
- Spring 1998, Tidewater Community College Norfolk Campus
- 1997-1998, Tidewater Community College Portsmouth Campus
- 1990-1993, Virginia Wesleyan College & Old Dominion University
- 1987-1990, Tidewater Community College Portsmouth Campus & Paul D. Camp Community College
- 1974-1975, University of Maryland & University of South Carolina, Rota, Spain

PUBLICATION:

- J. Arnold and J. Adam, A Simplified Model Of Wound Healing II (The Critical Size Defect In Two Dimensions) , *Mathematical and Computer Modelling*, 30,1999,47-60.

COMMUNITY ACTIVITIES:

- Children's Sunday School Teacher for First Baptist Church of Suffolk for 15 years
- Women's Missionary Union Member and Group Leader
- Member of the Auxiliary Organization of the Gideons
- Elementary School Room Mother
- Volunteer for Heart Fund, Cancer Fund
- Vacation Bible School Teacher